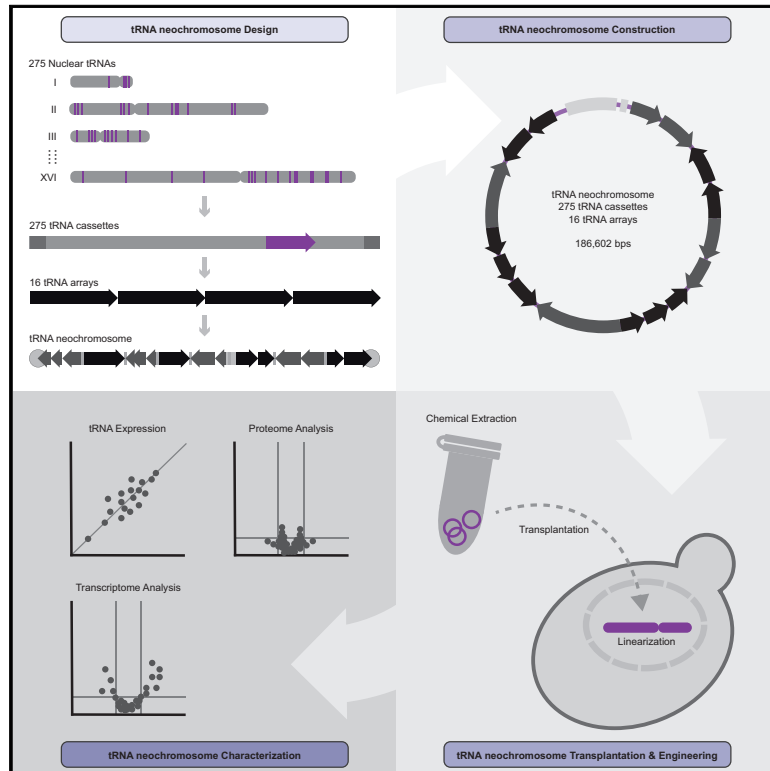


# Design, construction, and functional characterization of a tRNA neochromosome in yeast

## Graphical abstract



## Authors

Daniel Schindler, Roy S.K. Walker, Shuangying Jiang, ..., Lars M. Steinmetz, Jef D. Boeke, Yizhi Cai

## Correspondence

yizhi.cai@manchester.ac.uk

## In brief

A designer tRNA neochromosome containing all 275 nuclear tRNA genes of *Saccharomyces cerevisiae* reveals unexpected genomic plasticity and insights into both tRNA and chromosome biology.

## Highlights

- Designed, built, and characterized a neochromosome with 275 tRNA genes in yeast
- Additional tRNA genes burden the host cell, causing deletions or increased ploidy
- Chemical tRNA neochromosome extraction enables transplantation into new yeast strains
- Functional analysis reveals insights into tRNA and chromosomal biology

Article

# Design, construction, and functional characterization of a tRNA neochromosome in yeast

Daniel Schindler,<sup>1,2,3,25</sup> Roy S.K. Walker,<sup>4,5,25</sup> Shuangying Jiang,<sup>6</sup> Aaron N. Brooks,<sup>7</sup> Yun Wang,<sup>8,9</sup> Carolin A. Müller,<sup>10,11</sup> Charlotte Cockram,<sup>12</sup> Yisha Luo,<sup>1</sup> Alicia García,<sup>13</sup> Daniel Schraivogel,<sup>7</sup> Julien Mozziconacci,<sup>12</sup> Noah Pena,<sup>14</sup> Mahdi Assari,<sup>15</sup> María del Carmen Sánchez Olmos,<sup>2</sup> Yu Zhao,<sup>16</sup> Alba Ballerini,<sup>1</sup> Benjamin A. Blount,<sup>17,18</sup> Jitong Cai,<sup>19</sup> Lois Ogunlana,<sup>20</sup> Wei Liu,<sup>20</sup> Katarina Jönsson,<sup>20</sup> Dariusz Abramczyk,<sup>20</sup> Eva Garcia-Ruiz,<sup>1</sup> Tomasz W. Turowski,<sup>21</sup> Reem Swidah,<sup>1</sup> Tom Ellis,<sup>17,18</sup> Tao Pan,<sup>22</sup> Francisco Antequera,<sup>13</sup> Yue Shen,<sup>1,8,9</sup> Conrad A. Nieduszynski,<sup>10,11</sup> Romain Koszul,<sup>12</sup> Junbiao Dai,<sup>6</sup> Lars M. Steinmetz,<sup>7,23</sup> Jef D. Boeke,<sup>16,24</sup> and Yizhi Cai<sup>1,26,\*</sup>

<sup>1</sup>Manchester Institute of Biotechnology, University of Manchester, Manchester M1 7DN, UK

<sup>2</sup>Max Planck Institute for Terrestrial Microbiology, 35043 Marburg, Germany

<sup>3</sup>Center for Synthetic Microbiology (SYNMIKRO), Philipps-University Marburg, 35032 Marburg, Germany

<sup>4</sup>School of Engineering, Institute for Bioengineering, The University of Edinburgh, Edinburgh EH9 3BF, Scotland

<sup>5</sup>School of Natural Sciences and ARC Centre of Excellence in Synthetic Biology, Macquarie University, Sydney, NSW 2109, Australia

<sup>6</sup>CAS Key Laboratory of Quantitative Engineering Biology, Guangdong Provincial Key Laboratory of Synthetic Genomics and Shenzhen Key Laboratory of Synthetic Genomics, Shenzhen Institute of Synthetic Biology, Shenzhen Institute of Advanced Technology, Chinese Academy of Sciences, Shenzhen, China

<sup>7</sup>European Molecular Biology Laboratory (EMBL), Genome Biology Unit, 69117 Heidelberg, Germany

<sup>8</sup>BGI-Shenzhen, Beishan Industrial Zone, Shenzhen 518083, China

<sup>9</sup>Guangdong Provincial Key Laboratory of Genome Read and Write, BGI-Shenzhen, Shenzhen 518120, China

<sup>10</sup>Earlham Institute, Norwich Research Park, Norwich NR4 7UZ, UK

<sup>11</sup>School of Biological Sciences, University of East Anglia, Norwich NR4 7TU, UK

<sup>12</sup>Institut Pasteur, CNRS UMR 3525, Université Paris Cité, Unité Régulation Spatiale des Génomes, 75015 Paris, France

<sup>13</sup>Instituto de Biología Funcional y Genómica (IBFG), CSIC, Universidad de Salamanca, Salamanca, Spain

<sup>14</sup>Department of Molecular Genetics and Cell Biology, University of Chicago, Chicago, IL 60637, USA

<sup>15</sup>Department of Chemistry, University of Chicago, Chicago, IL 60637, USA

<sup>16</sup>Institute for Systems Genetics and Department of Biochemistry and Molecular Pharmacology, NYU Langone Health, New York, NY 10016, USA

<sup>17</sup>Imperial College Centre for Synthetic Biology, Imperial College London, London, UK

<sup>18</sup>Department of Bioengineering, Imperial College London, London, UK

<sup>19</sup>Department of Biomedical Engineering, Whiting School of Engineering, Johns Hopkins University, Baltimore, MD, USA

<sup>20</sup>School of Biological Sciences, The University of Edinburgh, Edinburgh EH9 3BF, Scotland

<sup>21</sup>Institute of Biochemistry and Biophysics PAS, Pawińskiego 5a, 02-106 Warszawa, Poland

<sup>22</sup>Department of Biochemistry and Molecular Biology, University of Chicago, Chicago, IL 60637, USA

<sup>23</sup>Department of Genetics and Stanford Genome Technology Center, Stanford University, Palo Alto, CA 94304, USA

<sup>24</sup>Department of Biomedical Engineering, NYU Tandon School of Engineering, Brooklyn, NY 11201, USA

<sup>25</sup>These authors contributed equally

<sup>26</sup>Lead contact

\*Correspondence: [yizhi.cai@manchester.ac.uk](mailto:yizhi.cai@manchester.ac.uk)

<https://doi.org/10.1016/j.cell.2023.10.015>

## SUMMARY

Here, we report the design, construction, and characterization of a tRNA neochromosome, a designer chromosome that functions as an additional, *de novo* counterpart to the native complement of *Saccharomyces cerevisiae*. Intending to address one of the central design principles of the Sc2.0 project, the ~190-kb tRNA neochromosome houses all 275 relocated nuclear tRNA genes. To maximize stability, the design incorporates orthogonal genetic elements from non-*S. cerevisiae* yeast species. Furthermore, the presence of 283 *rox* recombination sites enables an orthogonal tRNA SCRaMbLE system. Following construction in yeast, we obtained evidence of a potent selective force, manifesting as a spontaneous doubling in cell ploidy. Furthermore, tRNA sequencing, transcriptomics, proteomics, nucleosome mapping, replication profiling, FISH, and Hi-C were undertaken to investigate questions of tRNA neochromosome behavior and function. Its construction demonstrates the remarkable tractability of the yeast model and opens up opportunities to directly test hypotheses surrounding these essential non-coding RNAs.

## INTRODUCTION

Synthetic genomics is a nascent field of research that leverages advances in large-scale *de novo* DNA synthesis with rational design-based approaches of synthetic biology. Progressive advances in this field have led to the construction of viral genomes,<sup>1,2</sup> bacterial genomes,<sup>3,4</sup> and eukaryotic chromosomes.<sup>5–7</sup> Developments in eukaryotes include work of the international Synthetic Yeast Genome Project (Sc2.0), an international endeavor that aims to re-design and chemically synthesize a designer version of the *Saccharomyces cerevisiae* genome.

Sc2.0 is framed around three central design principles<sup>6,8</sup> that emphasize near wild-type fitness, the introduction of genetic flexibility to facilitate future research, and the removal of potentially unstable elements such as tRNA genes (tDNAs) and transposons. Since tRNA genes are collectively but not necessarily individually essential to cell viability, Sc2.0 design specifications dictate the relocation of all tDNAs onto a dedicated synthetic chromosome (termed a tRNA neochromosome), so that the overall abundance of tRNA isoacceptor gene copies in the final synthetic strain matches that of the wild-type genome.<sup>6</sup> Furthermore, design specifications include the removal of tRNA introns from those copies that contain them. In this study, we report the design, construction, and characterization of a tRNA neochromosome, a fully synthetic, designer chromosome that exists as an additional copy to the 16 native chromosomes of *S. cerevisiae*.

The genome of *S. cerevisiae* houses a total of 275 nuclear tRNA genes, including 1 pseudogene, dispersed throughout the genome.<sup>9</sup> tRNA genes are transcribed by RNA polymerase III (RNAPIII) and associated transcription factors by conserved dual promoter elements (A and B sequence blocks) located internally to the tDNA.<sup>10</sup> Owing to their central role in biology, tRNA molecules are evolutionarily conserved and essential to all known free-living organisms.

tDNAs are known genomic instability hotspots for at least two reasons. Polar replication fork collisions between components associated with heavily transcribed tRNA genes cause replication fork stall events, leading to DNA breakage and chromosomal instability.<sup>11–13</sup> Furthermore, highly repetitive retrotransposons of up to 6 kb in length, as well their solo long terminal repeat (LTR) derivatives of 300–400 bp, preferentially associate with regions upstream of tDNAs,<sup>14,15</sup> and thus they can act as hotspots for chromosomal recombination.<sup>16,17</sup> Our rationale is that removing repetitive elements and relocating tRNA genes onto a dedicated synthetic chromosome will lead to a synthetic yeast genome less susceptible to structural rearrangement and will isolate any instability caused by their presence.<sup>8</sup> We hypothesized that the function of tRNA genes are context independent and thus can be relocated onto a tRNA neochromosome. The tRNA neochromosome also serves as a chassis to systematically explore tRNA genetics through the *Dre-rox* synthetic chromosome rearrangement and modification by *loxP*-mediated evolution (SCRaMbLE) system, providing a technological platform to facilitate research into tRNA and chromosomal biology, and to demonstrate design-driven engineering biology approaches to enable the construction of future neochromosomes.

## RESULTS

### Design of the tRNA neochromosome

In contrast to other synthetic chromosomes of the Sc2.0 project, the tRNA neochromosome has no native counterpart in the yeast genome. As no pre-existing chromosome is available to serve as a template, the tRNA neochromosome was designed and built *de novo*. To rationalize the design process, we arranged each element of the tRNA neochromosome into defined layers of structural hierarchy (Figure 1A). The smallest of these layers consisted of 275 tRNA “cassettes” (~680 bp) concatenated into 16 tRNA “arrays” (2.6–23.3 kb; Methods S1), each designed to house tRNA genes from a single *S. cerevisiae* native chromosome (Figure 1A; Methods S1). These tRNA arrays in turn comprised “mega-arrays” consisting of one to three tRNA arrays oriented in tandem so as to be transcribed and replicated in the same direction (Figure 1B). Following linearization and release of functional telomere seed sequences through deployment of the telomerator system,<sup>18</sup> the circular tRNA neochromosome was converted into a true linear chromosome.

The design of the tRNA neochromosome was framed around a series of design specifications, largely intended to maximize its stability and ensure tRNA functionality. One of our primary design considerations was to limit homology with the host genome by incorporating DNA sequences that are largely orthogonal to the wild-type and synthetic yeast genome sequences. Overall, the majority (~89%) of the tRNA neochromosome sequences originate from non-*S. cerevisiae* yeast species. These orthogonal regions include tDNA flanking sequences, three origins of replication and four synthetic bidirectional replication termination (*TER*) sites assembled *de novo* and based on natural *Saccharomyces spp.* *Fob1* recognition sequences.

The tRNA neochromosome was designed to maintain tRNA copy number and codon specificity of all wild-type tRNA genes of *S. cerevisiae*. Since ensuring tRNA gene function took priority over orthogonality, tDNAs were not altered (excepting introns, which were removed from all 59 intron-containing tDNAs). To minimize host genome homology, each tRNA cassette incorporated flanking sequences from the yeasts *Ashbya (Eremothecium) gossypii* or *Eremothecium cymbalariae*. We selected these yeast species because of their close evolutionary relationship to *S. cerevisiae*.<sup>19,20</sup> Furthermore, *A. gossypii* lacks retrotransposons<sup>21</sup> and is thus not populated by the repetitive solo LTR elements that commonly reside upstream of *S. cerevisiae* tDNAs. Each 500-bp 5' flanking region was chosen to ensure a consistent spacing between each highly transcribed tRNA gene sequence (Figure 1A). The 40-bp 3' region was incorporated to ensure efficient tRNA transcriptional termination mediated by poly-thymidine residues that constitute the RNAPIII terminator.<sup>22</sup> All 3' tRNA flanking sequences should possess five or more thymidine residues required for transcriptional termination. Since tRNA genes are transcribed from an internal promoter, we did not envision a significant disruption of tRNA transcription. Each tDNA was assigned to flanking sequences (Methods S1) using a bioinformatic pipeline that additionally removes or alters unwanted elements from flanking sequences (Figure S1A; see STAR Methods for details). These elements included residual start codons, LTR repeats from *E. cymbalariae*, and overlapping regions from adjacent tDNAs

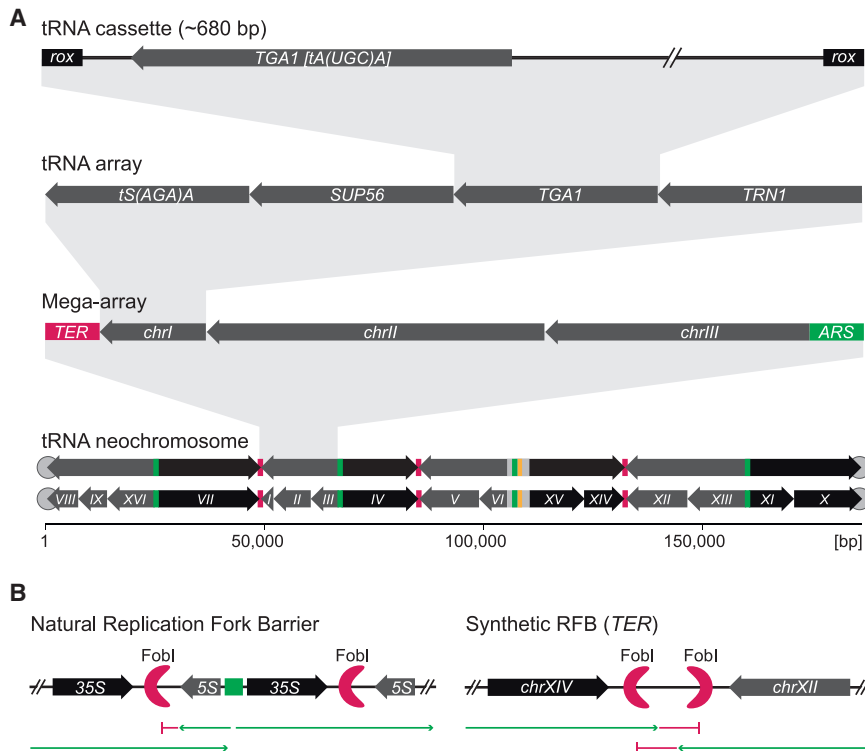


**Figure 1. Design and hierarchy of the tRNA neochromosome**

(A) The smallest level of hierarchy includes tRNA cassettes consisting of orthogonal 500-bp 5' and 40-bp 3' sequences flanking each tRNA gene. *rox* recombination sites flank each tRNA cassette. tRNA cassettes then form chromosome-specific tRNA arrays in which transcription of all tRNAs points in the same direction. tRNA arrays are in turn ordered into mega-arrays of approximately even size, with DNA replication and transcription oriented to proceed in the same direction. Autonomous replicating sequences (ARSs) are indicated in green, synthetic bidirectional termination sites (TER) are indicated in red, and pRS413 centromere region is indicated in orange. The tRNA neochromosome itself consists of 275 tRNA cassettes ordered in 16 tRNA arrays, which then comprise 8 mega-arrays. Telomeres are indicated by gray circles.<sup>18</sup>

(B) The synthetic bidirectional termination sites are based on the native rDNA replication fork blocking sites mediated by Fob1 and are intended to minimize potential collision events between the DNA replication and RNAPIII transcription machinery.

See also [Figure S1](#), [Methods S1](#), and [Data S1](#).

([Figure S1B](#)). Furthermore, a proof-of-principle experiment demonstrated that synthetic copies of single-copy, essential tRNA genes (*SUP61* (tS(CGA)C), *TRT2* (tT(CGU)K), and *TRR4* (tR(CCG)L)) were capable of successfully complementing deletion of their wild-type counterparts, with no significant effect of cell phenotype ([Figure S1C](#)). Similarly, removing an intron from the synthetic copy of tS(CGA)C did not result in a phenotype, in agreement with a previous study,<sup>23</sup> although a potential precursor accumulation and a single downstream deleterious synthetic genetic interaction was observed for tS(CGA)C.<sup>24</sup> In terms of additional evidence for function of individual synthetic tRNAs constructed according to this overarching design scheme, we note that the *chrII* and *chrXII* tRNA arrays, respectively, have previously demonstrated synthetic chromosome complementation through reversal of global upregulation of the *synII* translational machinery<sup>5</sup> as well as restoration of a fitness defect in *synXII*.<sup>25</sup>

### Neochromosome structure

The overall structure of the tRNA neochromosome ([Figure 1A](#)) was designed to encompass the fundamental features of typical eukaryotic chromosomes, including a centromere, telomeres, and origins of replication. The backbone for tRNA neochromosome assembly comprised the pRS413 centromeric vector, which itself houses the centromere region of chromosome VI (*CEN6*) fused to an origin of replication (*ARSH4*) and a *HIS3* marker.<sup>26</sup> Three orthogonal origins of replication from the yeast *Candida glabrata* ([Methods S1](#)) were introduced and positioned so as to ensure relatively even tRNA neochromosome replication ([Figure 1A](#)) with “early” and “strong” replication origins preferentially selected. Our circular design also enables us to chemically extract the neochromosome and transform it into a new yeast

background later<sup>27</sup> and also to conditionally linearize by introducing functional telomeres in any defined region using the telomerator system<sup>18</sup> ([Figure 3A](#)).

### Minimizing replication stress

A key consideration in our design was to maximize tRNA neochromosome stability, which included an overall aim of minimizing replication stress caused by polar replication fork collisions with tRNA gene transcription. tRNA genes are among the most highly transcribed in the cell.<sup>28,29</sup> It is also known that replication fork stall events in eukaryotes are influenced by the orientation of tDNA transcription relative to replication. When oriented to oppose incoming replication forks, they can induce blockage of the latter and induce chromosomal instability.<sup>12,30</sup> Therefore, to reduce replication stress and DNA damage caused by head-on replication fork stall events, we oriented tRNA arrays so that the direction of both replication and tRNA transcription were concordant ([Figure 1](#)). These formed mega-arrays that were designed to be of similar size (~20 kb each) to ensure replication progression as evenly as possible across the resulting ~40-kb replicons.

An inevitable challenge caused by the presence of multiple replication origins in our design is that a replication fork may progress beyond regions carrying co-oriented transcription units and may subsequently collide with tRNA transcription in opposing orientation. To limit this issue and minimize potentially destabilizing effects of head-on replication fork collisions with components associated with active tRNA transcription, we introduced four cassettes designed to block DNA replication in both directions. Our strategy intended to emulate the protective role of *TER* sites of the rDNA locus,<sup>31</sup> which are known to prevent

head-on collisions between the replication fork and the RNA polymerase I (RNAPI) transcriptional machinery of rDNA.<sup>32,33</sup> Each of the four designer bidirectional *TER* sites (*TERI* to *TERIV*; [Methods S1](#)) were designed to house two conserved Fob1 recognition sites, in opposite direction, with sequences based on the rDNA sequences of four non-*S. cerevisiae* *Saccharomyces* species ([Figure 1B](#)).

### An orthogonal recombinase system for tRNA copy-number adjustment

The Sc2.0 project leverages SCRaMble to generate combinatorial diversity in strains housing synthetic chromosomes.<sup>34</sup> To explore questions of tRNA genetics such as minimal and/or optimal combination of tRNA genes needed under a given condition, we introduced a second, independent site-specific recombinase system, based on the Dre-*rox* system,<sup>35,36</sup> to facilitate future studies. The positioning of *rox* recombination sites both upstream and downstream of each tRNA cassette ([Figure 1A](#)) is intended to provide the means to stochastically alter tDNA copy number. There is no evidence of any cross-reactivity between the Cre-*lox* and Dre-*rox* recombination systems.<sup>37</sup> A preliminary proof-of-principle experiment demonstrated that the Dre-*rox* system successfully induced a reduction in the number of tRNA cassettes on a tRNA array ([Figure S1D](#)). It should be noted that the tRNA neochromosome was constructed in a wild-type background with all native tRNA genes present. In the future, we will adjust tRNA copy number using the Dre-*rox* system once the fully synthetic Sc2.0 strain is available.

### Neochromosome construction

To construct the tRNA neochromosome from its constituent tRNA arrays, we employed an approach similar to the SwAP-In (Switching Auxotrophies Progressively by Integration) method described previously but without using a natural template.<sup>6,7</sup> This evolved into the eSwAP-In (extrachromosomal Switching Auxotrophies Progressively by Integration) approach described previously<sup>38</sup> and is referred to as such henceforth. This process applied recursive rounds of *in vivo* homologous recombination between a circular, intermediate “acceptor” assembly and a single “donor” tRNA array. Integration of each tRNA array was facilitated by two regions of homology: the outermost ~400-bp to ~600-bp DNA sequence already present in the growing neochromosome and a 500-bp “universal homologous region” (UHR) consisting of randomly generated DNA. The repeated swapping of the *LEU2* and *URA3* selective markers facilitated selection for each round of integration ([Figure 2A](#)). Successful integration of each tRNA array was verified through PCR, using specific primers designed to anneal with the 3' and 5' flanking region of each tRNA cassette ([Figure S11](#); [Methods S1](#)). The tRNA neochromosome was constructed in two independent strain backgrounds, in parallel, through a series of 15 subsequent rounds of integration into a circular acceptor vector housing the *chrVI* tRNA array. The first of these strains was the wild-type BY4741, and the second strain housed synthetic chromosome III, VI, and the right arm of IX (*synIII/VI/IXR*).<sup>6</sup> Subsequently, the circular tRNA neochromosome constructed in *synIII/VI/IXR* was subjected to chemical

extraction and spheroplast transformation into a “fresh” BY4741 strain, resulting in strain YCy1576.

### Neochromosome linearization and repair of structural variations

Initial tRNA neochromosome linearization experiments unexpectedly revealed structural variations of the tRNA neochromosome constructed in both strain backgrounds ([Figure S1H](#)). Notably, pulsed-field gel electrophoresis (PFGE) and next-generation sequencing (NGS) revealed complex structural variations of varying genomic sizes, including a doubling in size, of one BY4741 tRNA neochromosome variant ([Figure S1H](#)). In contrast, whole-genome sequencing of the tRNA neochromosome constructed in *synIII/VI/IXR* (YCy1576) revealed a single complex structural variation, consisting of an inversion, duplication, and deletion ([Figure 2B](#)). Furthermore, a total of eleven minor nucleotide variations outside the pRS413 backbone were detected, with nine having no predicted impact and two potentially inactivating one *rox* site each ([Methods S1](#)).

We elected to repair the structural variations of YCy1576 to generate the circular tRNA neochromosome consistent with our basal design. The structural variations of the resulting strain, YCy1677, were subsequently repaired by employing a two-step procedure mediated by the I-SceI homing endonuclease to remove the duplicated region, introduce the missing tRNA cassettes, and repair the inversion ([Figure 2B](#)). The final NGS-validated strain (YCy2508) was used for subsequent experiments.

### Spontaneous doubling in yeast genome ploidy and tRNA neochromosome instability in haploid cells

Unexpectedly, we observed a uniform increase in host strain ploidy from a haploid to a homozygous diploid (i.e., from  $1n$  to  $2n$  BY4741 *MATa/a* genotype). This was confirmed via the strain's ability to mate with *MAT $\alpha$*  strains, PCR-based mating-type tests,<sup>39</sup> and flow cytometry quantification of DNA content ([Figures 2C](#) and [S2](#)). In addition, flow cytometry revealed the same doubling in DNA content in a separate strain housing a tRNA neochromosome that had not undergone spheroplast transformation ([Figure S2](#)). Spontaneous alterations of cell ploidy in yeast have been associated with a stress response.<sup>40</sup> Therefore, we hypothesized that the increase in cell ploidy was a compensatory response to the presence of the tRNA neochromosome in wild-type haploid cells.

Given the apparent selective force manifesting as an increase cell ploidy, we later elected to maintain the tRNA neochromosome in the *MATa/a* genome-duplicated BY4741 background (YCy2508) for all subsequent functional studies. This rationale was supported by time course experiments performed in independent, tRNA neochromosome-transplanted haploid strains (BY4741 and BY4742), which revealed an apparent increase in tRNA neochromosome stability in the diploid background. Following haploid validation via flow cytometry ([Figure S3](#)), an increased number of internal deletions were observed in independent, freshly transformed haploid strains (BY4741 [YCy2837], BY4742 [YCy2838]), compared with that of the *MATa/a* diploid (YCy2508) and *MATa/ $\alpha$*  diploid (YCy2844) strains. After ~50 generations, deletions were detected in 2

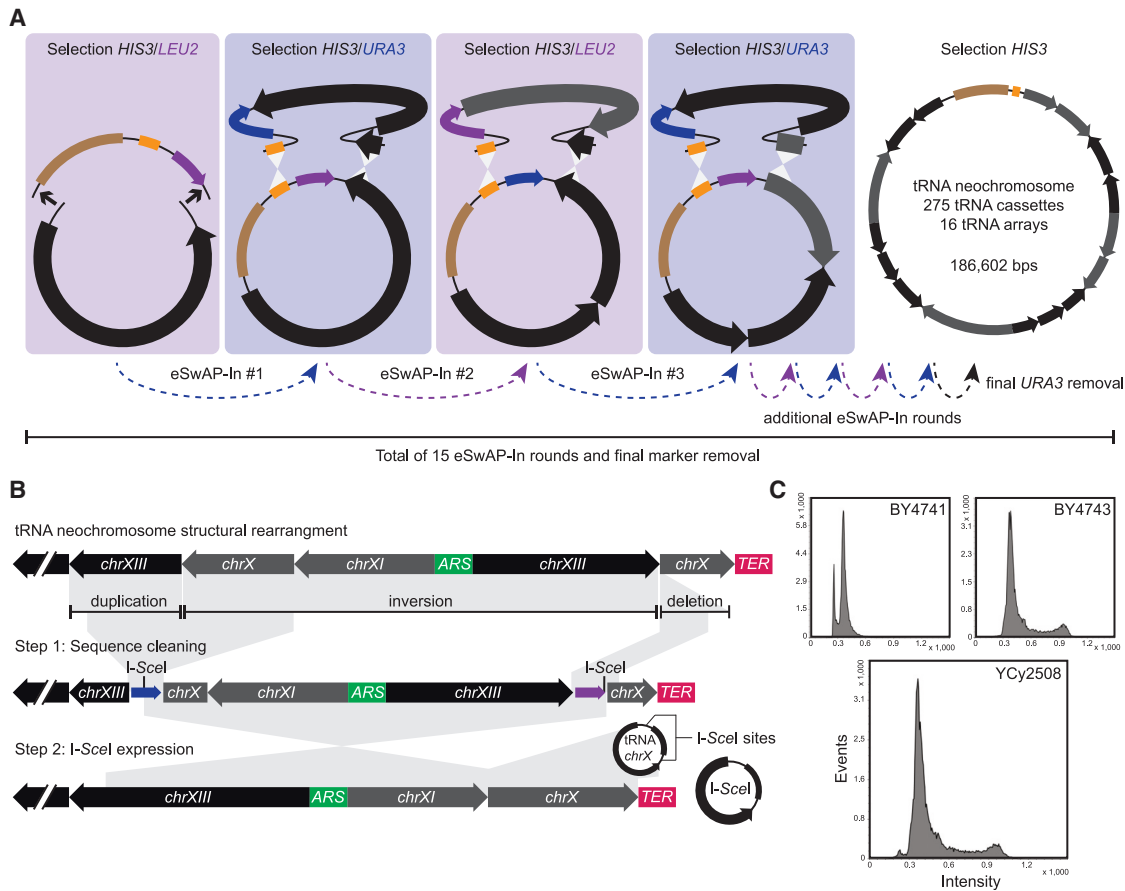


### Figure 2. Construction, debugging, and discovery of a whole-genome duplication

(A) tRNA neochromosome construction was performed in a stepwise manner through repeated rounds of *in vivo* homologous recombination in yeast. The brown bar denotes the pRS413 region of the eSwAP-In vector, and black and gray arrows denote tRNA arrays. *In vivo* homologous recombination is facilitated by two homology arms incorporating the last 350- to 680-bp sequence from the previous array and the 500-bp universal homologous region (UHR; shown in orange). Selection is conferred by the recursive swapping of *LEU2* and *URA3* markers.

(B) Following tRNA neochromosome construction, a complex structural rearrangement was observed consisting of a duplication, inversion, and deletion. This was then repaired using a strategy employing the rare-cutting I-SceI enzyme (see details in STAR Methods).

(C) An unexpected whole-genome duplication was observed; the *MATa/a* genotype that was verified by flow cytometry, diagnostic PCRs (Figure S2), and mating-type tests (data not shown).

See also Figures S1 and S2.

out of 8 diploid isolates, compared with 7 out of 8 haploid isolates (Figure S3).

### Linearization and sequencing of tRNA neochromosome strains reveals extensive genomic plasticity

To probe the effect of linearizing the tRNA neochromosome at different locations, a total of nine locations were selected (generating strains YCy2670 to YCy2678). Four were linearized at *TER* sites, two close to the centromere, and three at origins of replications (*ARS1* to *ARSIII*) (Figure 3A). Successful linearization and tRNA neochromosome size were verified via PFGE analysis. With the exception of one mitochondrially deficient  $\rho^-$  mutant (YCy2677), we observed no significant growth difference between isolates housing either circular or linearized variants (Figures 3B and S4). Notably, except for potential aneuploidies and sequence variations in several independent strains linear-

ized at non-*TER* positions (Figure S5), disruption of the replication profile of the tRNA neochromosome through linearization at origins of replication produced no significant impact on cell phenotype, compared with *TER* sites (*TERI-TERIV*) under 22 growth conditions (Figure S4). Overall, our results suggest that there is no significant difference in cell growth rate between linear or circular tRNA neochromosome variants and that the location chosen for linearization has no major impact on cell growth.

### tRNA-seq to characterize tRNA neochromosome expression

To examine whether tRNA genes on the tRNA neochromosome are transcribed when removed from their native genomic context, we performed tRNA sequencing (tRNA-seq). Because of extensive tRNA secondary and tertiary structures, combined

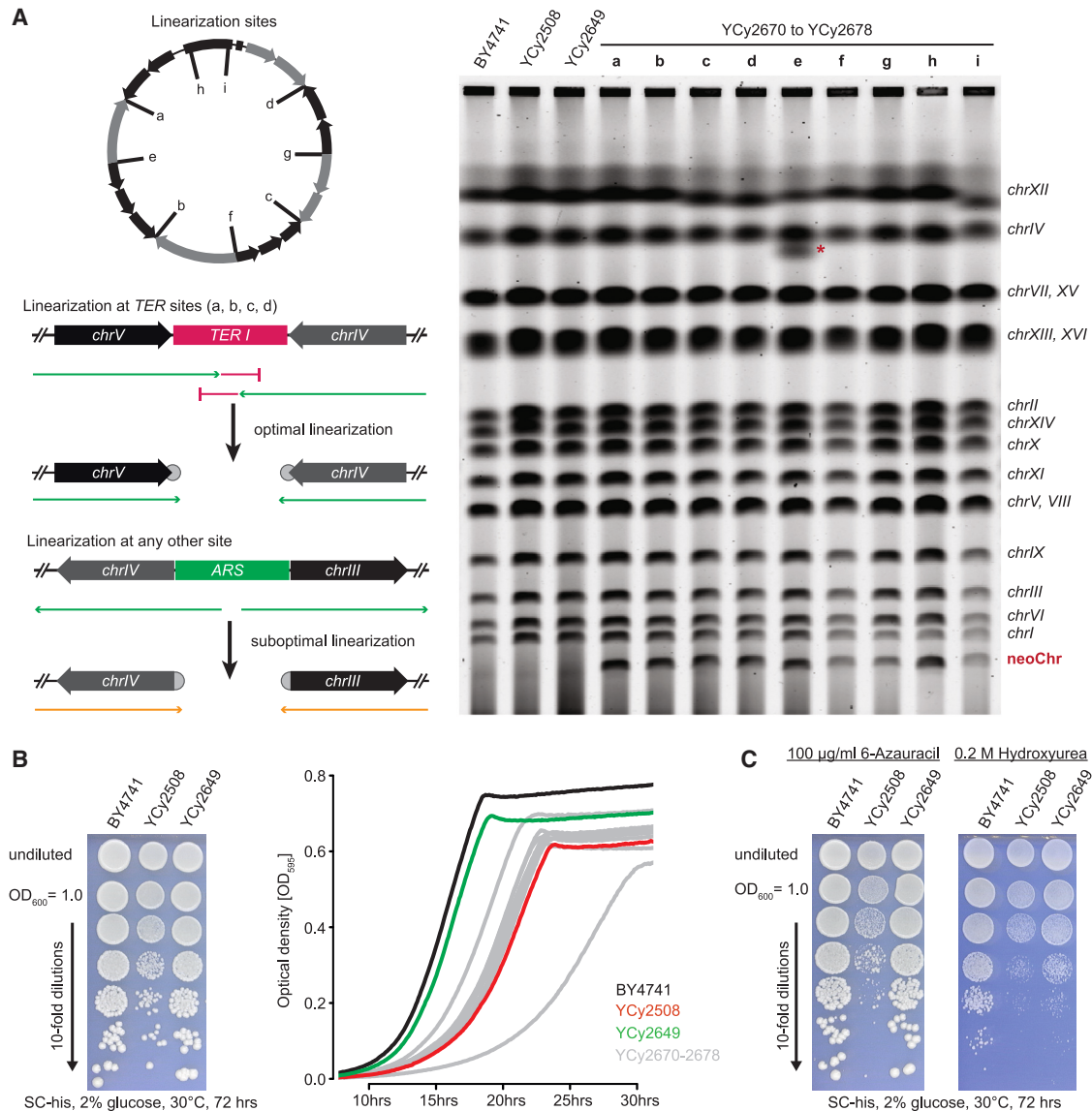


**Figure 3. Linearization and phenotypic characterization of the tRNA neochromosome**

(A) Left: indicates linearization at sites predicted to be optimal for the proper alignment of DNA replication and *RNAPIII* transcription (i.e., at *TER* sites) or sub-optimal for tRNA neochromosome linearization (i.e., at origins of replication). DNA replication aligned with transcription is indicated by green arrows, DNA-replication blocking by red, and colliding DNA replication and transcription by orange arrows. Right: pulsed-field gel electrophoresis (PFGE) of tRNA neochromosome strains and respective controls. Columns “a” to “i” (top) each represent the different linearization locations, as shown on the left panel, and were performed in YCy2508. YCy2649 has lost the tRNA neochromosome. The circular tRNA neochromosome (YCy2508) cannot be visualized by PFGE analysis because of topological trapping in agarose fibers. However, the linearized versions (YCy2670 to YCy2678) show a band on the expected height (indicated by neoChr). All chromosome bands are as expected, except for strain YCy2674 where a fraction of *chrXII* (red asterisk) shows a partial loss of the rDNA repeat (supported by NGS data, data not shown).

(B) Phenotypic growth assays indicate that the tRNA neochromosome strains have a growth defect that is recovered upon loss of the tRNA neochromosome. The growth differences between circular and linear strains are marginal (except for one strain that was later found to have partial loss of mitochondrial DNA).

(C) The tRNA neochromosome strains were benchmarked under 22 separate media conditions (cf. Figure S4) and compared with BY4741 + pRS413 and YCy2649. Only in the presence of 6-azauracil or 0.2 M hydroxyurea, the phenotype becomes more severe, indicating transcriptional and DNA-replication stress, respectively. See also Figure S4.

with the indistinguishability of individual locus expression of multi-gene tRNA species after tRNA processing, traditional RNA sequencing (RNA-seq) approaches are limited in terms of unbiased and global tRNA characterization. To overcome these chal-

lenges, we implemented a dedicated workflow and developed sensitive computational approaches for transcript-level quantification to distinguish closely related tRNA species (Figure 4A). We performed tRNA-seq on four strains with three biological

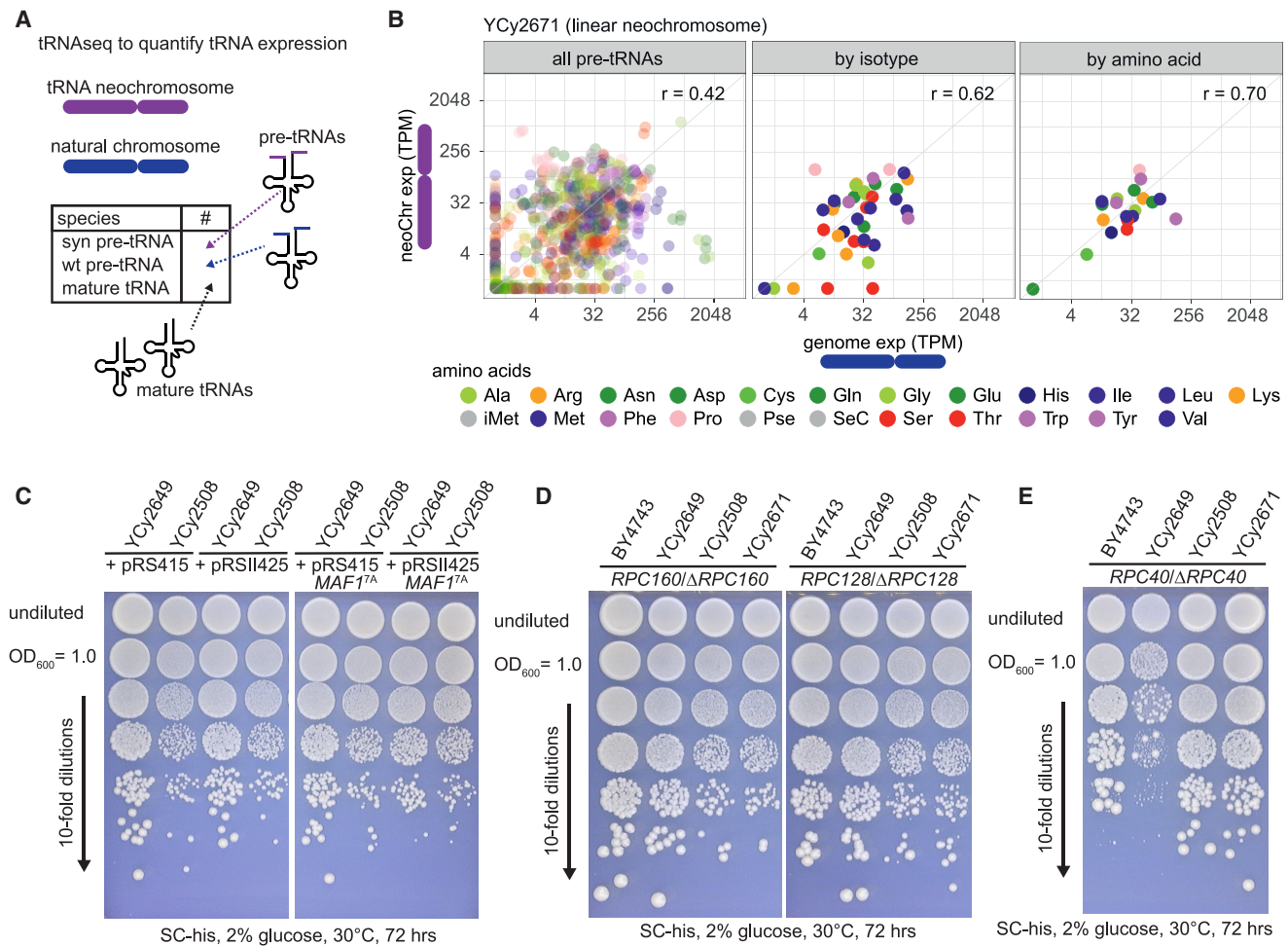


**Figure 4. tRNA expression analysis and phenotypic impact of RNAPIII activity reduction**

(A) tRNA-seq enables differentiation between the different tRNA loci based on the fraction of pre-tRNAs. Leading, tailing, and intron sequences allow for a clear separation of transcript origin.

(B) tRNA-seq data show that the expression levels of individual synthetic and native tRNA genes vary, sometimes dramatically. However, sorting tRNA expression by isotype or by amino acid indicates that overall expression levels appear to be relatively well balanced whether the source gene is native or synthetic.

(C) Overexpressing the constitutively active MAF1<sup>7A</sup> allele rescues the observed phenotype in the tRNA neochromosome strain. However, the growth of the control strain is reduced and almost matches the growth defect of the tRNA neochromosome strain when transformed with a high-copy plasmid (pRSII425) overexpressing MAF1<sup>7A</sup>. Interestingly, the growth of the tRNA neochromosome strain is not further reduced, potentially indicating that Maf1 is fully active in this strain to compensate for the consequences of tRNA overabundance.

(D) Reducing RNAPIII activity by deleting single-subunit alleles in the homodiploid did not show strong effects on growth recovery, neither in the circular nor in a linear tRNA neochromosome strain. *RPC160* and *RPC128* are shown as examples in comparison to the homodiploid control.

(E) *RPC40*, in contrast, produced a recovery in growth phenotype for both the circular and linear tRNA neochromosome strains. The control strain (BY4743 + pRS413) shows two types of colony sizes. Sequencing of two big and two small clones by Nanopore sequencing revealed that the small clones have a low abundance of mitochondrial DNA in comparison to the large clones (data not shown).

See also Figures S6 and S7 and Data S2 and S3.

replicates each, including the haploid and homozygous diploid controls (YCy2409 and YCy2649) and the circular (YCy2508) and a linear tRNA neochromosome strain (YCy2671). Leveraging leading and tailing pre-tRNAs sequences, we were able to identify the genomic origin of synthetic and wild-type tRNAs and to estimate their fractional expression (Figures 4A and 4B; Data S2).

Our analysis of pre-tRNAs revealed a similar expression pattern between the detected pre-tRNA abundances from the tRNA neochromosome and the genome aggregated by the 20 amino acids or 42 isoacceptor types, although individual tDNA

expression was not so well correlated (Figure 4B). Furthermore, our results revealed no significant alteration of tRNA expression caused by the removal of introns (Figure S6). We later validated our approach by implementing the multiplex small RNA sequencing (MSR-seq) method<sup>41</sup> that is especially well suited for the sequencing of mature and precursor tRNAs. Overall, our results were broadly similar with regard to the abundance of global pre-tRNAs (Figure S6; Data S3), with a more closely aligned correlation between synthetic and wild-type pre-tRNAs at the individual transcript level, based on upstream



reads ( $r^2 = 0.89\text{--}0.92$ ) and a less closely aligned correlation downstream ( $r^2 = 0.55\text{--}0.69$ ).

Northern blot analysis previously indicated a potential 5' tRNA maturation deficiency for the single-copy synthetic tRNA<sub>Ser</sub><sup>CGA</sup> (synSUP61).<sup>24</sup> Notably, we observed no difference in precursor tRNA levels for tRNA<sub>Ser</sub><sup>CGA</sup> for MSR-seq, which would presumably have manifested as an increase in read counts of the synthetic precursor form. Although some individual tRNAs may have altered precursor levels, on a global level we could not observe any evidence for a greatly increased accumulation of pre-tRNAs (Figure S6), which would presumably provide evidence for systematic tRNA maturation deficiencies on tRNA genes encoded by the tRNA neochromosome.

### Phenotypic characterization of the tRNA neochromosome

We observed a growth impact in homozygous diploid cells housing both linearized and circular variants of the tRNA neochromosome (YCy2670 to YCy2678), with an extended lag phase and an increase in doubling time of 19.2% ( $92.3 \pm 2.7$  min vs.  $110.0 \pm 2.6$  min; a rho<sup>-</sup> mutant was excluded from this calculation), compared with haploid and homozygous wild-type cells (Figure 3B). To confirm that the tRNA neochromosome is the cause of the growth defect, we selected for its spontaneous loss on non-selective media. The resulting isolate (YCy2649) reverted to a near-normal phenotype (Figure 3B), demonstrating that the tRNA neochromosome itself was responsible.

To further assess the potential cause of the phenotype, we subjected strains housing circular and linear versions of the tRNA neochromosome to a total of 22 solid media growth conditions (Figure S4). We observed a relative growth defect compared with the control under all conditions, with a more significant defect in the presence of 6-azauracil and hydroxyurea, indicating transcriptional elongation stress and replication stress, respectively (Figures 3C and S4). The latter phenotype on hydroxyurea also revealed a similar growth defect on the *MATa/a* diploid control strain (absent of the tRNA neochromosome), suggesting a potential phenotype caused by a change in the host genome or through whole-genome duplication. Notably, a similar effect for hydroxyurea was observed for growth phenotypes of a yeast strain possessing a *synVII* aneuploidy.<sup>42</sup> We observed no difference between the circular and linear variations of the tRNA neochromosome (Figure S4).

Given the relative doubling in the number of cellular tRNA genes, we set out to explore if reducing tRNA transcription might alleviate the observed cellular burden. RNAPIII is negatively regulated in a global manner by Maf1.<sup>43</sup> To increase gene copy number, two additional *MAF1* variants were introduced onto a high-copy (2-micron) plasmid under control of their natural promoter: the wild-type variant and a previously described constitutively active *MAF1*<sup>7A</sup> variant.<sup>44</sup> Both were introduced into YCy2649 and YCy2508. Furthermore, a second series of experiments investigated a reduction in RNAPIII abundance by individually deleting one copy of all 10 essential RNAPIII-specific subunits<sup>45</sup> of the 17-protein core complex, resulting in 10 heterozygous *MATa/a* strains. Overall, our results show that neither *MAF1* variant nor the majority of RNAPIII deletions produced any significant phenotypic effect on strains housing the tRNA neochromosome (Figures 4C, 4D, and S7).

We further decided to generate heterozygous deletions of the two large subunits of RNAPI (*RPC128* and *RPC160*) and two shared RNAPI and RNAPIII subunits (*RPC19* and *RPC40*). Our results (Figure 4E) indicate that eliminating one copy of *RPC40* deletion produced an apparent recovery of growth for tRNA neochromosome strains (although large and small colony sizes for both control strains were notable, with Nanopore sequencing revealing a reduction in mitochondrial DNA for the smaller colonies; data not shown). No significant changes in phenotype were observed following a reduction in *RPC128*, *RPC160*, and *RPC19* abundance. Rpc40 is necessary for the assembly of RNAPI and RNAPIII (but not RNAPII). Moreover, Rpc40 is necessary for retrotransposon insertion specificity.<sup>46–48</sup> Taken together, our results suggest that increased abundance of tRNA genes may at least be partially responsible for the observed phenotype. The combined reduction of both RNAPI and RNAPIII abundance may be beneficial to recover the growth phenotype.

### Transcriptome and proteome analysis of tRNA neochromosome strains

RNA-seq was performed on the circular and seven linear tRNA neochromosome variants, as well as the haploid and homozygous diploid control strains (Figures 5A and S8), respectively. Our results show a general upregulation of amino acid biosynthesis-related transcripts and a downregulation of ribosomal protein transcripts for all strains housing the tRNA neochromosome (Figure 5A). Proteomics was performed on the circular (YCy2508) and nine linear tRNA neochromosome variants (YCy2670–2676) (Figures 5B and S8), as well as the haploid (BY4741), homozygous diploid (YCy2649), and diploid (BY4743) control strain, revealing no significant changes at the individual protein level. However, at the collective level, we observed an increase in membrane-associated proteins and proteins associated with the endoplasmic reticulum and a reduction in proteins associated with the ribosome (Figure 5B), the latter of which correlating well with our transcriptomic data. Overall, neither transcriptome nor proteome analysis indicates a strong differential regulation of the DNA damage response.

### Nucleosome mapping

We subsequently investigated whether the clustering of tDNAs on the tRNA neochromosome might affect the general organization of its chromatin structure. Nucleosome occupancy maps were generated to investigate any potential for aberrant chromatin structure, such as mispositioning or nucleosome absence. Our results show that nucleosome positioning for genomic tRNAs is similar in all strains tested (Figure 6A). Notably, with the exception of a slight apparent variance in linker length, nucleosome positioning on both tRNA neochromosome variants is similar to that of genomic tRNAs, suggesting a relatively normal chromatin structure. Our data suggest that the typical 20-bp linker between two nucleosomes is reduced in the tRNA neochromosome variants, presumably due to the tight clustering of tDNAs. Our observations suggest that active transcription of tRNA genes may contribute to upstream and downstream nucleosome positioning. Aside from the high density of neochromosome tDNAs and an apparent difference in linker length,

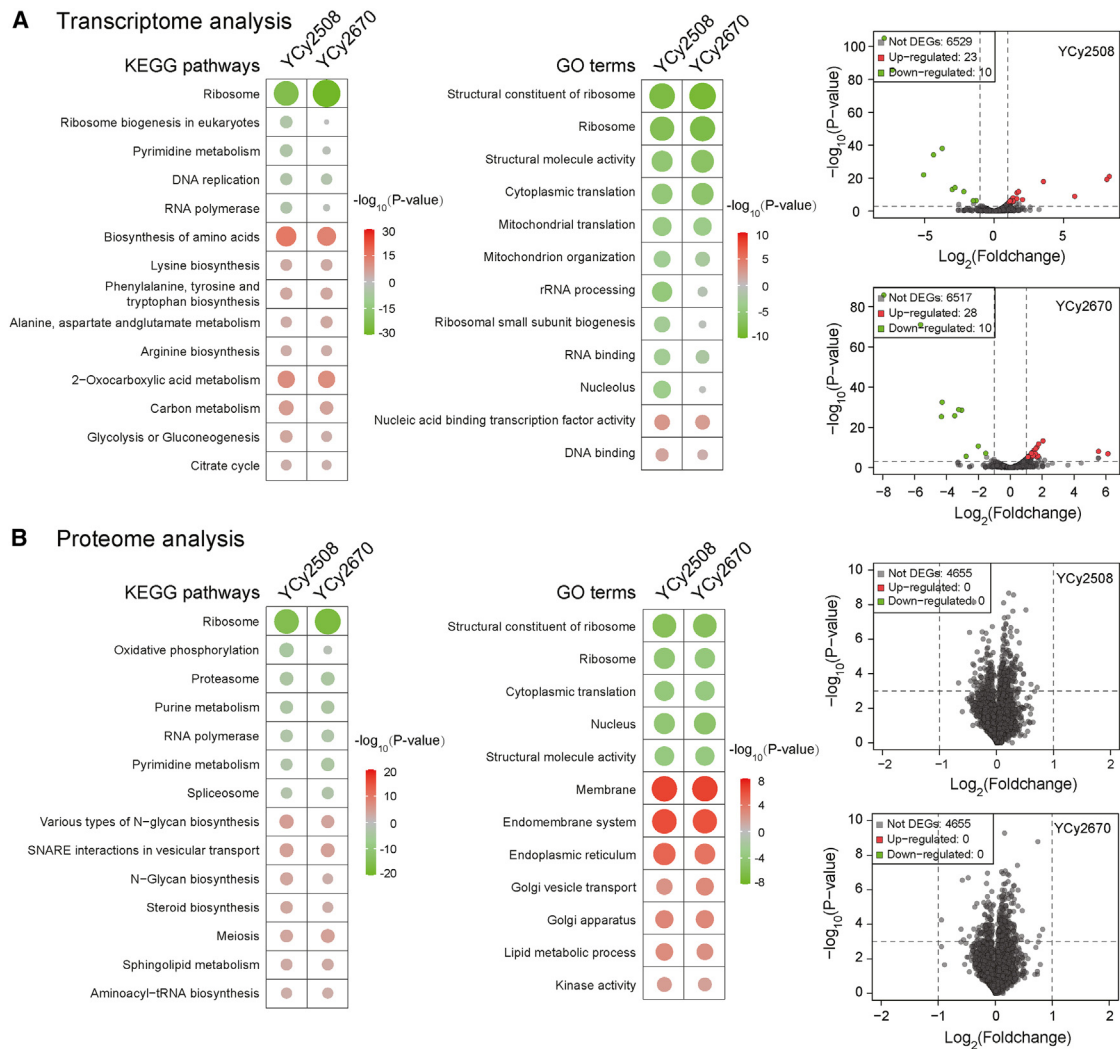


**Figure 5. Transcriptome and proteome analyses indicate an upregulation of amino acid biosynthesis and a general downregulation of ribosomal proteins**

(A) Differential expression of circular (YCy2508) and linear (YCy2670) tRNA neochromosome strains normalized to the homozygous diploid control strain (YCy2649). KEGG (left) and GO (right) analysis demonstrate a general upregulation of amino acid biosynthesis and a downregulation of translational processes. The volcano plots indicate that 33 and 38 individual mRNA transcripts associated with the latter are upregulated or downregulated, respectively. Upregulated and downregulated features are labeled in red and green, respectively, with both color intensity and circle sizes indicating significance level.

(B) Proteomic analysis of the circular and linear tRNA neochromosome strains (YCy2508 and YCy2670), respectively, normalized to the homozygous diploid control strain (YCy2649). KEGG and GO analysis globally show a similar pattern to that of transcriptomics. However, an additional increase in membrane-associated proteins and endoplasmic reticulum can be observed. Upregulated and downregulated features are labeled in red and green, respectively, with both color intensity and circle sizes indicating significance level.

See also [Figure S8](#) and [Data S5](#) and [S6](#).

nucleosome positioning adopts a rather orthodox pattern and is nearly indistinguishable from native positioning.

### Deep sequencing to determine the tRNA neochromosome replication profile

The tRNA neochromosome houses four origins of replication and four bidirectional *TER* sites. To explore how the tRNA neochromosome replicates, we performed deep sequencing of replicating cells normalized to the sequencing reads of non-replicating cells in both a circular (YCy2508) and a linear (YCy2671)

tRNA neochromosome variant ([Figure S5](#)). Our results show maxima of sequencing coverage co-localizing with each origin of replication and minima associated with the designed bidirectional *TER* sites ([Figure 6B](#)). Within the analysis it was observed that the tRNA neochromosome tends to have lower sequencing coverage, compared with the native chromosomes. To further investigate this observation, cells were normalized to G1 ( $\alpha$  factor arrest) ([Figures 6C](#) and [S5](#)). Interestingly, the tRNA neochromosome displayed an approximate abundance of 0.8, relative to the other chromosomes in G1 phase, but equal abundance in

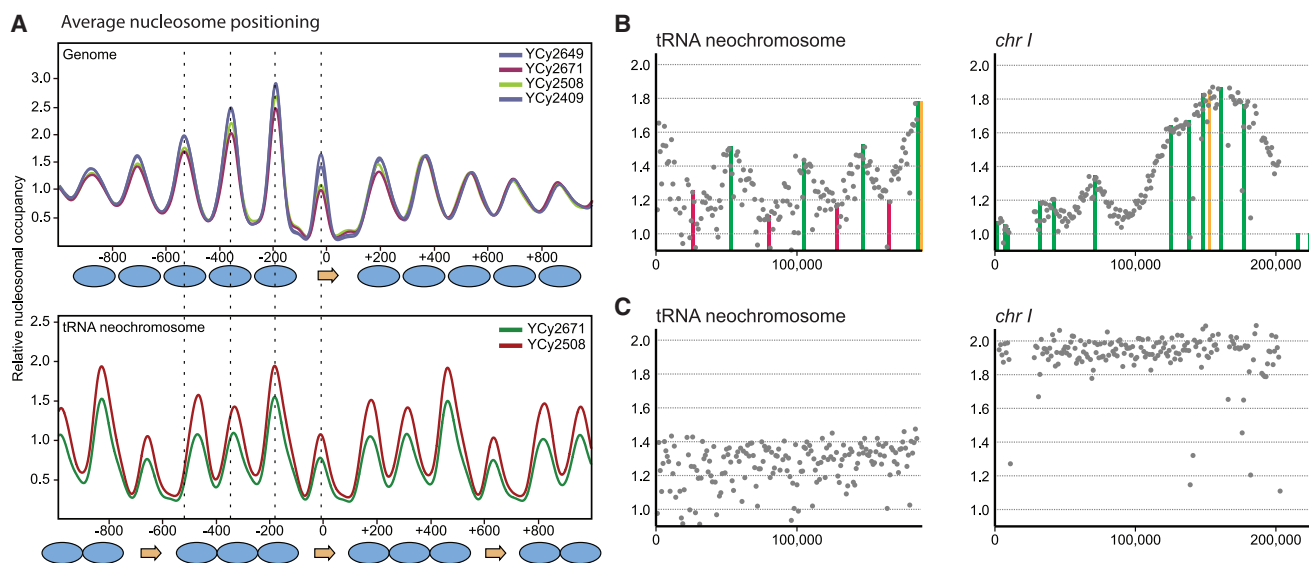


**Figure 6. Nucleosome positioning and replication pattern of the tRNA neochromosome**

(A) Averaged nucleosome positioning around tRNA genes on the native chromosomes are indistinguishable within all tested strains (top). The tRNA neochromosome nucleosome positioning is similar (bottom). However, based on the high density and the distance between two tRNA genes, the nucleosomes appear more compacted, as indicated by the dotted lines aligned to the dyad position of the three nucleosomes upstream of the tRNA in the genome (top).

(B) Replication pattern analysis indicates the functionality of origins of replication (green lines) and their time point of activation within the cell cycle for the circular tRNA neochromosome. Peaks correspond to initiation events, and valleys correspond to termination of DNA replication. In the case of the tRNA neochromosome, all origins from *C. glabrata* show apparent initiation events and associated valleys corresponding to termination sites (red lines). The position of the centromere is visualized by an orange line.

(C) Marker frequency analysis of cells synchronized to G1 shows a lower abundance of the tRNA neochromosome, compared with the native chromosomes. Synchronization at the end of S phase revealed a similar relative abundance between the tRNA neochromosome and native complement.

See also Figure S5.

G2, suggesting a heterogeneity in tRNA neochromosome copy number or partial tRNA neochromosome loss within the cell population. These data suggest that the tRNA neochromosome has the same abundance as the native chromosomes before cell division, but potentially aberrant segregation leads to the observed G1 effect, which we speculate may be one potential cause of the observed reduced growth rate.

### Intranuclear localization of the tRNA neochromosome

Evidence suggests that tDNAs influence the overall organization of the genome in the nuclear space.<sup>49–51</sup> Recently, the investigation of a yeast strain devoid of tRNA genes on *chrIII* and other synthetic chromosomes showed an impact on centromere clustering, but no significant influence on the large-scale architecture of the genome.<sup>52,53</sup> Given the designer structure of the tRNA neochromosome, we explored its position within the nuclear space and whether it modifies the global genome architecture using a combination of fluorescence *in situ* hybridization (FISH) and capture of chromosome conformation (Hi-C).

FISH experiments were performed using separate probes for *rox* recombination sites and rDNA repeats (5' Cy3 and 5' FAM, respectively) to identify the position of the tRNA neochromosome in the nuclear space. Our results show that the tRNA neochromosome does not co-localize with the rDNA signal in most cells of the homozygous diploid strain (YCy2508), with approximately half of the cells showing a clear separation of the two regions (Figure 7A). We validated the FISH results using live-cell

imaging (Figure 7B). A transcription activator-like effector construct (TAL-GFP) was designed to target *rox* sites and the nucleolus marked with Nop10-mCherry. We observed foci in cells housing the tRNA neochromosome, again with no significant co-localization of the *rox* signals and the nucleolus (Figures 7A and 7B). Overall, FISH and co-localization studies demonstrate no obvious co-localization of the tRNA neochromosome with the nucleolus.

We performed Hi-C of circular (YCy2508) and linear tRNA neochromosome variants (YCy2670–YCy2672). Furthermore, Hi-C is a convenient approach to investigate structural genomic rearrangements in genomes.<sup>54</sup> Here, the contact maps of both variants displayed a smooth pattern, with no evidence of unwanted structural rearrangement, further validating tRNA neochromosome integrity (Figure 7D). In addition, no obvious difference was observed between the circular and linear variants (data not shown). Intrachromosomal contacts were slightly enriched, compared with native wild-type yeast chromosomes. The greater intrinsic contacts observed within the tRNA neochromosome itself could correspond to a higher RNAPIII protein occupancy and transcription levels.<sup>55</sup> In addition, the contact maps show that the tRNA neochromosome centromere is enriched in contacts with the native centromeres (Figures 7C and 7F). The 3D representation of the 2D contact maps using Shrek3D<sup>56</sup> was reminiscent of those obtained for diploid wild type (BY4743). The plot of the contact frequency as a function of the genomic distance computed over the entire genome (p(s)

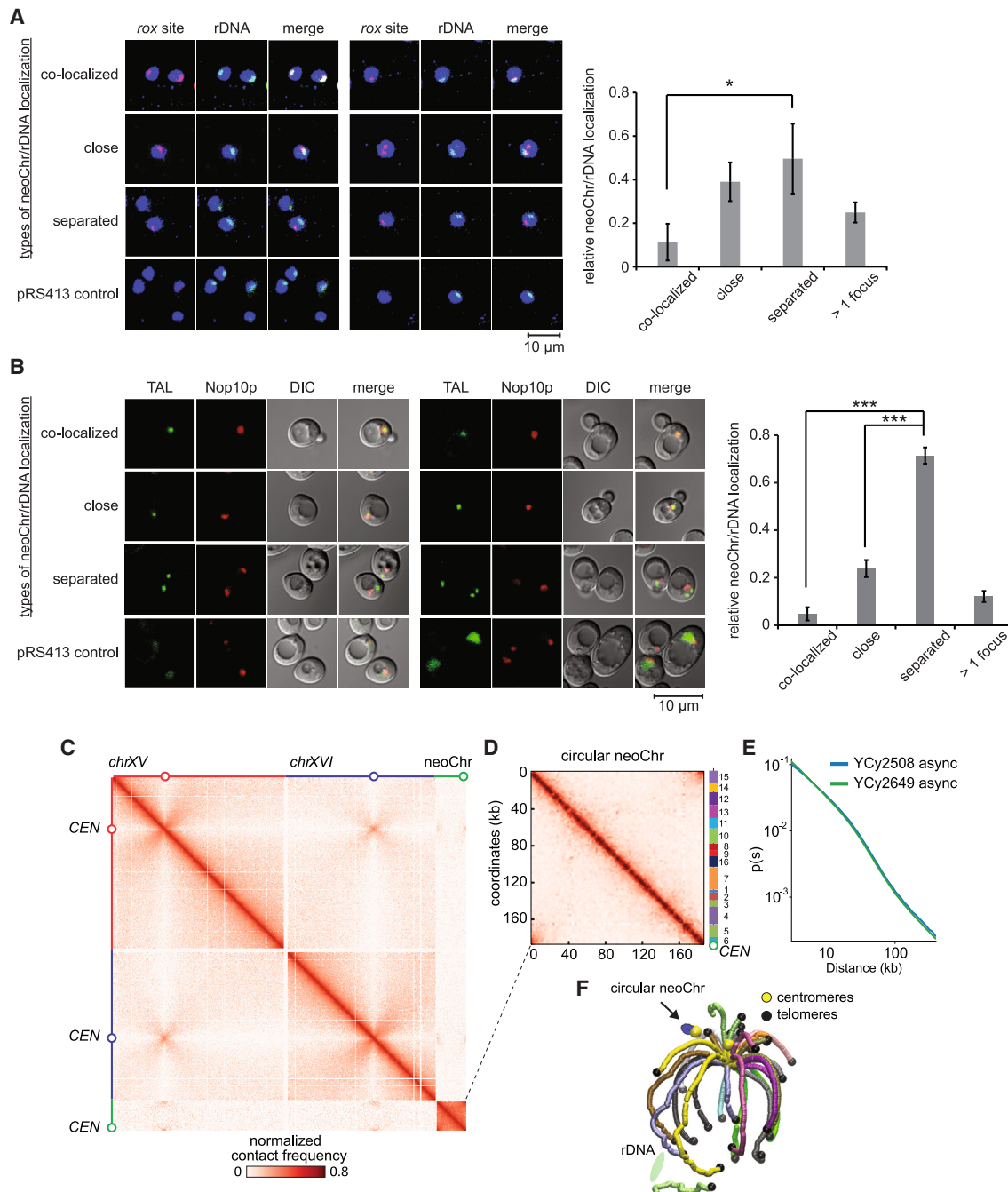


**Figure 7. Intracellular localization of the tRNA neochromosome**

(A, B, and F) The tRNA neochromosome shows no obvious co-localization with the nucleolus.

(A) The left panel displays representative FISH results, visualizing the observed modes of tRNA neochromosome localization (red) relative to the rDNA locus (green) in strain YCy2508. The bottom panel on the left represents a pRS413 control absent of *rox* localization. Percentage of the different localization modes are given in the histogram on the right (three strains  $n \geq 100$ , respectively). Error bars indicate the standard deviation of the three strains analyzed.  $^*0.01 < p < 0.05$ .

(B) Imaging results of live cells (JSY396 and JSY397). TAL: *rox*-probe-GFP, Nop10p:mCherry. The percentage of the different localization modes are given in the histogram (three clones  $n \geq 250$ , respectively). Error bars indicate the standard deviation of the three clones analyzed.  $^{***}p < 0.0001$ .

(C) Magnification of the genome-wide contact map of the circular tRNA neochromosome strain. The x and y axes represent chromosomes XV, XVI, and the tRNA neochromosome, respectively. The color scale reflects the frequency of contacts between two regions of the genome (arbitrary units [a.u.]) from white (rare contacts) to dark red (frequent contacts).

(D) Separate visualization of the circular tRNA neochromosome (YCy2508) showing the expected circularization signal at the edges of the contact map. No rearrangement is present.

(legend continued on next page)

curve; STAR Methods) was also conserved between the genomes of the tRNA neochromosome strain and a wild-type diploid strain, suggesting that the presence of the tRNA neochromosome has no direct impact on the average conformation of the native genome (Figure 7E).

## DISCUSSION

We have described here the design, construction, and characterization of a tRNA neochromosome, a fully synthetic designer chromosome that exists as an additional copy to the 16 native chromosomes of *S. cerevisiae*. The design of the tRNA neochromosome was custom for the purposes of the Sc2.0 project and represents a synthetic yeast chromosome designed without a natural template.

We observed a remarkable plasticity of both the tRNA neochromosome and the host genome, following construction. We speculate that the spontaneous increase in cell ploidy is a compensatory response to a cellular burden caused by a relative doubling in tRNA genes and consequent tRNA overabundance in a wild-type cell. The total RNA mass within a yeast cell consists to 80%–90% of rRNAs, 10%–15% of tRNAs, 3%–7% of mRNAs, and a small fraction of other RNAs (i.e., snRNAs, lncRNAs, etc.). However, if RNA mass is transferred to the actual number of molecules, tRNAs are the most abundant RNAs, exceeding the number of ribosomes 10-fold.<sup>29</sup> The high numerical abundance of tRNA molecules strengthens our hypothesis that the doubling of 275 highly transcribed tRNA genes results in a cellular burden, leading to a compensatory ploidy increase. Furthermore, recent work suggests that increases in ploidy in *S. cerevisiae* is a relatively common phenomenon, especially under conditions of stress.<sup>40,57</sup> We postulate that haploid cells are less amenable to compensate for this tDNA overabundance, potentially because of insufficient levels of aminoacyl-tRNA synthetases, with this conclusion supported by an apparent improvement in tRNA neochromosome stability in diploid cells. Despite our inconclusive results when attempting to downregulate tRNA expression through a constitutively active *MAF1*, our observations following transcriptomic and proteomic characterization further lend credence to the hypothesis that a relative doubling in the number of tRNA genes in haploids leads to an overabundance of uncharged tRNAs and thus a dysregulation of the translational machinery. This hypothesis extended to the conserved protein Gcn2, which is activated in response to uncharged tRNAs as a result of amino acid starvation. Gcn2 consequently phosphorylates the initiation factor eIF2- $\alpha$ , leading to the repression of protein synthesis.<sup>58</sup> However, we were unable to observe any significant increase in phosphorylation levels of eIF2- $\alpha$  (Figure S7) or in expression levels of the associated response gene, *GCN4*, from our transcriptomic data. Although we are unclear of the causes of the underlying phenotype, one possibility is that tRNA molecules are charged as normal, and the cellular response is independent of this pathway. For example, potential causes of the phenotype may be related to the effects of

amino acid sequestration or translational stalling. Future experiments into tRNA charging may shed light on this phenomenon.

Secondary observed phenomena include structural variations of the tRNA neochromosome and its unstable nature. Given the highly transcribed nature of tRNA genes, a general instability of the tRNA neochromosome is not unexpected. We postulate that the complex structural variations may be related to its circular intermediary structure, due to the known instability of ring chromosomes in higher eukaryotes,<sup>59</sup> and potential for complex variations (including duplications, deletions, or inversions) caused by dicentric or catenane formation.<sup>60,61</sup> Furthermore, its logical to assume that a general selection pressure exists in haploid cells against an intact tRNA neochromosome structure, ultimately leading to a reduction in its overall size.

Although the tRNA neochromosome conferred an expected cellular burden, we have not been able to pinpoint a singular cause, suggesting that the origin of this burden may be multifactorial. Aside from an overabundance of tRNA genes, we observed a different abundance in tRNA neochromosome read coverage during different stages of the cell cycle following replication profiling. One possible factor for this observed effect could be impaired chromosome segregation during mitosis leading to an unequal tRNA neochromosome exchange. We speculate this may be caused by an absence of convergent gene boundaries adjacent to the centromere, which are otherwise responsible for the trapping of cohesion.<sup>62</sup> Ultimately, elucidation and characterization attempts will greatly benefit once the tRNA neochromosome is introduced into the final synthetic yeast genome as part of Sc2.0, absent of its native tRNA copies.

tRNA-seq analysis demonstrates that the bulk of the tRNA genes of the tRNA neochromosome are expressed in a manner comparable to their wild-type counterparts. Overall, we did not observe a doubling in the total cellular tRNA pool, which suggests a buffering mechanism potentially caused by competition for RNAPIII. In contrast to the human genome where up to 50% of tRNA genes are reportedly silent,<sup>63,64</sup> MSR-seq shows expression for all tRNA genes, although with varying levels for the circular tRNA neochromosome (~250-fold) and the linear variant (~1,000-fold) in rich media, consistent with the known variability of tRNA expression within other genomes.<sup>64</sup> Although we previously identified a potential tRNA<sub>Ser</sub><sup>CGA</sup> maturation deficiency,<sup>24</sup> our global tRNA-seq analysis could not pinpoint accumulation of its precursor form and thus could not identify evidence of any global processing defects. It is possible that the structure of the 5' and 3' leader and trailer sequences influence the processing efficiency of RNase P: previous work has shown that complementary pairing between the 5' and 3' sequences affects RNase P cleavage and that these sequences may need to be separated for substrate recognition.<sup>65</sup>

As a designer biological structure, the tRNA neochromosome provides opportunities to study how such entities function within the cell. Replication profiling provided evidence of replication fork firing with associated troughs located near *TER* sites.

(E) Plot of the contact probability  $p$  as a function of genomic distance  $s$  (log scale) for the contact maps of either the tRNA neochromosome strain (YCy2508) or a strain (YCy2649), during exponential growth.

(F) 3D representation of the contact map showing the clustering of the tRNA neochromosome (blue chromosome) in the vicinity of the centromere cluster and distal to the rDNA locus.

Interestingly, nucleosome mapping data demonstrate that tRNA expression may contribute to the positioning of the nucleosomes. Nucleosome positioning differs slightly, compared with that found in the genome, with a shorter linker between individual nucleosomes presumably caused by a higher overall density and shorter distances between tDNAs than are observed in the native genome. Furthermore, FISH and Hi-C provide conclusive evidence that the tRNA neochromosome does not co-localize with the nucleolus, supporting the tethering hypothesis proposed recently.<sup>66</sup> Finally, we expect that the Dre-rox recombination system will be a powerful future system to address questions of tRNA genetics in a systematic manner, especially once the fully synthetic Sc2.0 strain is available.

Overall, this study has shown the remarkable tolerance of baker's yeast to support the presence of an additional neochromosome housing 275 tRNA genes. Looking beyond the Sc2.0 project, this work demonstrates the application of these designer structures and the benefits of radically re-engineering the host cell machinery. Future designer neochromosomes will provide a means to address fundamental questions of biology through the refactoring of genetic components in a systematic manner,<sup>67</sup> introduce characteristics into designer industrial strains,<sup>68</sup> provide a chassis to incorporate large-scale metabolic pathways, and provide the means to further understand aspects of chromosome biology through a “build to understand” approach. Given rapid technological advances and reduced costs of DNA synthesis, we anticipate the routine construction of custom neochromosomes, leading to tangible applications in the near future.

### Limitations of the study

Our study explored the design, construction, and functional characterization of a tRNA neochromosome in yeast. However, as this chromosome was constructed in a wild-type cell, further work is required to determine if and how these “synthetic” tRNA genes will complement the loss of all 275 wild-type tRNA genes once the final Sc2.0 strain is complete. This limitation extends to the systematic loss of tRNA introns; more recent evidence suggests that some tRNA introns may indeed have a physiological role,<sup>23</sup> and so future variants will likely benefit from their presence. We acknowledge that future experimental analysis is required to investigate whether tRNA modifications are altered in any way. Transplanting the tRNA neochromosome into a fully synthetic yeast background lacking all native tRNAs will allow a systematic study of this aspect. Also, further work is required to more fully investigate tRNA neochromosome segregation during mitosis or whether the tRNA flanking sequences influence tRNA expression. We introduced bidirectional *TER* sites into the tRNA neochromosome design. Although DNA-replication profiling displayed associated troughs adjacent to these regions, further work is required to definitively determine their function.

### CONSORTIA

This work is part of the international Synthetic Yeast Genome (Sc2.0) consortium. The chromosome design and building consortium includes research groups worldwide: Boeke Lab at Johns Hopkins University and New York University (led chromosomes I, III, IV, VI, VIII, and IX); Chandrasegaran lab at Johns

Hopkins (led chromosomes III and IX); Cai Lab at University of Edinburgh and University of Manchester (led chromosomes II and VII and tRNA neochromosome); Yue Shen's team at BGI-Research SHENZHEN (led chromosomes II, VII, and XIII); Y.J. Yuan's team at Tianjin University (led chromosomes V and X); Dai Lab at Tsinghua University and Shenzhen Institute of Advanced Technology, CAS (led chromosome XII); Ellis Lab at Imperial College London (led chromosome XI); Sakkie Pretorius and Ian Paulsen's team at Macquarie University (led chromosomes XIV and XVI); Matthew Wook Chang's team at National University of Singapore (led chromosome XV); Bader and Boeke Labs at Johns Hopkins University (led design and workflow); and Build-A-Genome undergraduate teams at Johns Hopkins University and Loyola University Maryland (contributed to chromosomes I, III, IV, VIII, and IX). The Sc2.0 consortium includes numerous other participants who are acknowledged on the project website, [www.syntheticyeast.org](http://www.syntheticyeast.org).

### STAR★METHODS

Detailed methods are provided in the online version of this paper and include the following:

- KEY RESOURCES TABLE
- RESOURCE AVAILABILITY
  - Lead contact
  - Materials availability
  - Data and code availability
- EXPERIMENTAL MODEL AND STUDY PARTICIPANT DETAILS
  - *S. cerevisiae* strains and growth conditions
  - Yeast transformation
- METHOD DETAILS
  - Automating flanking sequence assignment to tRNA genes
  - Manually curated design differences
  - Neochromosome design
  - Origins of replication and design of replication termination sites
  - Universal homologous region
  - Assembly of tRNA arrays
  - Neochromosome construction (eSwAP-In)
  - PCR Tags method and conditions
  - Repair of tRNA neochromosome structural variations
  - Whole genome sequencing
  - Chemical extraction and transfer of the tRNA neochromosome
  - Neochromosome linearization
  - Pulsed field gel electrophoresis (PFGE)
  - tRNA neochromosome stability assay
  - Nanopore sequencing
  - Tecan growth curve assay
  - Single-copy, essential, tRNA gene complementation
  - Dre recombinase-induced tRNA copy number adjustment: proof-of-concept
  - Ploidy determination by flow cytometry
  - Fluorescent in situ hybridization (FISH)
  - Live cell imaging

- RNA-seq analysis
- Proteome analysis
- Preparation of mononucleosomal DNA and generation of nucleosomal occupancy maps
- Hi-C analysis
- tRNAseq: RNA isolation, tRNA library preparation and sequencing
- MSR-Seq
- Western blot analysis
- Replication timing profiles

● **QUANTIFICATION AND STATISTICAL ANALYSIS**

**SUPPLEMENTAL INFORMATION**

Supplemental information can be found online at <https://doi.org/10.1016/j.cell.2023.10.015>.

**ACKNOWLEDGMENTS**

This work was supported by UK Biotechnology and Biological Sciences Research Council (BBSRC) grants BB/M005690/1, BB/P02114X/1, and BB/W014483/1; a Volkswagen Foundation “Life? Initiative” Grant (Ref. 94 771); an Engineering and Physical Sciences Research Council (EPSRC) Fellowship EP/V05967X/1; and a European Research Council (ERC) Consolidator Award EP/Y024753/1 to Y.C. D. Schindler is supported by the Max Planck Society in the framework of the MaxGENESYS project. R.S.K.W., at the University of Edinburgh, was supported by EPSRC studentship (1419736) and the Bill and Melinda Gates Foundation (OPP1140908) to Y.C. R.S.K.W., as part the *Yeast 2.0* initiative at Macquarie University, is financially supported by Bioplatforms Australia, the New South Wales (NSW) Chief Scientist and Engineer, and the Australian Research Council (ARC) Centre of Excellence in Synthetic Biology. N.P. is supported by NIH/R01GM113194 supplement. M.A. and T.P. are supported by NIH/NHGRI RM1HG012780. M.d.C.S.O. is supported by the International Max Planck Research School for Principles of Microbial Life: from molecules to cells, from cells to interactions. F.A. is supported by a grant from the Spanish Ministry of Science and Innovation (PID2020-118423GB-I00). C.A.N. acknowledges support from the Biotechnology and Biological Sciences Research Council (BBSRC), part of UK Research and Innovation, grant BB/N016858/1; Core Capability Grant BB/CCG1720/1; and the National Capability (BBS/E/T/000PR9814). J.D. is supported by a Royal Society Newton Advanced Fellowship (NAFR2\180590) hosted by Y.C. J.D.B. was supported by NSF grants MCB-1026068, MCB-1443299, MCB-1616111, and MCB-1921641. We thank Anita Dornes, Patricia Bedrunka, and Gert Bange for using their equipment and materials for western blot analysis.

**AUTHOR CONTRIBUTIONS**

Conceptualization, J.D.B. and Y.C.; coordination, J.D.B. and Y.C.; design and construction of the tRNA neochromosome, D. Schindler, R.S.K.W., Y.L., J.D.B., and Y.C.; design of experiments, D. Schindler, R.S.K.W., F.A., Y.S., C.A.N., R.K., J.D., L.M.S., J.D.B., and Y.C.; conducting experiments, D. Schindler, R.S.K.W., S.J., A.N.B., Y.W., C.A.M., C.C., A.G., D. Schraivogel, J.M., M.A., M.d.C.S.O., Y.Z., A.B., L.O., W.L., K.J., D.A., E.G.-R., T.W.T., and R.S.; data analysis, D. Schindler, R.S.K.W., A.N.B., Y.W., C.A.M., C.C., A.G., D. Schraivogel, J.M., N.P., J.C., B.A.B., T.W.T., T.E., T.P., F.A., Y.S., C.A.N., R.K., J.D., L.M.S., J.D.B., and Y.C.; writing – original draft, D. Schindler, R.S.K.W., and Y.C.; writing – review & editing, all authors.

**DECLARATION OF INTERESTS**

J.D.B. is a Founder and Director of CDI Labs, Inc.; a Founder of and consultant to Neochromosome, Inc.; a Founder, SAB member of, and consultant to ReOpen Diagnostics, LLC; and serves or served on the Scientific Advisory Board of the following: Logomix, Inc., Modern Meadow, Inc., Rome Therapeu-

tics, Inc., Sample6, Inc., Sangamo, Inc., Tessera Therapeutics, Inc., and the Wyss Institute.

Received: October 6, 2022

Revised: September 22, 2023

Accepted: October 12, 2023

Published: November 8, 2023

**REFERENCES**

1. Smith, H.O., Hutchison, C.A., 3rd, Pfannkoch, C., and Venter, J.C. (2003). Generating a synthetic genome by whole genome assembly: phiX174 bacteriophage from synthetic oligonucleotides. *Proc. Natl. Acad. Sci. USA* 100, 15440–15445. <https://doi.org/10.1073/pnas.2237126100>.
2. Cello, J., Paul, A.V., and Wimmer, E. (2002). Chemical synthesis of poliovirus cDNA: generation of infectious virus in the absence of natural template. *Science* 297, 1016–1018. <https://doi.org/10.1126/science.1072266>.
3. Gibson, D.G., Glass, J.I., Lartigue, C., Noskov, V.N., Chuang, R.Y., Algire, M.A., Benders, G.A., Montague, M.G., Ma, L., Moodie, M.M., et al. (2010). Creation of a bacterial cell controlled by a chemically synthesized genome. *Science* 329, 52–56. <https://doi.org/10.1126/science.1190719>.
4. Fredens, J., Wang, K., de la Torre, D., Funke, L.F.H., Robertson, W.E., Christova, Y., Chia, T., Schmied, W.H., Dunkelmann, D.L., Beránek, V., et al. (2019). Total synthesis of *Escherichia coli* with a recoded genome. *Nature* 569, 514–518. <https://doi.org/10.1038/s41586-019-1192-5>.
5. Shen, Y., Wang, Y., Chen, T., Gao, F., Gong, J., Abramczyk, D., Walker, R., Zhao, H., Chen, S., Liu, W., et al. (2017). Deep functional analysis of synll, a 770-kilobase synthetic yeast chromosome. *Science* 355, eaaf4791. <https://doi.org/10.1126/science.aaf4791>.
6. Richardson, S.M., Mitchell, L.A., Stracquadanio, G., Yang, K., Dymond, J.S., DiCarlo, J.E., Lee, D., Huang, C.L., Chandrasegaran, S., Cai, Y., et al. (2017). Design of a synthetic yeast genome. *Science* 355, 1040–1044. <https://doi.org/10.1126/science.aaf4557>.
7. Annaluru, N., Muller, H., Mitchell, L.A., Ramalingam, S., Stracquadanio, G., Richardson, S.M., Dymond, J.S., Kuang, Z., Scheifele, L.Z., Cooper, E.M., et al. (2014). Total synthesis of a functional designer eukaryotic chromosome. *Science* 344, 55–58. <https://doi.org/10.1126/science.1249252>.
8. Dymond, J.S., Richardson, S.M., Coombes, C.E., Babatz, T., Muller, H., Annaluru, N., Blake, W.J., Schwerzmann, J.W., Dai, J., Lindstrom, D.L., et al. (2011). Synthetic chromosome arms function in yeast and generate phenotypic diversity by design. *Nature* 477, 471–476. <https://doi.org/10.1038/nature10403>.
9. Hani, J., and Feldmann, H. (1998). tRNA genes and retroelements in the yeast genome. *Nucleic Acids Res.* 26, 689–696.
10. Geiduschek, E.P., and Kassavetis, G.A. (2001). The RNA polymerase III transcription apparatus. *J. Mol. Biol.* 310, 1–26. <https://doi.org/10.1006/jmbi.2001.4732>.
11. Admire, A., Shanks, L., Danzl, N., Wang, M., Weier, U., Stevens, W., Hunt, E., and Weinert, T. (2006). Cycles of chromosome instability are associated with a fragile site and are increased by defects in DNA replication and checkpoint controls in yeast. *Genes Dev.* 20, 159–173. <https://doi.org/10.1101/gad.1392506>.
12. Hamperl, S., Bocek, M.J., Saldivar, J.C., Swigut, T., and Cimprich, K.A. (2017). Transcription-replication conflict orientation modulates R-Loop levels and activates distinct DNA damage responses. *Cell* 170, 774–786.e19. <https://doi.org/10.1016/j.cell.2017.07.043>.
13. Deshpande, A.M., and Newlon, C.S. (1996). DNA replication fork pause sites dependent on transcription. *Science* 272, 1030–1033. <https://doi.org/10.1126/science.272.5264.1030>.
14. Ji, H., Moore, D.P., Blomberg, M.A., Braiterman, L.T., Voytas, D.F., Nat-soulis, G., and Boeke, J.D. (1993). Hotspots for unselected Ty1 transposition events on yeast chromosome III are near tRNA genes and LTR sequences. *Cell* 73, 1007–1018.

15. Mularoni, L., Zhou, Y., Bowen, T., Gangadharan, S., Wheelan, S.J., and Boeke, J.D. (2012). Retrotransposon Ty1 integration targets specifically positioned asymmetric nucleosomal DNA segments in tRNA hotspots. *Genome Res.* 22, 693–703. <https://doi.org/10.1101/gr.129460.111>.
16. Mieczkowski, P.A., Lemoine, F.J., and Petes, T.D. (2006). Recombination between retrotransposons as a source of chromosome rearrangements in the yeast *Saccharomyces cerevisiae*. *DNA Repair* 5, 1010–1020. <https://doi.org/10.1016/j.dnarep.2006.05.027>.
17. Dunham, M.J., Badrane, H., Ferea, T., Adams, J., Brown, P.O., Rose- nzwieg, F., and Botstein, D. (2002). Characteristic genome rearrange- ments in experimental evolution of *Saccharomyces cerevisiae*. *Proc. Natl. Acad. Sci. USA* 99, 16144–16149.
18. Mitchell, L.A., and Boeke, J.D. (2014). Circular permutation of a synthetic eukaryotic chromosome with the telomerase. *Proc. Natl. Acad. Sci. USA* 111, 17003–17010. <https://doi.org/10.1073/pnas.1414399111>.
19. Dietrich, F.S., Voegeli, S., Brachat, S., Lerch, A., Gates, K., Steiner, S., Mohr, C., Pöhlmann, R., Luedi, P., Choi, S., et al. (2004). The *Ashbya gossypii* genome as a tool for mapping the ancient *Saccharomyces cerevisiae* genome. *Science* 304, 304–307. <https://doi.org/10.1126/science.1095781>.
20. Wendland, J., and Walther, A. (2011). Genome evolution in the Eremothecium clade of the *Saccharomyces* complex revealed by comparative genomics. *G3 (Bethesda)* 1, 539–548. <https://doi.org/10.1534/g3.111.001032>.
21. Dietrich, F.S., Voegeli, S., Kuo, S., and Philippsen, P. (2013). Genomes of *Ashbya fungi* isolated from insects reveal four mating-type loci, numerous translocations, lack of transposons, and distinct gene duplications. *G3 (Bethesda)* 3, 1225–1239. <https://doi.org/10.1534/g3.112.002881>.
22. Braglia, P., Percudani, R., and Dieci, G. (2005). Sequence context effects on Oligo(dT) termination signal recognition by *Saccharomyces cerevisiae* RNA polymerase III. *J. Biol. Chem.* 280, 19551–19562. <https://doi.org/10.1074/jbc.M412238200>.
23. Hayashi, S., Mori, S., Suzuki, T., Suzuki, T., and Yoshihisa, T. (2019). Impact of intron removal from tRNA genes on *Saccharomyces cerevisiae*. *Nucleic Acids Res.* 47, 5936–5949. <https://doi.org/10.1093/nar/gkz270>.
24. Zhao, Y., Coelho, C., Hughes, A.L., Lazar-Stefanita, L., Yang, S., Brooks, A.N., Walker, R.S.K., Zhang, W., Lauer, S., Hernandez, C., et al. (2022). Debugging and consolidating multiple synthetic chromosomes reveals combinatorial genetic interactions. <https://doi.org/10.1101/2022.04.11.486913>.
25. Zhang, W., Zhao, G., Luo, Z., Lin, Y., Wang, L., Guo, Y., Wang, A., Jiang, S., Jiang, Q., Gong, J., et al. (2017). Engineering the ribosomal DNA in a megabase synthetic chromosome. *Science* 355, 1049. <https://doi.org/10.1126/science.aaf3981>.
26. Sikorski, R.S., and Hieter, P. (1989). A system of shuttle vectors and yeast host strains designed for efficient manipulation of DNA in *Saccharo- myces cerevisiae*. *Genetics* 122, 19–27.
27. Noskov, V.N., Chuang, R.Y., Gibson, D.G., Leem, S.H., Larionov, V., and Kouprina, N. (2011). Isolation of circular yeast artificial chromosomes for synthetic biology and functional genomics studies. *Nat. Protoc.* 6, 89–96. <https://doi.org/10.1038/nprot.2010.174>.
28. Dieci, G., Fiorino, G., Castelnuovo, M., Teichmann, M., and Pagano, A. (2007). The expanding RNA polymerase III transcriptome. *Trends Genet.* 23, 614–622. <https://doi.org/10.1016/j.tig.2007.09.001>.
29. Waldron, C., and Lacroute, F. (1975). Effect of growth rate on the amounts of ribosomal and transfer ribonucleic acids in yeast. *J. Bacteriol.* 122, 855–865. <https://doi.org/10.1128/jb.122.3.855-865.1975>.
30. Deshpande, A.M., and Newlon, C.S. (1992). The ARS consensus sequence is required for chromosomal origin function in *Saccharomyces cerevisiae*. *Mol. Cell. Biol.* 12, 4305–4313.
31. Brewer, B.J., Lockshon, D., and Fangman, W.L. (1992). The arrest of replication forks in the rDNA of yeast occurs independently of transcrip- tion. *Cell* 71, 267–276.
32. Takeuchi, Y., Horiuchi, T., and Kobayashi, T. (2003). Transcription- dependent recombination and the role of fork collision in yeast rDNA. *Genes Dev.* 17, 1497–1506. <https://doi.org/10.1101/gad.1085403>.
33. Rothstein, R., Michel, B., and Gangloff, S. (2000). Replication fork pausing and recombination or "gimme a break". *Genes Dev.* 14, 1–10.
34. Shen, Y., Stracquadanio, G., Wang, Y., Yang, K., Mitchell, L.A., Xue, Y., Cai, Y., Chen, T., Dymond, J.S., Kang, K., et al. (2016). SCRaMbLE gener- ates designed combinatorial stochastic diversity in synthetic chromo- somes. *Genome Res.* 26, 36–49. <https://doi.org/10.1101/gr.193433.115>.
35. Sauer, B., and McDermott, J. (2004). DNA recombination with a hetero- specific Cre homolog identified from comparison of the pac-c1 regions of P1-related phages. *Nucleic Acids Res.* 32, 6086–6095. <https://doi.org/10.1093/nar/gkh941>.
36. Liu, W., Luo, Z., Wang, Y., Pham, N.T., Tuck, L., Pérez-Pi, I., Liu, L., Shen, Y., French, C., Auer, M., et al. (2018). Rapid pathway prototyping and engineer- ing using in vitro and in vivo synthetic genome SCRaMbLE-in methods. *Nat. Commun.* 9, 1936. <https://doi.org/10.1038/s41467-018-04254-0>.
37. Anastassiadis, K., Fu, J., Patsch, C., Hu, S., Weidlich, S., Duerschke, K., Buchholz, F., Edenhofer, F., and Stewart, A.F. (2009). Dre recombinase, like Cre, is a highly efficient site-specific recombinase in *E. coli*, mamma- lian cells and mice. *Dis. Model. Mech.* 2, 508–515. <https://doi.org/10.1242/dmm.003087>.
38. Mitchell, L.A., McCulloch, L.H., Pingley, S., Berger, H., Bosco, N., Brosh, R., Bulajić, M., Huang, E., Hogan, M.S., Martin, J.A., et al. (2021). *De novo* assembly and delivery to mouse cells of a 101 kb functional human gene. *Genetics* 218, iyab038. <https://doi.org/10.1093/genetics/iyab038>.
39. Huxley, C., Green, E.D., and Dunham, I. (1990). Rapid assessment of *S. cerevisiae* mating type by PCR. *Trends Genet.* 6, 236. [https://doi.org/10.1016/0168-9525\(90\)90190-h](https://doi.org/10.1016/0168-9525(90)90190-h).
40. Harari, Y., Ram, Y., Rappoport, N., Hadany, L., and Kupiec, M. (2018). Spontaneous changes in ploidy are common in yeast. *Curr. Biol.* 28, 825–835.e4. <https://doi.org/10.1016/j.cub.2018.01.062>.
41. Watkins, C.P., Zhang, W., Wylder, A.C., Katanski, C.D., and Pan, T. (2022). A multiplex platform for small RNA sequencing elucidates multi- faceted tRNA stress response and translational regulation. *Nat. Comm- un.* 13, 2491. <https://doi.org/10.1038/s41467-022-30261-3>.
42. Shen, Y., Gao, F., Wang, Y., Wang, Y., Zheng, J., Gong, J., Zhang, J., Luo, Z., Schindler, D., Deng, Y., et al. (2022). Dissecting aneuploidy phe- notypes by constructing Sc2.0 chromosome VII and SCRaMbLEing syn- thetic disomic yeast. <https://doi.org/10.1101/2022.09.01.506252>.
43. Pluta, K., Lefebvre, O., Martin, N.C., Smagowicz, W.J., Stanford, D.R., El- lis, S.R., Hopper, A.K., Sentenac, A., and Boguta, M. (2001). Maf1p, a negative effector of RNA polymerase III in *Saccharomyces cerevisiae*. *Mol. Cell. Biol.* 21, 5031–5040. <https://doi.org/10.1128/MCB.21.15.5031-5040.2001>.
44. Huber, A., Bodenmiller, B., Uotila, A., Stahl, M., Wanka, S., Gerrits, B., Aebersold, R., and Loewith, R. (2009). Characterization of the rapamy- cin-sensitive phosphoproteome reveals that Sch9 is a central coordi- nator of protein synthesis. *Genes Dev.* 23, 1929–1943. <https://doi.org/10.1101/gad.532109>.
45. Wild, T., and Cramer, P. (2012). Biogenesis of multisubunit RNA polymer- ases. *Trends Biochem. Sci.* 37, 99–105. <https://doi.org/10.1016/j.tibs.2011.12.001>.
46. Mann, C., Buhler, J.M., Treich, I., and Sentenac, A. (1987). RPC40, a unique gene for a subunit shared between yeast RNA polymerases A and C. *Cell* 48, 627–637. [https://doi.org/10.1016/0092-8674\(87\)90241-8](https://doi.org/10.1016/0092-8674(87)90241-8).
47. Lalo, D., Carles, C., Sentenac, A., and Thuriaux, P. (1993). Interactions between three common subunits of yeast RNA polymerases I and III. *Proc. Natl. Acad. Sci. USA* 90, 5524–5528. <https://doi.org/10.1073/pnas.90.12.5524>.
48. Bridier-Nahmias, A., Tchalikian-Cosson, A., Baller, J.A., Menuoni, R., Fayol, H., Flores, A., Saïb, A., Werner, M., Voytas, D.F., and Lesage, P. (2015). Retrotransposons. An RNA polymerase III subunit determines



- sites of retrotransposon integration. *Science* 348, 585–588. <https://doi.org/10.1126/science.1259114>.
49. Thompson, M., Haeusler, R.A., Good, P.D., and Engelke, D.R. (2003). Nucleolar clustering of dispersed tRNA genes. *Science* 302, 1399–1401. <https://doi.org/10.1126/science.1089814>.
50. Chen, M., and Gartenberg, M.R. (2014). Coordination of tRNA transcription with export at nuclear pore complexes in budding yeast. *Genes Dev.* 28, 959–970. <https://doi.org/10.1101/gad.236729.113>.
51. Duan, Z., Andronescu, M., Schutz, K., McIlwain, S., Kim, Y.J., Lee, C., Shendure, J., Fields, S., Blau, C.A., and Noble, W.S. (2010). A three-dimensional model of the yeast genome. *Nature* 465, 363–367. <https://doi.org/10.1038/nature08973>.
52. Hamdani, O., Dhillon, N., Hsieh, T.S., Fujita, T., Ocampo, J., Kirkland, J.G., Lawrimore, J., Kobayashi, T.J., Friedman, B., Fulton, D., et al. (2019). tRNA genes affect chromosome structure and function via local effects. *Mol. Cell Biol.* 39, e00432–e00418. <https://doi.org/10.1128/MCB.00432-18>.
53. Mercy, G., Mozziconacci, J., Scolari, V.F., Yang, K., Zhao, G., Thierry, A., Luo, Y., Mitchell, L.A., Shen, M., Shen, Y., et al. (2017). 3D organization of synthetic and scrambled chromosomes. *Science* 355, eaaf4597. <https://doi.org/10.1126/science.aaf4597>.
54. Marie-Nelly, H., Marbouty, M., Cournac, A., Flot, J.-F., Liti, G., Parodi, D.P., Syan, S., Guillén, N., Margeot, A., Zimmer, C., and Koszul, R. (2014). High-quality genome (re)assembly using chromosomal contact data. *Nat. Commun.* 5, 5695. <https://doi.org/10.1038/ncomms6695>.
55. Bignaud, A., Cockram, C., Allemand, E., Mozziconacci, J., Espeli, O., and Koszul, R. (2022). Transcriptional units form the elementary constraining building blocks of the bacterial chromosome. <https://doi.org/10.1101/2022.09.16.507559>.
56. Lesne, A., Riposo, J., Roger, P., Cournac, A., and Mozziconacci, J. (2014). 3D genome reconstruction from chromosomal contacts. *Nat. Methods* 11, 1141–1143. <https://doi.org/10.1038/nmeth.3104>.
57. Harari, Y., Ram, Y., and Kupiec, M. (2018). Frequent ploidy changes in growing yeast cultures. *Curr. Genet.* 64, 1001–1004. <https://doi.org/10.1007/s00294-018-0823-y>.
58. Kubota, H., Ota, K., Sakaki, Y., and Ito, T. (2001). Budding yeast GCN1 binds the GI domain to activate the eIF2alpha kinase GCN2. *J. Biol. Chem.* 276, 17591–17596. <https://doi.org/10.1074/jbc.M011793200>.
59. McClintock, B. (1938). The production of homozygous deficient tissues with mutant characteristics by means of the aberrant mitotic behavior of ring-shaped chromosomes. *Genetics* 23, 315–376.
60. Guilhaume, R.S., Meloni, V.F., Kim, C.A., Pellegrino, R., Takeno, S.S., Spinner, N.B., Conlin, L.K., Christofolini, D.M., Kulikowski, L.D., and Melaragno, M.I. (2011). Mechanisms of ring chromosome formation, ring instability and clinical consequences. *BMC Med. Genet.* 12, 171. <https://doi.org/10.1186/1471-2350-12-171>.
61. Pristayzhnyuk, I.E., and Menzorov, A.G. (2018). Ring chromosomes: from formation to clinical potential. *Protoplasma* 255, 439–449. <https://doi.org/10.1007/s00709-017-1165-1>.
62. Paldi, F., Alver, B., Robertson, D., Schalbetter, S.A., Kerr, A., Kelly, D.A., Baxter, J., Neale, M.J., and Marston, A.L. (2020). Convergent genes shape budding yeast pericentromeres. *Nature* 582, 119–123. <https://doi.org/10.1038/s41586-020-2244-6>.
63. Thornlow, B.P., Hough, J., Roger, J.M., Gong, H., Lowe, T.M., and Corbett-Deitig, R.B. (2018). Transfer RNA genes experience exceptionally elevated mutation rates. *Proc. Natl. Acad. Sci. USA* 115, 8996–9001. <https://doi.org/10.1073/pnas.1801240115>.
64. Thornlow, B.P., Armstrong, J., Holmes, A.D., Howard, J.M., Corbett-Deitig, R.B., and Lowe, T.M. (2020). Predicting transfer RNA gene activity from sequence and genome context. *Genome Res.* 30, 85–94. <https://doi.org/10.1101/gr.256164.119>.
65. Ziehler, W.A., Day, J.J., Fierke, C.A., and Engelke, D.R. (2000). Effects of 5' leader and 3' trailer structures on pre-tRNA processing by nuclear RNase P. *Biochemistry* 39, 9909–9916.
66. Belagal, P., Normand, C., Shukla, A., Wang, R., Léger-Silvestre, I., Dez, C., Bhargava, P., and Gadal, O. (2016). Decoding the principles underlying the frequency of association with nucleoli for RNA polymerase III-transcribed genes in budding yeast. *Mol. Biol. Cell* 27, 3164–3177. <https://doi.org/10.1091/mbc.E16-03-0145>.
67. Postma, E.D., Dashko, S., van Breemen, L., Taylor Parkins, S.K., van den Broek, M., Daran, J.-M., and Daran-Lapujade, P. (2021). A supernumerary designer chromosome for modular *in vivo* pathway assembly in *Saccharomyces cerevisiae*. *Nucleic Acids Res.* 49, 1769–1783. <https://doi.org/10.1093/nar/gkaa1167>.
68. Kutyna, D.R., Onetto, C.A., Williams, T.C., Goold, H.D., Paulsen, I.T., Pretorius, I.S., Johnson, D.L., and Borneman, A.R. (2022). Construction of a synthetic *Saccharomyces cerevisiae* pan-genome neo-chromosome. *Nat. Commun.* 13, 3628. <https://doi.org/10.1038/s41467-022-31305-4>.
69. Langmead, B., and Salzberg, S.L. (2012). Fast gapped-read alignment with Bowtie 2. *Nat. Methods* 9, 357–359. <https://doi.org/10.1038/nmeth.1923>.
70. Langmead, B., Trapnell, C., Pop, M., and Salzberg, S.L. (2009). Ultrafast and memory-efficient alignment of short DNA sequences to the human genome. *Genome Biol.* 10, R25. <https://doi.org/10.1186/gb-2009-10-3-r25>.
71. Kechin, A., Boyarskikh, U., Kel, A., and Filipenko, M. (2017). cutPrimers: A new tool for accurate cutting of primers from reads of targeted next generation sequencing. *J. Comput. Biol.* 24, 1138–1143. <https://doi.org/10.1089/cmb.2017.0096>.
72. Martin, M. (2011). Cutadapt removes adapter sequences from high-throughput sequencing reads. *EMBnet.journal* 17. <https://doi.org/10.14806/ej.17.1.200>.
73. Anders, S., and Huber, W. (2010). Differential expression analysis for sequence count data. *Genome Biol.* 11, R106. <https://doi.org/10.1186/gb-2010-11-10-r106>.
74. de Sena Brandine, G., and Smith, A.D. (2019). Falco: high-speed FastQC emulation for quality control of sequencing data. *F1000Res* 8, 1874. <https://doi.org/10.12688/f1000research.21142.2>.
75. Liao, Y., Smyth, G.K., and Shi, W. (2014). featureCounts: an efficient general purpose program for assigning sequence reads to genomic features. *Bioinformatics Oxf. Engl.* 30, 923–930. <https://doi.org/10.1093/bioinformatics/btt656>.
76. Kim, D., Paggi, J.M., Park, C., Bennett, C., and Salzberg, S.L. (2019). Graph-based genome alignment and genotyping with HISAT2 and HISAT-genotype. *Nat. Biotechnol.* 37, 907–915. <https://doi.org/10.1038/s41587-019-0201-4>.
77. McKenna, A., Hanna, M., Banks, E., Sivachenko, A., Cibulskis, K., Kernytsky, A., Garimella, K., Altshuler, D., Gabriel, S., Daly, M., et al. (2010). The Genome Analysis Toolkit: a MapReduce framework for analyzing next-generation DNA sequencing data. *Genome Res.* 20, 1297–1303. <https://doi.org/10.1101/gr.107524.110>.
78. Sprouffske, K., and Wagner, A. (2016). Growthcurver: an R package for obtaining interpretable metrics from microbial growth curves. *BMC Bioinformatics* 17, 172. <https://doi.org/10.1186/s12859-016-1016-7>.
79. Robinson, J.T., Thorvaldsdóttir, H., Winckler, W., Guttman, M., Lander, E.S., Getz, G., and Mesirov, J.P. (2011). Integrative genomics viewer. *Nat. Biotechnol.* 29, 24–26. <https://doi.org/10.1038/nbt.1754>.
80. Wen, B., Zhou, R., Feng, Q., Wang, Q., Wang, J., and Liu, S. (2014). IQuant: an automated pipeline for quantitative proteomics based upon isobaric tags. *Proteomics* 14, 2280–2285. <https://doi.org/10.1002/pmic.201300361>.
81. Girardot, C., Scholtalbers, J., Sauer, S., Su, S.Y., and Furlong, E.E. (2016). Je, a versatile suite to handle multiplexed NGS libraries with unique molecular identifiers. *BMC Bioinformatics* 17, 419. <https://doi.org/10.1186/s12859-016-1284-2>.
82. Li, H. (2018). Minimap2: pairwise alignment for nucleotide sequences. *Bioinformatics Oxf. Engl.* 34, 3094–3100. <https://doi.org/10.1093/bioinformatics/bty191>.

83. Quintales, L., Soriano, I., Vázquez, E., Segurado, M., and Antequera, F. (2015). A species-specific nucleosomal signature defines a periodic distribution of amino acids in proteins. *Open Biol.* 5, 140218. <https://doi.org/10.1098/rsob.140218>.
84. Li, H., Handsaker, B., Wysoker, A., Fennell, T., Ruan, J., Homer, N., Marth, G., Abecasis, G., and Durbin, R.; 1000 Genome Project Data Processing Subgroup (2009). The Sequence Alignment/Map format and SAMtools. *Bioinformatics Oxf. Engl.* 25, 2078–2079. <https://doi.org/10.1093/bioinformatics/btp352>.
85. Patro, R., Duggal, G., Love, M.I., Irizarry, R.A., and Kingsford, C. (2017). Salmon provides fast and bias-aware quantification of transcript expression. *Nat. Methods* 14, 417–419. <https://doi.org/10.1038/nmeth.4197>.
86. Danecek, P., Bonfield, J.K., Liddle, J., Marshall, J., Ohan, V., Pollard, M.O., Whitwham, A., Keane, T., McCarthy, S.A., Davies, R.M., and Li, H. (2021). Twelve years of SAMtools and BCFtools. *GigaScience* 10, giab008. <https://doi.org/10.1093/gigascience/giab008>.
87. Pimentel, H., Bray, N.L., Puente, S., Melsted, P., and Pachter, L. (2017). Differential analysis of RNA-seq incorporating quantification uncertainty. *Nat. Methods* 14, 687–690. <https://doi.org/10.1038/nmeth.4324>.
88. Chen, Y., Chen, Y., Shi, C., Huang, Z., Zhang, Y., Li, S., Li, Y., Ye, J., Yu, C., Li, Z., et al. (2018). SOAPnuke: a MapReduce acceleration-supported software for integrated quality control and preprocessing of high-throughput sequencing data. *GigaScience* 7, 1–6. <https://doi.org/10.1093/gigascience/gix120>.
89. Milne, I., Stephen, G., Bayer, M., Cock, P.J., Pritchard, L., Cardle, L., Shaw, P.D., and Marshall, D. (2013). Using Tablet for visual exploration of second-generation sequencing data. *Brief. Bioinform.* 14, 193–202. <https://doi.org/10.1093/bib/bbs012>.
90. Lowe, T.M., and Chan, P.P. (2016). TRNAscan-SE On-line: integrating search and context for analysis of transfer RNA genes. *Nucleic Acids Res.* 44, W54–W57. <https://doi.org/10.1093/nar/gkw413>.
91. Ma, J., Chen, T., Wu, S., Yang, C., Bai, M., Shu, K., Li, K., Zhang, G., Jin, Z., He, F., et al. (2019). iProX: an integrated proteome resource. *Nucleic Acids Res.* 47, D1211–D1217. <https://doi.org/10.1093/nar/gky869>.
92. Gietz, R.D., and Woods, R.A. (2002). Transformation of yeast by lithium acetate/single-stranded carrier DNA/polyethylene glycol method. *Methods Enzymol.* 350, 87–96.
93. Schattner, P., Brooks, A.N., and Lowe, T.M. (2005). The tRNAscan-SE, snoscan and snoGPS web servers for the detection of tRNAs and snoRNAs. *Nucleic Acids Res.* 33, W686–W689. <https://doi.org/10.1093/nar/gki366>.
94. Cooper, E.M., Müller, H., Chandrasegaran, S., Bader, J.S., and Boeke, J.D. (2012). The build-a-genome course. In *Gene Synthesis: Methods and Protocols*, J. Peccoud, ed. (Humana Press), pp. 273–283. [https://doi.org/10.1007/978-1-61779-564-0\\_20](https://doi.org/10.1007/978-1-61779-564-0_20).
95. Gibson, D.G., Young, L., Chuang, R.Y., Venter, J.C., Hutchison, C.A., 3rd, and Smith, H.O. (2009). Enzymatic assembly of DNA molecules up to several hundred kilobases. *Nat. Methods* 6, 343–345. <https://doi.org/10.1038/nmeth.1318>.
96. Burgers, P.M.J., and Percival, K.J. (1987). Transformation of yeast spheroplasts without cell fusion. *Anal. Biochem.* 163, 391–397. [https://doi.org/10.1016/0003-2697\(87\)90240-5](https://doi.org/10.1016/0003-2697(87)90240-5).
97. Hage, A.E., and Houseley, J. (2013). Resolution of budding yeast chromosomes using pulsed-field gel electrophoresis. *Methods Mol. Biol.* 1054, 195–207. [https://doi.org/10.1007/978-1-62703-565-1\\_13](https://doi.org/10.1007/978-1-62703-565-1_13).
98. Scherthan, H., and Loidl, J. (2010). FISH as a tool to investigate chromosome behavior in budding yeast. *Methods Mol. Biol.* 659, 363–377. [https://doi.org/10.1007/978-1-60761-789-1\\_28](https://doi.org/10.1007/978-1-60761-789-1_28).
99. Shi, D., Han, T., Chu, X., Lu, H., Yang, X., Zi, T., Zhao, Y., Wang, X., Liu, Z., Ruan, J., et al. (2021). An isocaloric moderately high-fat diet extends lifespan in male rats and *Drosophila*. *Cell Metab.* 33, 581–597.e9. <https://doi.org/10.1016/j.cmet.2020.12.017>.
100. Wang, Y., Yang, F., Gritsenko, M.A., Wang, Y., Claus, T., Liu, T., Shen, Y., Monroe, M.E., Lopez-Ferrer, D., Reno, T., et al. (2011). Reversed-phase chromatography with multiple fraction concatenation strategy for proteome profiling of human MCF10A cells. *Proteomics* 11, 2019–2026. <https://doi.org/10.1002/pmic.201000722>.
101. González, S., García, A., Vázquez, E., Serrano, R., Sánchez, M., Quintales, L., and Antequera, F. (2016). Nucleosomal signatures impose nucleosome positioning in coding and noncoding sequences in the genome. *Genome Res.* 26, 1532–1543. <https://doi.org/10.1101/gr.207241.116>.
102. Soriano, I., Morafraila, E.C., Vázquez, E., Antequera, F., and Segurado, M. (2014). Different nucleosomal architectures at early and late replicating origins in *Saccharomyces cerevisiae*. *BMC Genomics* 15, 791. <https://doi.org/10.1186/1471-2164-15-791>.
103. Lazar-Stefanita, L., Scolari, V.F., Mercy, G., Muller, H., Guérin, T.M., Thierry, A., Mozziconacci, J., and Koszul, R. (2017). Cohesins and condensins orchestrate the 4D dynamics of yeast chromosomes during the cell cycle. *EMBO J.* 36, 2684–2697. <https://doi.org/10.15252/emboj.201797342>.
104. Dauban, L., Montagne, R., Thierry, A., Lazar-Stefanita, L., Bastié, N., Gadal, O., Cournac, A., Koszul, R., and Beckouët, F. (2020). Regulation of cohesin-mediated chromosome folding by Eco1 and other partners. *Mol. Cell* 77, 1279–1293.e4. <https://doi.org/10.1016/j.molcel.2020.01.019>.
105. Zaborske, J.M., Narasimhan, J., Jiang, L., Wek, S.A., Dittmar, K.A., Freimoser, F., Pan, T., and Wek, R.C. (2009). Genome-wide analysis of tRNA charging and activation of the eIF2 kinase Gcn2p. *J. Biol. Chem.* 284, 25254–25267. <https://doi.org/10.1074/jbc.M109.000877>.
106. Collart, M.A., and Oliviero, S. (2001). Preparation of yeast RNA. *Curr. Protoc. Mol. Biol.* Chapter 13, Unit13.12. <https://doi.org/10.1002/0471142727.mb1312s23>.
107. Katanski, C.D., Watkins, C.P., Zhang, W., Reyer, M., Miller, S., and Pan, T. (2022). Analysis of queuosine and 2-thio tRNA modifications by high throughput sequencing. *Nucleic Acids Res.* 50, e99. <https://doi.org/10.1093/nar/gkac517>.
108. Awan, A.R., Blount, B.A., Bell, D.J., Shaw, W.M., Ho, J.C.H., McKiernan, R.M., and Ellis, T. (2017). Biosynthesis of the antibiotic nonribosomal peptide penicillin in baker's yeast. *Nat. Commun.* 8, 15202. <https://doi.org/10.1038/ncomms15202>.
109. Lindeboom, T.A., Olmos, M.d.C.S., Schulz, K., Brinkmann, C.K., Rojas, A.A.R., Hochrein, L., and Schindler, D. (2022). L-SCRaMbLE creates large-scale genome rearrangements in synthetic *Sc2.0* chromosomes. <https://doi.org/10.1101/2022.12.12.519280>.
110. Batrakou, D.G., Müller, C.A., Wilson, R.H.C., and Nieduszynski, C.A. (2020). DNA copy-number measurement of genome replication dynamics by high-throughput sequencing: the sort-seq, sync-seq and MFA-seq family. *Nat. Protoc.* 15, 1255–1284. <https://doi.org/10.1038/s41596-019-0287-7>.
111. Krzywinski, M., Schein, J., Birol, I., Connors, J., Gascoyne, R., Horsman, D., Jones, S.J., and Marra, M.A. (2009). Circos: an information aesthetic for comparative genomics. *Genome Res.* 19, 1639–1645. <https://doi.org/10.1101/gr.092759.109>.
112. Müller, C.A., and Nieduszynski, C.A. (2012). Conservation of replication timing reveals global and local regulation of replication origin activity. *Genome Res.* 22, 1953–1962. <https://doi.org/10.1101/gr.139477.112>.

## STAR★METHODS

### KEY RESOURCES TABLE

REAGENT or RESOURCE	SOURCE	IDENTIFIER
<b>Bacterial and virus strains</b>		
<i>Escherichia coli</i> DH5 $\alpha$	Invitrogen	Cat# 18258012
<i>Escherichia coli</i> Top10	Invitrogen	Cat# C4040-10
<b>Chemicals, peptides, and recombinant proteins</b>		
1 kb Plus DNA Ladder	New England Biolabs (NEB)	Cat# N3200L
5-Fluoroorotic acid (5-FOA)	Formedium	Cat# 5FOA10
Agencourt AMPure XP	Beckman Coulter	Cat# A63881/A63882
Biotin-14-dCTP	Fisher Scientific	Cat# 10022582
Certified Megabase Agarose	Bio-Rad	Cat# 1613108
cOmplete™ Protease inhibitor-cocktail	Roche	Cat# 4693116001
Covaris microTUBE Snap-Cap AFA Fiber	Covaris	Cat# 520045
DMSO	Sigma Aldrich	Cat# D8418-100ML
Deoxynucleotide (dNTP) Solution Set	NEB	Cat# N0446S
DreamTaq Green PCR Master Mix (2X)	Thermo Fisher	Cat# K1082
Dynabeads™ Streptavidin C1	Fisher Scientific	Cat# 10202333
Formaldehyde	Sigma Aldrich	Cat# F8775
Glycine	Sigma	Cat# G7126
GoTaq G2 Green Master Mix	Promega UK Limited	Cat# M7823
Herring sperm DNA	Promega UK Limited	Cat# D1815
Lambda PFG Ladder	NEB	Cat# N0341S
Lithium acetate dihydrate	Sigma Aldrich	Cat# L4158-250G
Lyticase	Sigma Aldrich	Cat# L2524-50KU
<i>N</i> -Lauroylsarcosine sodium salt	Sigma Aldrich	Cat# L9150-100G
PEG 3350	Sigma Aldrich	Cat# P4338-1KG
PEG 8000	Sigma Aldrich	Cat# P2139-500G
PhosSTOP™	Roche	Cat# 4906845001
Phusion polymerase	NEB	Cat# M0530L
Plasmid-Safe™ ATP-Dependent DNase	Epicentre	Cat# E3101K
Primary antibody: $\alpha$ -Tubulin	Cell Signaling Technology	Cat# 2144; RRID:AB_2210548
Primary antibody: Anti-HA	Sigma Aldrich	Cat# H6908; RRID:AB_260070
Primary antibody: Phospho-eIF2 $\alpha$ (Ser51)	Cell Signaling Technology	Cat# 3398; RRID:AB_2096481
Proteinase K from <i>Tritirachium album</i>	Sigma Aldrich	Cat# P4850-1ML
Q5 polymerase	NEB	Cat# M0491L
Restriction enzymes	NEB	N/A
RNase A	Qiagen	Cat# 19101
RNase cocktail	Invitrogen	Cat# AM2286
Rubidium chloride	Sigma Aldrich	Cat# R2252-100G
SeaKem LE agarose	Lonza	Cat# 50001
Secondary antibody: Anti-rabbit IgG, HRP-linked	Cell Signaling Technology	Cat# 7074; RRID:AB_2099233
Sodium deoxycholate	Sigma Aldrich	Cat# D6750-100G
Sytox Green	Invitrogen	Cat# S7020
T4 DNA Ligase	New England Biolabs	Cat# M0202L
T4 DNA Polymerase	New England Biolabs	Cat# M0203L
T5 exonuclease	NEB	Cat# M0663S

(Continued on next page)

**Continued**

REAGENT or RESOURCE	SOURCE	IDENTIFIER
Taq ligase	NEB	Cat# M0208L
Zymolyase 20T from <i>Arthrobacter luteus</i>	MP Bio	Cat# MP08320921
<b>Experimental models: organisms/strains</b>		
See <a href="#">Methods S1</a> for <i>Saccharomyces cerevisiae</i> strains used in this study	This study	N/A
<b>Oligonucleotides</b>		
'PCR Tags' are listed in <a href="#">Methods S1</a>	IDT	N/A
<b>Recombinant DNA</b>		
Plasmids are listed in <a href="#">Methods S1</a> and sequences are provided as Genbank files in <a href="#">Data S4</a> .	N/A	N/A
<b>Software and algorithms</b>		
Bowtie2	Langmead and Salzberg <sup>69</sup> and Langmead et al. <sup>70</sup>	<a href="http://bowtie-bio.sourceforge.net/bowtie2/index.shtml">http://bowtie-bio.sourceforge.net/bowtie2/index.shtml</a>
cutadapt v1.15 and v4.4	Kechin et al. <sup>71,72</sup>	<a href="https://cutadapt.readthedocs.io/en/stable/">https://cutadapt.readthedocs.io/en/stable/</a>
DESeq2 v1.30.1	Anders and Huber <sup>73</sup>	<a href="https://bioconductor.org/packages/release/bioc/html/DESeq2.html">https://bioconductor.org/packages/release/bioc/html/DESeq2.html</a>
FastQC v0.10.1 and v0.11.9	de Sena Brandine and Smith <sup>74</sup>	<a href="https://www.bioinformatics.babraham.ac.uk/projects/fastqc/">https://www.bioinformatics.babraham.ac.uk/projects/fastqc/</a>
featureCounts v2.0.1	Liao et al. <sup>75</sup>	N/A
Hisat2 v2.1.0	Kim et al. <sup>76</sup>	<a href="http://daehwankimlab.github.io/hisat2/">http://daehwankimlab.github.io/hisat2/</a>
GATK v2.7	McKenna et al. <sup>77</sup>	<a href="https://gatk.broadinstitute.org/hc/en-us">https://gatk.broadinstitute.org/hc/en-us</a>
Growthcurver	Sprouffske and Wagner <sup>78</sup>	<a href="https://github.com/cran/growthcurver">https://github.com/cran/growthcurver</a>
Guppy	Oxford Nanopore Technologies	<a href="https://nanoporetech.com/">https://nanoporetech.com/</a>
IGV Viewer and IGV 2.5.2	Robinson et al. <sup>79</sup>	<a href="https://software.broadinstitute.org/software/igv/">https://software.broadinstitute.org/software/igv/</a>
IQuant	Wen et al. <sup>80</sup>	N/A
Je	Girardot et al. <sup>81</sup>	<a href="https://gbcs.embl.de/portal/tiki-index.php?page=Je">https://gbcs.embl.de/portal/tiki-index.php?page=Je</a>
Mascot	Matrix Science Inc	<a href="https://www.matrixscience.com/">https://www.matrixscience.com/</a>
Minimap2	Li <sup>82</sup>	<a href="https://github.com/lh3/minimap2">https://github.com/lh3/minimap2</a>
NUCwave	Quintales et al. <sup>83</sup>	<a href="http://nucleosome.usal.es/nucwave/">http://nucleosome.usal.es/nucwave/</a>
PySam	Li et al. <sup>84</sup>	<a href="https://github.com/pysam-developers/pysam">https://github.com/pysam-developers/pysam</a>
R / RStudio	R studio	<a href="https://www.r-project.org/">https://www.r-project.org/</a> <a href="https://www.rstudio.com/">https://www.rstudio.com/</a>
Salmon v1.2.1	Patro et al. <sup>85</sup>	N/A
Samtools	Li et al. <sup>84</sup> and Danecek et al. <sup>86</sup>	<a href="http://www.htslib.org/">http://www.htslib.org/</a>
Sleuth v0.30.0	Pimentel et al. <sup>87</sup>	<a href="https://pachterlab.github.io/sleuth/">https://pachterlab.github.io/sleuth/</a>
Snapgene	GSL Biotech LLC	<a href="http://www.snapgene.com/">http://www.snapgene.com/</a>
SOAPnuke	Chen et al. <sup>88</sup>	N/A
Tablet v1.21.02	Milne et al. <sup>89</sup>	N/A
tRNAscan-SE v.2.0	Lowe and Chan <sup>90</sup>	<a href="http://lowelab.ucsc.edu/tRNAscan-SE/">http://lowelab.ucsc.edu/tRNAscan-SE/</a>
<b>Deposited data</b>		
Code for tRNA gene assignment to flanking sequences	This study	<a href="https://github.com/the-cai-lab/tRNA-neochr">https://github.com/the-cai-lab/tRNA-neochr</a>
Raw sequencing reads	This study	NCBI BioProject: PRJNA884518
Proteomics raw data	This study	iProX: PXD037209
MSR-seq raw data	This study	NCBI GEO: GSE243449

## RESOURCE AVAILABILITY

### Lead contact

Further information and requests for resources and reagents should be directed to and will be fulfilled by the lead contact, Yizhi Cai ([yizhi.cai@manchester.ac.uk](mailto:yizhi.cai@manchester.ac.uk)).

### Materials availability

This study did not generate new unique reagents. Plasmids and strains generated in this study are available from the [lead contact](#) on request.

### Data and code availability

- WGS data, tRNAseq data, RNA-seq data, nucleosome positioning data and Hi-C data is deposited at SRA with NCBI BioProject number PRJNA884518. Proteome data is deposited at iProX<sup>91</sup> with accession number PXD037209. MSR-seq data is deposited at NCBI GEO with accession number GSE243449. All data is publicly accessible at the date of publication.
- Code for assigning tRNA genes to flanking sequences is available on the GitHub repository (<https://github.com/the-cai-lab/tRNA-neochr>).
- Any additional information required to reanalyze the data reported in this study is available from the [lead contact](#) upon request.

## EXPERIMENTAL MODEL AND STUDY PARTICIPANT DETAILS

### *S. cerevisiae* strains and growth conditions

All yeast strains were derivatives of S288C and grown at 30°C unless otherwise specified. A full list of strains used may be found in [Methods S1](#). Yeast cells were grown in either YEP/YPD media (10 g/L yeast extract, 20 g/L peptone and with or without 0.64 g/L tryptophan) or Synthetic Complete (SC) media lacking the indicated amino acids, both supplemented with 2% glucose if not stated otherwise. Standard solid media contained 2% agar and cultures were incubated at 30°C. Liquid cultures were cultivated according to standard procedures in glass tubes on a TC-7 roller drum (New Brunswick).

### Yeast transformation

Yeast transformation was undertaken according to a modified protocol described by Daniel Gietz and Woods<sup>92</sup>. Briefly, yeast strains were inoculated into 10 mL of liquid media and incubated with rotation at 30°C overnight. Overnight cultures were then re-inoculated to an optical density of 600nm ( $OD_{600}$ ) = 0.1 and incubated with rotation to a target  $OD_{600}$  of between 0.5 and 1. Cells were then centrifuged at 2,103 *g* for 5 minutes, washed with 10 mL sterile ddH<sub>2</sub>O and centrifuged again. Cell pellets were washed with 10 mL of 0.1 M LiOAc, centrifuged at 2,103 *g* for 5 minutes. 50 μL of cells were mixed with 5 to 10 μL of transforming DNA, 36 μL of 1M LiOAc, 19 μL ddH<sub>2</sub>O, 25 μL 10 mg/mL herring sperm carrier DNA and 240 μL of 44% PEG 3350. Transformations were incubated at 30°C for 30 minutes before adding 36 μL of DMSO and heat-shock at 42°C for 15 minutes. Cells were pelleted and incubated in 400 μL of 5 mM CaCl<sub>2</sub> at room temperature for 10 minutes and plated onto selective media.

## METHOD DETAILS

### Automating flanking sequence assignment to tRNA genes

An algorithm ([Figure S1A](#)) and associated scripts (<https://github.com/the-cai-lab/tRNA-neochr>) were used to assign tRNA genes to respective flanking sequences recovered from the *A. gossypii* and *E. cymbalariae* genome. These were based on custom Python scripts with BiPython modules. *S. cerevisiae* tRNA gene sequences (lacking introns), and *A. gossypii*/*E. cymbalariae* 5' and 3' flanking sequences were recovered from Genbank files downloaded from the NCBI genome database (accession numbers may be found in [Methods S1](#)), with metadata exported to comma separated value (.csv) files. All tRNA gene anticodons were determined (*i.e.* independently verified) by 'calling' a program compiled from the source code of tRNAscan-SE.<sup>93</sup> We developed an algorithm to preferentially map tRNA genes to flanking sequence based on the following design parameters: (1) tRNA genes of *S. cerevisiae* should match flanking sequences in *A. gossypii* and *E. cymbalariae*, in that order of preference, based on relative orientation and matching anticodon where possible. (2) Flanking sequences should only be assigned to tRNA genes once. (3) tRNA genes will lack introns. (4) All 3' tRNA flanking sequences should possess five or more thymidine residues required for transcriptional termination. (5) The 500 bp 5' flanking sequences should not contain unwanted features. (6) *rox* recombination sites will flank each tRNA cassette. To address the 5<sup>th</sup> design parameter above, scripts were used to remove and alter unwanted features in tRNA flanking sequences (summarized in [Figure S1B](#)), and include the translational silencing of gene starts, avoidance of those with overlapping regions and the removal of Solo LTR sequences for *E. cymbalariae*. Some tRNA genes were discarded from the available pool altogether. Following tRNA gene/flanking sequence assignment, tRNA cassettes were concatenated into tRNA arrays and generated as Genbank output files. Sixteen tRNA arrays ([Figure 1A](#); [Data S1](#)), consisting of concatenated tRNA cassettes, housed tRNA genes from each of the sixteen respective *S. cerevisiae* chromosomes were re-organized so that relative tRNA gene orientation was unidirectional for each array. The

unidirectionality was deemed potentially important to assure that the directions of replication forks and RNAPIII were always congruent. Furthermore, tRNA genes in tRNA arrays were aggregated by chromosome in a modular manner to both facilitate the construction of the tRNA neochromosome itself, and additionally, complement the loss of tRNA genes on individual synthetic chromosomes as part of the Sc2.0 project<sup>24</sup> and to assist in debugging of synthetic chromosomes. [Methods S1](#) details a full list of each *S. cerevisiae* tRNA gene and its associated assigned flanking sequence. [Data S1](#) includes the output file generated from scripts, including annotated tRNA arrays and metadata on tRNA genes and their associated flanking sequences. tRNA gene flanking sequences were also obtained from the yeast, *Kluyveromyces lactis*, but were not used in our final design.

### Manually curated design differences

The *chrVI* tRNA array was manually designed prior to the development of custom scripts. In this instance, 20 bp 3' flanking sequences from *A. gossypii* were incorporated (with the exception of the tG(GCC)F1 (SC.t6.4) tRNA cassette, which utilized a 40 bp 3' flanking sequence to capture the full poly-T sequence). Furthermore, the *chrVI* tRNA retains SfiI restriction sites which were used to experimentally 'flip' two tRNA cassettes from their wild-type orientation and ensure unidirectionality. For this reason, the orders of the tG(GCC)F1 (SC.t6.4) and tY(GUA)F1 (SC.t6.5) tRNA cassettes are reversed. Finally, following manual sequence validation of the tRNA neochromosome following flanking sequence assignment, a further four tRNA cassettes were observed to house unwanted features and were thus manually assigned different flanking sequences. These tRNA genes included *tV(AAC)G1* (SC.t07.12), *tV(AAC)H* (SC.t08.02), *tL(UAA)J* (SC.t10.17) and *tL(UAG)L2* (SC.t12.12) ([Methods S1](#)).

### Neochromosome design

The tRNA neochromosome itself was manually designed *in silico* from constituent tRNA arrays using Snapgene (Chicago, USA) and was used as a reference point for the design of eSwAP-In vectors used in its construction. The designed and sequenced tRNA neochromosome sequences are deposited at NCBI BioProject PRJNA351844.

### Origins of replication and design of replication termination sites

ARS elements were obtained from *Candida glabrata* (*chrF-444*, *chrL-615* and *chrM-794*; sequences listed in [Methods S1](#)). These were chosen on the basis of an intergenic

ORC-binding motif that closely resembles the motif found in all *S. cerevisiae* origins. The ARS *chrM-794* origin of replication was later observed to unexpectedly house an unannotated tRNA gene from *Candida glabrata* (revealed to be *chrM.tna11-GlyGCC*). Bidirectional replication termination sites (sequences listed in [Methods S1](#)) were designed to contain two conserved Fob1 recognition sites as follows: **TERI**: A hybrid between the *TER2* and *TER1* sites of *Saccharomyces paradoxus* and the *TER1* and *TER2* sites of *Saccharomyces uvarum*. **TERII**: A hybrid between the *TER2* and *TER1* sites of *Saccharomyces kudriavzevii* and the *TER1* and *TER2* sites of *Saccharomyces pastorianus*. **TERIII**: A hybrid between the *TER2* and *TER1* of *Saccharomyces mikatae* and the *TER1* of *Saccharomyces paradoxus* with a modified *TER2* hybrid containing a flipped middle spacer region. **TERIV**: A hybrid between the *TER2* of *Saccharomyces paradoxus* and the *TER1* site of *Saccharomyces uvarum* as well as the *TER1* of *Saccharomyces kudriavzevii* and *TER2* of *Saccharomyces pastorianus* (with some minor modifications). *TER* sites I-IV were synthesized by Twist Biosciences (San Francisco, USA).

### Universal homologous region

The Universal Homologous Region (UHR) was designed using a Perl script to produce a sequence of randomly-generated DNA 500 bp in length. This sequence was subjected to BLAST (<https://blast.ncbi.nlm.nih.gov/Blast.cgi>) against the *S. cerevisiae* genome, with no significant homology found. This DNA sequence is listed in [Methods S1](#). The UHR was synthesized *de novo* from overlapping oligonucleotides using the overlap-extension PCR method from the Build-A-Genome course.<sup>94</sup>

### Assembly of tRNA arrays

The *chrI* tRNA array was synthesized *de novo* from overlapping oligonucleotides into four 'building blocks' containing 100 bp overlapping regions using the overlap-extension PCR method from the Build-A-Genome course<sup>94</sup> and assembled using Gibson Assembly before verification with Sanger sequencing (Edinburgh Genomics, Edinburgh, UK). tRNA arrays over 10 kb in size were initially synthesized as sequences less than 10 kb and later combined into a linearized pRS413 acceptor plasmid using either Gibson Assembly<sup>95</sup> or *in vivo* homologous recombination in BY4741 using the LioAC transformation method.<sup>92</sup> To facilitate assembly, 100 bp overlapping region was incorporated into the central region of each split tRNA array. tRNA arrays (listed in [Methods S1](#)) were synthesized *de novo* by Wuxi Qinglan Biotech Co. Ltd (Yixing City, China), except for the *chrVIII*, *chrIX* and *chrXVI* tRNA arrays that were synthesized by Thermo Fisher Scientific (Renfrew, UK). Once constructed, tRNA genes were excised from their respective backbone using terminal restriction sites. All DNA constructs were verified using standard methods (colony PCR, restriction digest fingerprinting and Sanger sequencing).

### Neochromosome construction (eSwAP-In)

We developed an approach (later referred to as eSwAP-In) to construct the tRNA neochromosome, although this approach differs in key aspects to that described by Mitchell et al.<sup>38</sup> and are noted as follows. tRNA arrays were introduced into specialized eSwAP-In

vectors to facilitate construction. These vectors housed genetic elements required for the eSwAP-In process, including both the *LEU2* or *URA3* auxotrophic markers and a 500 bp ‘Universal Homologous Region’ (UHR). tRNA arrays were excised from their backbone using flanking restriction sites (Methods S1), with eSwAP-In vectors linearized using the *SmaI* restriction enzyme. tRNA arrays were inserted into their respective eSwAP-In vector using Gibson Assembly or *in vivo* homologous recombination in BY4741 facilitated by two homologous 330 bp to 650 bp ‘bridge’ sequences amplified using PCR (cf. Figure S1F). These bridge sequences also introduced functional elements to the growing neochromosome, including the origins of replication and the bidirectional *TER* sites (cf. Figure S1G). An exception was the first tRNA array (*chrVI*), which was instead ligated into a *LEU2* eSwAP-In vector (indicated by small arrows in the first panel) to provide a start point for tRNA neochromosome construction and the *CEN/ARS* and *HIS3* marker required for *in vivo* function. The primers used to amplify each bridge sequences were designed to house the necessary 40 bp overhangs for subsequent assembly. Neochromosome construction was performed in a stepwise manner (cf. Figure 2A) using repeated rounds of *LEU2* and *URA3* marker swapping in BY4741 and *synIII/VI/IXR*. Each tRNA array and sequences necessary for eSwAP-In were first recovered from their backbone using flanking *NotI* or *FseI* restriction enzymes and transformed into yeast containing the growing circular neochromosome. Candidate isolates were re-streaked onto selective agar for single colonies to induce loss of any prior auxotrophic marker before replica-plating onto agar lacking histidine (SC-His), leucine (SC-Leu) and uracil (SC-Ura), respectively, to determine the correct phenotype. Verification of the intact neochromosome was then performed using the PCR Tags (Methods S1). Finally, to facilitate the integration of the telomerase cassette for subsequent linearization, the residual *URA3* marker was ‘popped-out’ on 5-FOA following the final round of tRNA neochromosome construction. This was undertaken by introducing a second homologous 500 bp UHR located upstream of the *URA3* marker (introduced as a PCR ‘bridge’ during construction of the eSwAP-In vector) (cf. Figures S1F and S1G).

### PCR Tags method and conditions

To screen for candidate isolates, primers were designed to anneal to the 5′ and 3′ flanking sequence of each tRNA cassette to produce an amplicon of approximately 400 bp to 600 bp. After each round of eSwAP-In, an initial set of one to six primer pairs were used to screen colonies for an intact tRNA neochromosome before undertaking a full set of PCR Tags for all 275 tRNA cassettes. Crude genomic DNA was generated by incubating yeast isolates at 95°C in 50 μL of 20 mM NaOH for 10 minutes or the MasterPure™ Yeast DNA Purification Kit (Lucigen). PCR Tag analysis was performed either by adding 1.8 μL of yeast lysate used as template DNA to 6.25 μL of 2X GoTaq® Green Master Mix (Promega), 4.75 μL of nuclease-free water and 400 nM of each primer or by adding 1 μL of yeast lysate to 5 μL of DreamTaq Green PCR Master Mix (2X) (ThermoFisher Scientific) plus 4 μL of nuclease-free water with 200 nM of each primer. PCR reactions were performed as follows: 95°C for 2 min followed by 30 cycles of 95°C /2 min 30 s, 50°C /1 min 15 s, 72°C /1 min 45 s followed by a 72°C /5 min extension time (GoTaq) or 95°C for 2 min followed by 40 cycles of 95°C /20 s, 52°C /45 s, 72°C /1 min 30 s followed by a 72°C /2 min extension time (DreamTaq). 8-10 μL aliquots of each reaction were then run on a 1.5-2% TAE agarose gel. A full list of PCR Tag primers used may be found in Methods S1; a representative example gel may be found in Figure S2D.

### Repair of tRNA neochromosome structural variations

The structural variation observed in YCy1576 was repaired as follows. Initially, *URA3* and *LEU2* markers, each coupled with an *I-SceI* recognition site, were simultaneously integrated upstream and downstream of the structural re-arrangement, deleting the duplicated part of the *chrXIII* tRNA array and the partially complete *chrX* tRNA array (YCy2411). In the second round of repair, two plasmids were co-transformed. The first plasmid (*KANMX* marker) contained the *chrX* tRNA array flanked by *I-SceI* recognition sites; the second (*MET15* marker) housed a galactose inducible *I-SceI* overexpression construct. Subsequent induction of *I-SceI* expression facilitated the release of the *chrX* tRNA array from the first plasmid and generation of two neochromosome fragments. The presence of 500 bp homologous sequences on the three fragments facilitated recombination-mediated integration of the *chrX* tRNA array and the repair of the inversion to generate the final tRNA neochromosome (YCy2508) (cf. Figure 2B). Single colonies were selected on SC-His-Met + 5-FOA with 2% galactose agar plates. Candidates were screened with primers to detect the correct homologous recombination borders as well as the missing tRNA cassettes of the *chrX* tRNA array before full PCR Tag analysis, size verification *via* PFGE and short read sequencing was performed resulting in the final strain YCy2508. The raw reads of YCy2508 are deposited at NCBI BioProject PRJNA351844 (SAMN30265401).

### Whole genome sequencing

Yeast genomic DNA was prepared from 5 mL stationary phase culture either with the MasterPure™ Yeast DNA Purification Kit (Lucigen) according to the manufacturer guidelines or using the Cetyl Trimethyl Ammonium Bromide (CTAB) DNA extraction method. Briefly, cells were harvested at 4,000 g for 4 min, resuspended in 1 mL extraction buffer (2% CTAB, 100 mM Tris, 1.4 M NaCl and 10 mM EDTA, pH 8.0) and transferred into a 2 mL screw-top tube containing ~50 mg 425–600 μm washed glass beads (Sigma). Cells were lysed by vortexing for 10 min at maximum speed followed by incubation for 10 min at 65°C. Cell debris was removed by centrifugation at maximum speed for 2 min and supernatant was transferred to a 2 mL tube, 4 μL of 100 mg/mL RNase (Qiagen) was added, followed by incubation at 37°C for 15 min. 700 μL of chloroform was added, mixed carefully and centrifuged at maximum speed for 2 min. The aqueous phase was transferred into a 1.5 mL reaction tube containing ~0.6 volumes of isopropanol. Thorough mixing was performed with the precipitate collected by centrifugation at maximum speed for 10 min. The resulting supernatant was discarded

and the pellet was washed with 500  $\mu$ L 70% ethanol followed by centrifuging for 5 min at maximum speed. The supernatant was decanted and the tube was again pulse-centrifuged with the residual alcohol removed with a pipette followed by air drying for 2–5 min. The pellet was subsequently resuspended in 100  $\mu$ L of H<sub>2</sub>O. DNA library preparation was performed using the Nextera XT kit (Illumina). Tagmentation, inactivation, and library amplification were performed following kit instructions and using commercial reagents. Amplified libraries were purified using 1.8 $\times$  volumes AMPure XP beads and eluted in 10  $\mu$ L nuclease-free water. Library yield was quantified using the Qubit high-sensitivity DNA kit and library quality was determined on an Agilent Bioanalyzer (high-sensitivity DNA assay). Samples were pooled and 150 bp paired-end reads were generated on an Illumina NextSeq 500. Alternatively, PCR-free whole genome sequencing was performed using the Sanger Institute service. Samples were normalized so that 500 to 1000 ng of input DNA enters the process. DNA was fragmented to 450 bp using a Covaris LE220 sonicator prior to library construction. During library construction fragmented DNA was purified ready for end-repair, A-tailing and unique dual indexed adapter ligation with no amplification step. Libraries were quantified using qPCR and then pooled and 150 bp paired-end reads were generated on an Illumina HiSeqX. Sequencing reads QC, data processing and analysis were performed using standard procedures, clean reads were mapped to the respective reference sequence using Bowtie2 v2.3.5.1 with default parameters.<sup>70</sup> GATK v2.7<sup>77</sup> and SAMtools v0.1.19<sup>84</sup> were used in conjunction with IGV for analysis.

### Chemical extraction and transfer of the tRNA neochromosome

Extraction and transfer of circular neochromosome variants from one cell to another was undertaken according to the method described by Noskov et al.<sup>27</sup> The Plasmid Maxi Kit (Qiagen) with QS solution (1.5 M NaCl, 100 mM MOPS, 15% v/v isopropanol) and PlasmidSafe (Epicentre) were used *in lieu* of the Qiagen Large Construct Kit and Qiagen exonuclease, respectively. Purified neochromosome DNA was then transformed into BY4741 and BY4742 using the spheroplast transformation method described by Burgers and Percival<sup>96</sup> Increased volumes were used during transformation, with 12  $\mu$ L of neochromosome DNA added to 300  $\mu$ L of spheroplasts. Transformed spheroplasts were then added to 10 mL of molten SC-Ura or SC-His TOP agar (SC-Ura or SC-His media containing 1 M sorbitol and 2.5% agar; held at 45°C), gently mixed, and poured directly onto petri dishes containing 10 mL of SC-Ura or SC-His SORB (SC-Ura or SC-His media containing 0.9 M sorbitol, 2% agar and 3% glucose). The plates were then incubated at 30°C for four days before the appearance of sufficiently large colonies.

### Neochromosome linearization

Telomere seed sequence integration and neochromosome linearization was performed according to the method described by Mitchell and Boeke<sup>18</sup> Following the integration of the telomerase cassette into defined regions of the neochromosome, strains were transformed with a plasmid expressing the I-SceI homing endonuclease under a control of a *GAL1* promoter. Isolates were then inoculated into 10 mL of SC-His-Ura-Leu (2% glucose) and incubated with rotation at 30°C overnight. Once saturated, cultures were washed once with sterile PBS (phosphate buffered saline) solution and re-inoculated into 10 mL of SC-His-Leu containing either 2% galactose (for induction of I-SceI) or 2% glucose (negative control) to a target OD<sub>600</sub> of 0.05 and incubated with rotation at 30°C for 24 hours. After 24 hours of growth, cultures were serially-diluted by a factor of 1 in 1,000 and plated onto SC-His + 5-FOA (1 mg/mL). Approximate efficiency of linearization was inferred by comparing the number of colonies of galactose-induced cultures with those cultured in glucose (normalized for cell density). After three days of growth, yeast isolates were verified using a colony PCR with primers designed to anneal with each arm of the telomerase cassette and to screen for the presence or absence of the junction region at the I-SceI cut site.

### Pulsed field gel electrophoresis (PFGE)

Plug preparation and pulsed-field gel electrophoresis (PFGE) was performed according to previously described methods by Hage and Houseley<sup>97</sup> PFGE was undertaken by running samples on a 1.3% agarose gel in 0.5 X TBE solution at 14°C on a Bio-Rad clamped homogenous electric field (CHEF) apparatus (CHEF-DR III). 6 V/cm were used with a ramped switch time of 15–25 s for 24 h. Alternatively, samples were run for 15 h with a switch time of 60 s, followed by a further 15 h with a switch time of 120 s at a 120° angle. The resulting gel was stained with 1 X SYBR Safe (ThermoFisher Scientific) and imaged using a Fujifilm FLA-5100 or Typhoon Trio (GE) laser scanning system. The identity and size of the tRNA neochromosome was inferred by lambda ladders run on the same gel and/or the known molecular karyotype of BY4741.

### tRNA neochromosome stability assay

Overnight cultures of haploid BY4741, BY4742 and diploid *MATa/a* and *MATa/α* containing the tRNA neochromosome (YCy2837, YCy2838, YCy2508 and YCy2844) were inoculated as biological triplicates into 20 mL SC-His to a starting OD<sub>600</sub> of 0.1. Every 24 h, cultures were back diluted to OD<sub>600</sub> 0.1 and glycerol stocks were prepared over a time-course of seven days corresponding to approximately 50 generations. On the seventh day, dilution series were plated on SC-His media and four randomly selected candidates per strain were tested with a subset of the PCR Tag primers via colony PCR. DNA of 2 mL overnight culture was extracted with the MasterPure™ Yeast DNA Purification Kit (Lucigen) and whole PCR Tag analysis was performed on population level to test the general presence of all tRNAs within the population (data not shown). Selected candidates were submitted to Nanopore sequencing to identify the location of recombination.



### Nanopore sequencing

High-molecular weight DNA extraction was performed according to a modified Qiagen Genomic-tip 100/g protocol. Yeast cultures were grown to early stationary phase ( $OD_{600}$  of approximately 10) and an equivalent  $OD_{600}$  of 250 were harvested with centrifugation at 5,000 *g*. Spheroplasts were generated by incubating resuspended yeast pellets in 4 mL of Y1 buffer supplemented with 250 U lyticase (Sigma Aldrich) at 37°C for 1 hour. Spheroplasts were then harvested at 800 *g* for 10 minutes at 4°C. The pellet was resuspended in G2 Buffer with 20  $\mu$ L RNase A (100 mg/mL) (Qiagen) and 125  $\mu$ L RNase Cocktail (Invitrogen). After incubation for 5 min at RT, 100  $\mu$ L Proteinase K (Sigma Aldrich) was added and incubated for 1 hour at 50°C. The lysate was cleared by centrifuging at 5,000 *g* for 15 min at 4°C before loading onto the column. The remaining procedure was performed according to the manufacturer's guidelines. DNA quality was assessed via gel-electrophoresis, NanoDrop™ 2000 spectrophotometer and Qubit 4 fluorometer using the dsDNA BR reagents. Library preparation was performed using the SQK-LSK109 and the Native Barcoding kits (EXP-NDB104 and EXP-NDB114) according to the manufacturing guidelines. The only alteration was to increase the DNA mass 5-fold to match the required starting material molarity, DNA is approx. 50 kb in size based on our initial PFGE analysis (data not shown). Sequencing was performed on a MinION Mk1B device (Oxford Nanopore Technologies) using flow cell chemistry R9.4.1 (FLO-MIN106D). Base calling was performed using Guppy and minimap2 was used for sequence alignments. Samtools and IGV were used for data analysis.

### Tecan growth curve assay

Growth curve analysis was performed in a Tecan F200 plate reader in 96-well flat bottom plates (Corning) with 150  $\mu$ L of medium inoculated to a starting  $OD_{600}$  of 0.05. Plates were sealed with TopSeal-A PLUS (Perkin Elmer). The following kinetic parameters were run with a varying number of cycles (289 cycles for approx. 24 h at 30°C): 2:23 min orbital shaking (1.5 mm amplitude), 2:23 min linear shaking (2 mm amplitude) followed by OD measurement at 595 nm. Data was analyzed and visualized with custom R scripts and the R package Growthcurver.<sup>78</sup>

### Single-copy, essential, tRNA gene complementation

To assay synthetic tRNA functionality on an individual level, three, single-copy tRNA genes were investigated: *SUP61* (*tS(CGA)C*), *TRT2* (*tT(CGU)K*) and *TRR4* (*tR(CCG)L*). All three tRNA genes are essential in *S. cerevisiae*. Synthetic variants of each were integrated into the *HO* locus of BY4741, with *URA3* used as a selective marker for integration. Wild-type copies of each essential tRNA gene were removed by PCR-amplifying a *KanMX* marker with 40 bp homology arms specific to the surrounding region of each tRNA gene (viability was supported by episomal copies of each). Removal of wild-type tRNA genes and integration into the *HO* locus was verified using colony PCR, with primer pairs designed to amplify the junction regions of each locus. Following induced loss of each respective episomal copy, biological duplicates of these strains (YCy896 to YCy905) and a wild-type control (BY4741 + pRS416) were inoculated into 10 mL of SC-Ura and incubated with rotation overnight at 30°C. Overnight cultures were then adjusted to a normalized  $OD_{600}$  of 0.03 in sterile PBS (phosphate buffered saline) solution, serially diluted, and spotted side-by-side onto SC-Ura selective media (Figure S1C). Plates were then incubated at 30°C for three days.

### Dre recombinase-induced tRNA copy number adjustment: proof-of-concept

A proof-of-concept with Dre recombinase was performed on the *chrVI* tRNA array in BY4741. The *chrVI* tRNA array contained 10 tRNA genes from *chrVI* and one tRNA gene from *chrV*. The pRS413-*chrVI*-tRNA array was first transformed into BY4741, followed by a second transformation with pRS415-P<sub>SCW11</sub>-*DreEBD*.<sup>36</sup> The double transformed strain was cultured in SC-His-Leu liquid medium overnight and re-inoculated to  $OD_{600}$  of 0.1 into two tubes, one with a 7 h induction of 1  $\mu$ M  $\beta$ -estradiol and the other un-induced. Following induction, cells were plated onto SC-His, with single colonies picked for plasmid extraction and recovery in *E. coli*. XbaI restriction sites were subsequently used to excise the *chrVI* tRNA array from its plasmid backbone and generate a restriction map indicating the relative reduction in the number of tRNA cassettes. Sanger sequencing was then used to determine the full genotype information of the remaining tRNA genes.

### Ploidy determination by flow cytometry

The ploidy of yeast cells was determined using SYTOX Green stained fixed cells in a SH800S Cell Sorter (Sony Biotechnology). Briefly, cells were grown to an  $OD_{600}$  of approx. 0.5 with 2 mL of cells collected (4 min at 2,000 *g*), washed with filtered H<sub>2</sub>O and fixed in 1 mL 70% EtOH. Fixed cells were washed twice in 1 mL filter sterilized 50 mM sodium citrate followed by resuspension in 1 mL 50 mM sodium citrate with RNase A (final conc. 0.25 mg/mL) and incubation at 50°C for 1 h. Subsequently Proteinase K was added with a final conc. of 0.4 mg/mL followed by 1 h at 50°C before harvesting the cells (4 min 2,000 *g*). Cell pellets were resuspended in 1 mL 50 mM sodium citrate with Sytox Green (5 mM stock; 1:5,000 diluted) and subsequently measured in the SH800S Cell Sorter. Known haploid (BY4741) and diploid (BY4743) control strains were always used as standards.

### Fluorescent in situ hybridization (FISH)

Yeast strains (YCy2508, YCy2649) were cultured in 3 mL of SC-His overnight at 30°C before back-diluting into 5 mL fresh SC-His ( $OD_{600}$  = 0.1), and subsequently grown to a concentration of approx.  $2 \times 10^7$  cells per mL. Slides and hybridization of probes were prepared according to Scherthan and Loidl<sup>98</sup> Hybridization reactions were performed using 6  $\mu$ L of a 3  $\mu$ M 5'-Cy3 labelled probe (5'-taactttaataatgccaatttttaagta-3') for the rox recombination sites, and 3  $\mu$ L the three 3  $\mu$ M 5'-FAM labelled probes, targeting the

5S rDNA according to Thompson et al.,<sup>49</sup> for rDNA sequences, respectively. Slides were imaged using a Nikon A1 confocal microscope with a 60x objective. Three different derivatives of YCy2508 which lost different PCR Tags were used for the imaging with  $n = >100$  cells for each derivative. Results were merged and used to calculate the percentage of cells with different localization patterns.

### Live cell imaging

Yeast strains (JSY396 and JSY397) were cultured into 3 mL of SC-His overnight at 30°C before back-dilution into 5 mL fresh SC-His ( $OD_{600} = 0.15$ ) and grown 5 hours prior imaging. Cells were harvested and washed with H<sub>2</sub>O. Live cell imaging was performed on a Nikon A1 confocal microscope with a 60x objective. The recognition sequence of the constructed TAL-GFP is 5'-ttaaataattggcattat-3'. The results of four clones of JSY396 were used to calculate the percentage of cells with different patterns. More than 250 cells for each clone were counted.

### RNA-seq analysis

The strains with 3 biological replicates were prepared using sample preparation methods established previously for transcriptome analysis.<sup>5</sup> The total RNA was prepared using the Omega Bio-tek Yeast RNA Kit (CAT# R6870-02). A 200-400bp RNA-seq library was prepared by the MGIEasy™ RNA Library Prep Kit V3.0 (CAT# 1000006384). The transcriptome sequencing was performed with the BGISEQ-500 platform. For transcriptomic analysis, reads were mapped to genome sequence by hisat2 v2.1.0,<sup>76</sup> assigned read counts for each gene by featureCounts v2.0.1<sup>75</sup> and differentially expressed genes were analyzed by DESeq2 v1.30.1.<sup>73</sup> Genes were assessed for significantly differential expression if the  $\log_2(\text{Foldchange})$  was  $>1$  or  $<-1$ , and if the raw P value fell below the threshold of the 5% Family Wise Error Rate (FWER) after Bonferroni correction (threshold =  $7.62E-6$ ). To identify differentially active biological processes between tRNA neochromosome strains and its native control strains, gene enrichment analyses were performed as described previously<sup>5</sup> using yeast KEGG pathways and yeast Gene Ontology (GO) annotations. The significance of each KEGG pathway and GO term in genes was individually identified using the hyper-geometric test and Chi-squared test the threshold P-value  $<0.001$ .

### Proteome analysis

The strains with 3 biological replicates were prepared using sample preparation methods established previously for proteome analysis.<sup>5</sup> Yeast protein was extracted with Urea, reduced, alkylated, and digested with trypsin.<sup>99</sup> The protein identification and quantification performed by tandem mass spectrometry. The proteins were labeled by Thermo Scientific TMT pro 16plex Label Reagent Set (CAT# A44522) according to the manufacturer's instructions, and then the labeled peptides were fractionated with high pH reversed-phase (RP) chromatography method<sup>100</sup> and analyzed by a Q Exactive™ HF-X mass spectrometer (Thermo Fisher Scientific, San Jose, CA) coupled with an online High-Performance Liquid Chromatography (HPLC, Thermo Scientific™ UltiMate™ 3000 UHPLC system). For proteomic analysis, Mascot and IQuant<sup>80</sup> were used for protein identification and quantification. The differential expression proteins were identified if the  $\log_2(\text{Foldchange})$  was  $>1$  or  $<-1$ , and the P value  $<0.001$ . The Gene enrichment analyses of KEGG pathways and Gene Ontology were performed as above description.

### Preparation of mononucleosomal DNA and generation of nucleosomal occupancy maps

*S. cerevisiae* cultures of 200 mL at  $0.8 \times 10^7$  cells/mL were collected for preparation of mononucleosomal DNA. Cells were treated with 10 mg of Zymolyase 20T for 5 minutes at 30°C to generate spheroplasts. Mononucleosomal fragments were generated by digesting DNA with 300 units/mL of micrococcal nuclease (MNase) at 37°C for 10 minutes. The amount of MNase was optimized experimentally to generate an 80:20 ratio of mononucleosomes to dinucleosomes, as described by González et al.,<sup>101</sup> Soriano et al.<sup>102</sup> Mononucleosomal DNA was recovered from 1.5% agarose gels to prepare sequencing libraries following the Illumina protocol. They were sequenced in an Illumina NextSeq 500 platform using the paired-end protocol. Reads were aligned using Bowtie<sup>70</sup> to the *S. cerevisiae* (SacCer 3) genome or to the tRNA neochromosome sequence. Alignment files were processed using the NUCwave algorithm<sup>83</sup> to generate the nucleosome occupancy maps.

### Hi-C analysis

Hi-C experiments were performed following the protocol described in Lazar-Stefanita et al.<sup>103</sup> and adapted in Dauban et al.<sup>104</sup> Briefly,  $1$  to  $3 \times 10^9$  cells in 150 mL synthetic medium were crosslinked using 3% formaldehyde. Quenching of formaldehyde was performed using 300 mM glycine at 4°C for 20 min. Fixed cells were recovered through centrifugation, washed, and stored at -80°C. The Hi-C library was generated using a DpnII restriction enzyme as described in Lazar-Stefanita et al.,<sup>103</sup> except that after the protein digestion step the DNA was purified using AMPure XP beads. The DNA Hi-C libraries were sheared into 300 bp using a Covaris S220 apparatus (Covaris) and the biotin-labeled fragments were selectively captured by Dynabeads Myone Streptavidin C1. The sequencing library was generated using Invitrogen Colibri PS DNA Library Prep Kit for Illumina, following manufacturer instructions.

### tRNAseq: RNA isolation, tRNA library preparation and sequencing

Yeast total RNA was depleted from rRNA and sRNAs, followed by library preparation and Illumina sequencing. Yeast strains were grown in liquid cultures in SC-His medium until reaching  $OD_{600}$  of 0.9. Cells were harvested by centrifugation, washed once with

water, with cell pellets corresponding to an OD<sub>600</sub> of 9 OD subsequently frozen. Total RNA was then isolated from cell pellets using Epicentre Masterpure Yeast RNA Kit, which were processed with 4 times the volume of chemistry of the Epicentre kit; all remaining steps were done as described by the manufacturer (including DNaseI digest to remove residual DNA). 8 μg of isolated total RNA was separated from rRNA using the Illumina RiboZero Gold for Yeast rRNA removal kit, resulting in around 1.8 μg of rRNA-depleted RNA. sRNAs below 200 nt were subsequently enriched using the Ambion MirVana miRNA Isolation kit (according to manufacturer's instructions), resulting in around 300 ng of RNA. RNAs were checked for successful rRNA depletion and sRNA depletion using an Agilent Bioanalyzer RNA 6000 Nano. Illumina sequencing ready libraries were prepared using NEBNext Small RNA Library Prep Set for Illumina following the manufacturer's instructions and checked on a Bioanalyzer DNA 1000. Illumina sequencing was performed on an Illumina NextSeq 500. tRNA quantification and differential expression testing Illumina sequencing data were quality controlled with FastQC v0.10.1.<sup>74</sup> Sequencing adapters were trimmed with cutadapt v1.15.<sup>71</sup> tRNAs were quantified at the transcript-level with Salmon v1.2.1<sup>85</sup> using both pre-tRNA and mature tRNA transcript models. tRNAs were detected *de novo* using tRNAscan-SE v.2.0<sup>90</sup> on the tRNA neochromosome reference sequence. pre-tRNAs were modified with 10 nucleotide additional leader and trailer sequences based on the genomic coordinates. tRNAs derived from synthetic and native chromosomes were aggregated in a single reference transcriptome. The identical reference transcriptome was used to quantify each sample, independent of neochromosome presence, allowing for determination of misquantification rates on the neochromosome. Additional small RNA species were downloaded from Ensembl. Salmon was run with both sequence and position bias modelling enabled and in paired end mode. Differential expression testing was performed with Sleuth v0.30.0.<sup>87</sup>

### MSR-Seq

Yeast total RNA was extracted as described before.<sup>105,106</sup> Briefly, 5 mL yeast cells were cultured in SC-His medium to OD<sub>600</sub> of 1.0 prior to harvesting by centrifugation. Cell pellets were resuspended in lysis buffer (10 mM Tris-HCl pH 8.5, 5 mM EDTA, 2% SDS), and mixed with acetate-saturated phenol/CHCl<sub>3</sub> at pH 4.5 (Ambion cat# AM9720). The tubes were vortexed using MP FastPrep-24 5G Homogenizer, with 6 cycles of 30 seconds shaking and 30 seconds cool down. Following cold centrifugation at 18,600 g for 10 minutes, the upper aqueous layers were collected to a new tube and mixed with equal volume of cold acetate-saturated phenol/CHCl<sub>3</sub> solution for another round of extraction. Then, the aqueous layers were collected and mixed with 1/10 volume of 3M sodium acetate pH 5 and 2.5 volume of cold 100% ethanol. RNA was precipitated at -80°C for 30 minutes, then centrifuged at 18,600 g for 10 minutes. RNA pellets were washed with 500 μL of cold 80% ethanol, dried in air, and finally resuspended in water. One μg total RNA from each sample was used to build multiplex small RNA sequencing (MSR-seq) libraries as previously reported.<sup>41</sup> Sequencing was done using Illumina NEXT-seq, 80 bp read1, 150 bp read2. MSR-seq data analysis was performed as described previously.<sup>41</sup> Briefly, starting from index demultiplexed fastq data, paired end reads were split by internal barcode sequence using Je<sup>81</sup> demultiplex with options BPOS = BOTH BM = READ 1 LEN = 4:6 FORCE = true C = false 6. Barcode sequences are available on Github at [https://github.com/ckatanski/Q\\_paper](https://github.com/ckatanski/Q_paper).<sup>107</sup> Next read 2 files were used to map with bowtie2<sup>69</sup> with the following parameters: -q -p 10 -local -no-unal. Reads were mapped to curated list of non-redundant tRNA genes using custom yeast gene references from both BY4741 native chromosomes and neo-chromosome. Bowtie2 output sam files were converted to bam files, then sorted using samtools. Next, IGV<sup>79</sup> was used to collapse reads into 1 nt window. IGV output.wig files were reformatted using custom python scripts (available on GitHub at [https://github.com/ckatanski/Q\\_paper](https://github.com/ckatanski/Q_paper)). The bowtie2 output Sam files were also used as input for a custom python script using PySam, a python wrapper for SAMTools<sup>84</sup> to sum all reads that mapped to each gene. Data were visualized with custom R scripts. All custom scripts are available on GitHub (<https://github.com/ckatanski/CHRIS-seq>).

### Western blot analysis

For Western blot analysis, eIF2- $\alpha$  was C-terminally tagged with the Human influenza hemagglutinin (HA) tag in strains BY4741 (YCy2409), YCy2508 and YCy2671. Strains were generated by the previously described CRISPR-Cas9 methodology<sup>108,109</sup> to ensure both alleles are tagged in the tRNA neochromosome strains. This resulted in strains BY4741 eIF2- $\alpha$ -HA pRS413 (SLy129), YCy2508 eIF2- $\alpha$ -HA (SLy135), YCy2671 eIF2- $\alpha$ -HA (SLy138). HA-fusions were validated by Sanger sequencing and the presence of the tRNA neochromosome was validated by PCRTags. The HA tag was necessary because the sourced commercial antibody for eIF2- $\alpha$  did not allow detection in *S. cerevisiae*. For Western blot analysis, the strains were cultured in 200 mL SC-His medium in 1000 mL baffled flasks at 30°C with shaking at 200 rpm until OD<sub>600</sub> = 0.5. 100 mL were harvested and the remaining culture was grown until OD<sub>600</sub> = 0.8 followed by treatment with 10 mM 3-Amino-1,2,4-triazole (3AT) for 1-hour prior to harvest (3AT inhibits His3 and induces phosphorylation of eIF2- $\alpha$ ). Pellets were resuspended in 1 mL HNH buffer (50 mM HEPES pH 7.5, 150 mM NaCl, 50 mM NaF, 5 mM EDTA, 0.1% NP40, 0.1% Triton, 0.1% protease [cOmplete™ Protease inhibitor-cocktail, Roche] and phosphatase inhibitor [PhosSTOP™, Roche]) and poured in liquid N<sub>2</sub> to generate frozen droplets. Samples were then lysed using a CryoMill (Retsch MM 200). The resulting powder was resuspended in HNH buffer to a final OD<sub>600</sub> = 80 and the corresponding amount of 5X protein sample buffer (74 mM Tris-HCl, pH 8.0, 6.25% SDS, 10%  $\beta$ -mercaptoethanol, 20% glycerol) was added prior loading 10 μL of each sample on the SDS-PAGE (Tris-Glycine-20%). Proteins were blotted onto Immuno-Blot PVDF membrane (BioRad) using a Trans-Blot Turbo Transfer System (BioRad). The settings for eIF2- $\alpha$  were mixed molecular weight: 7 min, 1.3 A, up to 25 V, for  $\alpha$ -Tubulin transfer the time was increased to 10 min. The membranes were washed in 20 mL TBS for 5 min prior blocking with 10% milk in TBS-T (eIF2- $\alpha$  and  $\alpha$ -Tubulin) or 10% milk in PBS-T (eIF2- $\alpha$ -HA) for 2 h. Primary antibody treatment was done overnight at 4°C. For eIF2- $\alpha$ -HA antibody treatment was done in 5% milk in PBS-T (antibody: 1/10,000) and for eIF2- $\alpha$  (Ser51) and  $\alpha$ -Tubulin in TBS-T with 5% BSA (antibody: 1/5,000). Membranes

were washed three times with TBS-T (eIF2- $\alpha$  and  $\alpha$ -Tubulin) or PBS-T (eIF2- $\alpha$ -HA) for 5 min respectively prior secondary antibody incubation (anti-rabbit IgG, 1/2,000) in 5% milk in TBS-T (eIF2- $\alpha$  and  $\alpha$ -Tubulin) or PBS-T (eIF2- $\alpha$ -HA) for 1 h. Membranes were washed three times accordingly with either TBS-T or PBS-T for 5 min prior detection on an Azure Imager using SuperSignal West Femto (ThermoScientific).

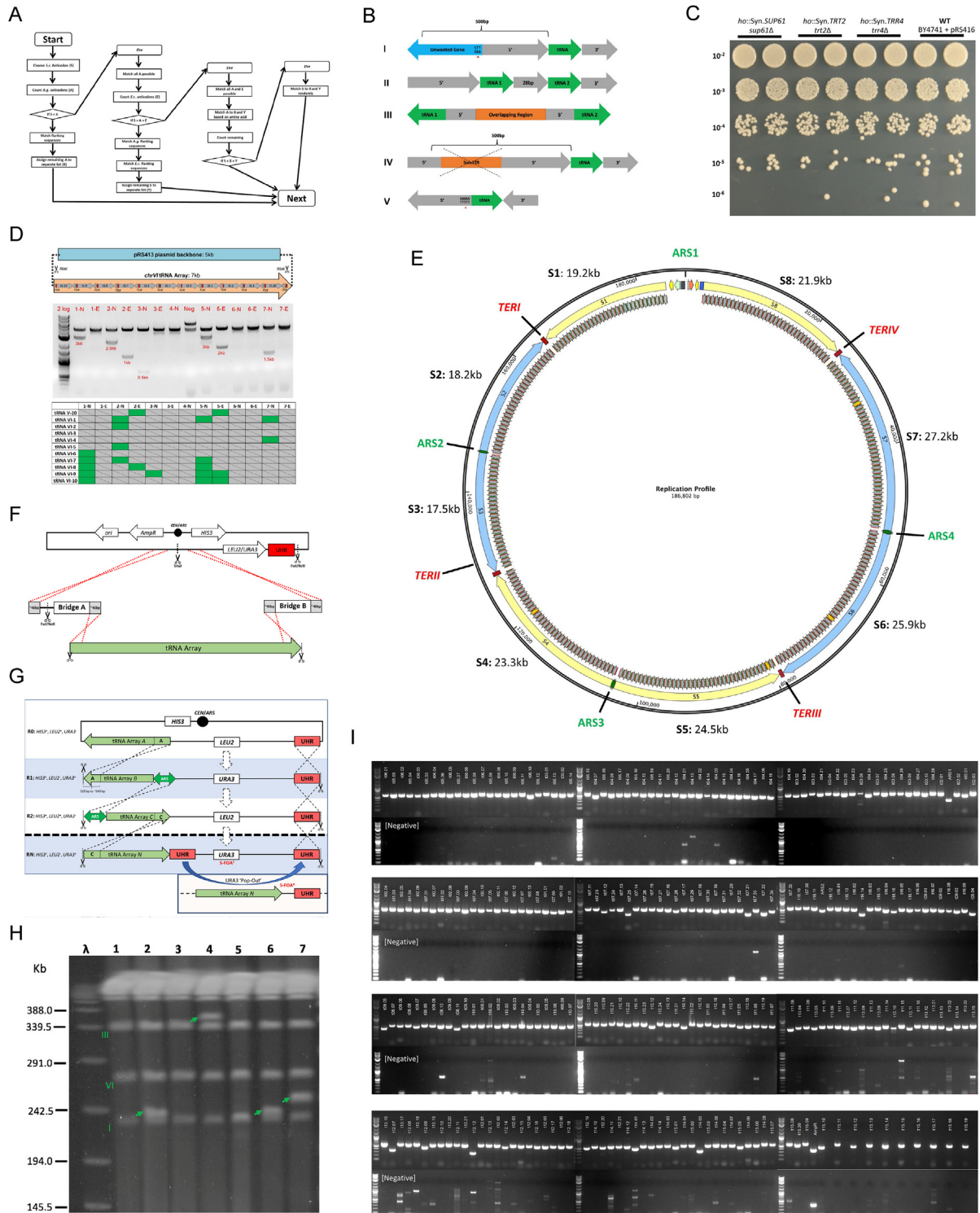
### Replication timing profiles

Relative replication time was determined by sort-seq as described previously.<sup>110</sup> Briefly, replicating (S phase) and non-replicating (G2 phase) cells were enriched from an asynchronously growing culture by FACS based on DNA content. As controls, G1 phase ( $\alpha$  factor arrest) and G2 phase (nocodazole arrest) samples were also collected. For each sample, genomic DNA was extracted and subjected to Illumina sequencing to measure relative DNA copy number. Replication timing profiles were generated by normalizing the replicating (sorted S phase) sample read count to the non-replicating (sorted G2 phase) sample read count in 1 kb windows. The ratio was normalized to a baseline of one to control for differences in number of reads between the samples.

### QUANTIFICATION AND STATISTICAL ANALYSIS

Statistical analyses used in this study included the Mann–Whitney U test and the Pearson correlation coefficient and are indicated in the corresponding figure legends. The software used for statistical analysis is indicated in the [key resources table](#).

# Supplemental figures



(legend on next page)

**Figure S1. Design and construction of the tRNA neochromosome, related to Figures 1 and 2**

(A) Flow chart of algorithm used to assign *S. cerevisiae* tDNAs to flanking sequences of *A. gossypii* and *E. cymbalariae*. The flow chart formed the basis of programming scripts used to generate the tRNA arrays of the tRNA neochromosome. The first stage of the algorithm identified a single anticodon family of *S. cerevisiae* (S) and assigned *A. gossypii* (A) flanking sequences with the same anticodon based on the available pool. The remaining unassigned flanking sequences were then added to a separate list (X). For tDNAs that cannot be assigned *A. gossypii* flanking sequences based on this principle (IF S>A), the second stage of the algorithm performed the same process of assignment based on tRNA flanking sequences from *E. cymbalariae* (E), and unassigned flanking sequences were again added to a separate list (Y). For tRNA genes that cannot be assigned flanking sequences by matching anticodon from either of these two species (IF S>A+E), tDNAs were assigned flanking sequences based on matching amino acid from the two *A. gossypii* and *E. cymbalariae* lists (X and Y). Finally, the remaining tDNAs that cannot match any of these conditions were randomly assigned flanking sequences irrespective of anticodon, amino acid, or species.

(B) Graphical representation depicting the removal/alteration of unwanted features in tDNA flanking sequences. Otherwise, tDNAs and their associated flanking sequences were discarded from the available “pool.” (BI) Unwanted genes in 5′ flanking sequence. Partially transcribed gene “starts” identified in the 5′ flanking sequence were translationally silenced by altering the “ATG” start codon to the “AAG” lysine codon (denoted by the red asterisk). (BII) Co-transcribed tDNAs separated by a 28-bp spacer region. The 5′ flanking sequence of tRNA 1 and the 3′ flanking sequence of tRNA 2 may be used (or otherwise discarded). (BIII) Shared 5′ flanking sequence between two divergent tDNAs. Only one of the two tRNA flanking sequences may be used based on relative anticodon requirement (or otherwise discarded). (BIV) Solo LTR observed in 5′ flanking sequences of *E. cymbalariae*. The solo LTR was removed, with the 5′ flanking sequence extended to incorporate the full 500 bp. (BV) Potentially misannotated tRNA orientation. This was inferred by the presence of a poly-thymidine residue in the 5′ flanking sequence (denoted by the red asterisk) and its absence in the 3′ flanking sequence. These tRNA flanking sequences were discarded from the available pool.

(C) Phenotypic colony morphology of each strain housing a synthetic copy of each essential tRNA gene. The figure demonstrates that synthetic single-copy tRNA genes (*SUP61* (tS(CGA)C), *TRT2* (tT(CGU)K), and *TRR4* (tR(CCG)L)) can complement the absence of each wild-type copy in BY4741 with no observable effect on colony size. Serial dilution and spotting of each strain (biological replicates) were undertaken onto SC-Ura. The dilution factor of each yeast sample is indicated on the left of the diagram.

(D) Dre recombinase-induced tRNA copy-number adjustment: proof-of-concept. Upper diagram: illustrative map of the *chrVI* tRNA array on pRS413. The tRNA array consists of 10 tRNA genes from *chrVI*, and one from *chrV*. *Rox* recombination sites are indicated in red. Middle: XbaI digestion pattern of plasmids recovered from BY4741 subjected to induction with Dre recombinase. The 5-kb band corresponds to pRS413, the second band of varying sizes corresponds to loss of tRNA genes on the array. Neg, negative control strain with tRNA array and empty pRS415 vector; N, non-induced; E, estradiol induced. Bottom: sequencing analysis of isolates housing the *chrVI* tRNA array following post-induction with Dre recombinase. Green: tRNA gene remains; gray boxes: tRNA gene is lost. The loss pattern of the tRNA genes indicates leaky expression of P<sub>SCW11</sub>-DreEBD, as previously indicated for Cre.<sup>8,34</sup>

(E) DNA-replication profile of the tRNA neochromosome. The tRNA neochromosome was divided into eight mega-arrays (S1–S8; replication length in kb is denoted in the above figure), with each oriented away from the leading edge of the replication fork from four origins of replication (*ARS1*: *ARSH4*; *ARS2*: *chrF-444*; *ARS3*: *chrL-615*; *ARS4*: *chrM-794*). The latter three origins were obtained from *C. glabrata*. Yellow and blue arrows indicate orientation of tRNA genes and direction of replication fork. Replication termination sites (red; *TER1* to *TERIV*) were introduced at relatively even inter-origin distance to terminate replication at defined regions. The diagram was generated using SnapGene software ([www.snapgene.com](http://www.snapgene.com)).

(F) Introducing tRNA arrays into *LEU2* or *URA3* eSwAP-In vectors. Two 330-bp to 650-bp “bridge” sequences were amplified using PCR to facilitate construction, using either Gibson Assembly or *in vivo* homologous recombination in yeast. Each bridge sequence was amplified using primers designed to contain the 40 bp of homology required for assembly, together with a single FseI or NotI restriction cut site (bridge A). Furthermore, these bridge sequences additionally served the purpose of providing homologous regions required for tRNA neochromosome construction (bridge A was the last segment of DNA from the latter round of construction, bridge B represents homology for a future round). Scissors with dotted lines represent restriction enzyme cut sites. The eSwAP-In vector contained a single SmaI restriction cut site to facilitate linearization.

(G) Alternate representation of tRNA neochromosome construction and “pop-out” of the *URA3* marker. The figure elaborates on the process of tRNA neochromosome construction. The black dot indicates the centromere, tRNA arrays are indicated by colored arrows, auxotrophic markers by green arrows, and the 500-bp UHR with a red box. The FseI/NotI restriction sites are indicated by scissors and black dotted lines. During round 1, the “A” region of tRNA array B facilitates homologous recombination, with the *LEU2* marker replaced with the *URA3* marker. For all future rounds, marker swapping may be facilitated with any region of homology (e.g., ARS elements as denoted in the above figure), with the UHR remaining static. To induce *URA3* pop-out (bottom), a second UHR is introduced to facilitate homologous recombination. *URA3* converts 5-fluoroorotic acid (5-FOA) into the toxic 5-fluorouracil—only cells that remove functionality of the *URA3* gene will survive.

(H) Pulsed-field gel pattern of strains housing linear and circular variants of the tRNA neochromosome constructed in BY4741. The above gel image shows an unexpected heterogeneity in tRNA neochromosome size. Lanes 1 and 3 are strains housing circular variants, lanes 2 and 6 are replicate isolates (n = 2) of strains housing a neochromosome linearized at *TERIII* (~240 kb band), lanes 4 and 7 are replicate isolates of strains housing a neochromosome linearized at *TERII* (~350- and ~250-kb bands, respectively), and lane 5 is a wild-type empty plasmid control. The expected size of the tRNA neochromosome is ~187 kb. Wild-type yeast chromosomes are indicated by Roman numerals, and bands corresponding to the neochromosome are indicated by green arrows.

(I) Representative PCR tag analysis of the tRNA neochromosome. PCR tag names are denoted at the top (a full list may be found in [Methods S1](#)). The negative control (bottom) was undertaken on BY4741 + pRS413. “AmpR” denotes a positive control designed to amplify *bla* on pRS413.

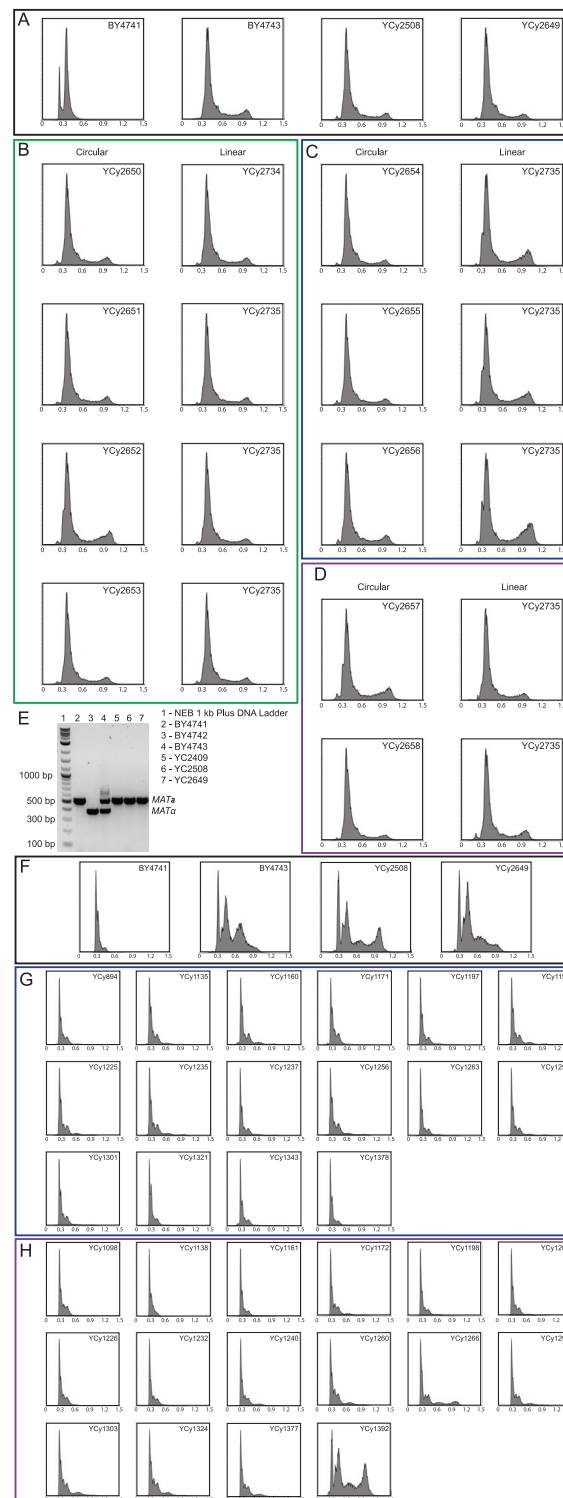


**Figure S2. Ploidy and mating-type determination of tRNA neochromosome strains, related to Figure 2**

(A–D) 100,000 total events were detected, and each histogram consists of a minimum of 70,000 gated events. y axis displays number of events and x axis intensity (a.u.  $\times$  1,000).

(A) DNA content analysis of haploid BY4741 and the diploid strains BY4743, YCy2508, and YCy2649 serving as controls for (B)–(D).

(B–D) DNA content analysis to determine the ploidy of strains pre- and post-linearization, all strains show the pattern for diploid DNA content.

(B) Strains linearized at the *TER* sites.

(legend continued on next page)

---

(C) Strains linearized at *ARS* sequences. The strains show a higher proportion of cells with 4-n DNA content in contrast to all other strains. However, this seems not to influence the phenotype of the strains under the tested conditions (Figure S4).

(D) Strains linearized close to *CEN*.

(E) Multiplexed *MAT*-locus PCR according to Huxley et al.<sup>39</sup> with universal- (5'-AGTCACATCAAGATCGTTTATG-3'), *MATa*-specific (5'-ACTCCACTTCAAG-TAAGAGTTTG-3'; ~500 bp) and *MATα*-specific primers (5'-GCACGGAATATGGGACTACTT-3'; ~400 bp). Analysis confirms that the final tRNA neochromosome strain is *MATa*. Taking the results together, as well as the ability of the strains to mate with *MATα*-strains (data not shown), suggest a whole-genome duplication resulting in a *MATa/a* genotype.

(F) Ploidy determination of individual intermediary strains following each round of eSwAP-In. DNA content analysis of haploid BY4741 and the diploid strains BY4743, YCy2508, and YCy2649 serving as controls for (G) and (H).

(G) Consecutive eSwAP-In rounds of all tRNA arrays in BY4741.

(H) Consecutive eSwAP-In rounds of all tRNA arrays in YLM896 (or *synIII/VI/IXR*; purple). 100,000 total events were detected for each sample, and each histogram consists of a minimum of 50,000 events. y axis displays number of events and x axis intensity (a.u. × 1,000). YCy1392 presumably underwent a whole-genome duplication independent of spheroplast transformation.



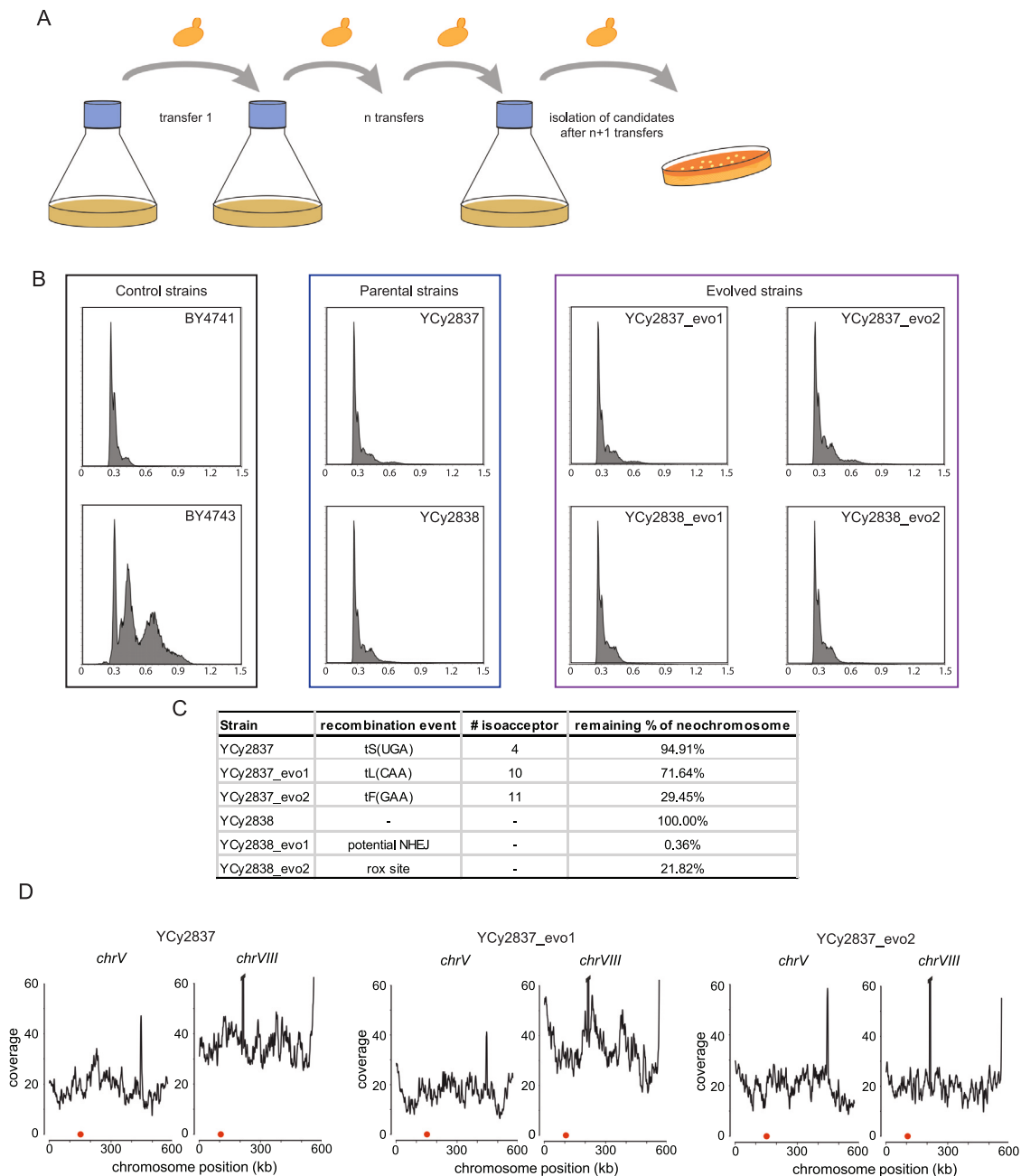


**Figure S3. Time course experiment for tRNA neochromosome stability, related to Figure 2**

(A) The time course experiment was performed as batch transfer where yeast cultures were back-diluted every 24 h to an OD<sub>600</sub> of 0.1. Single isolates were obtained after serial dilution and plated onto SC-His medium.

(B) Flow cytometry analysis of DNA content of the starting strains and four evolved isolates in comparison to BY4741 and BY4743. All tested strains are haploid. 100,000 total events were detected for each sample, and each histogram consists of a minimum of 50,000 events. y axis displays number of events and x axis intensity.

(C) Structural variations in the tRNA neochromosome detected by Nanopore sequencing of the parental strains and evolved isolates.

(D) Nanopore sequencing revealed an aneuploidy for *chrVIII* in the parental strain and the evolved strain containing >70% of the tRNA neochromosome content, while the aneuploidy is lost in the strain only containing 30% of the tRNA neochromosome content. Visualization of *chrV* serves as a reference for the average genome coverage in each sequencing experiment. Red dot indicates position of CEN, CUP1-1/CUP1-2 amplification in *chrVIII* exceeds y axis scale, and data are omitted for visualization purpose.

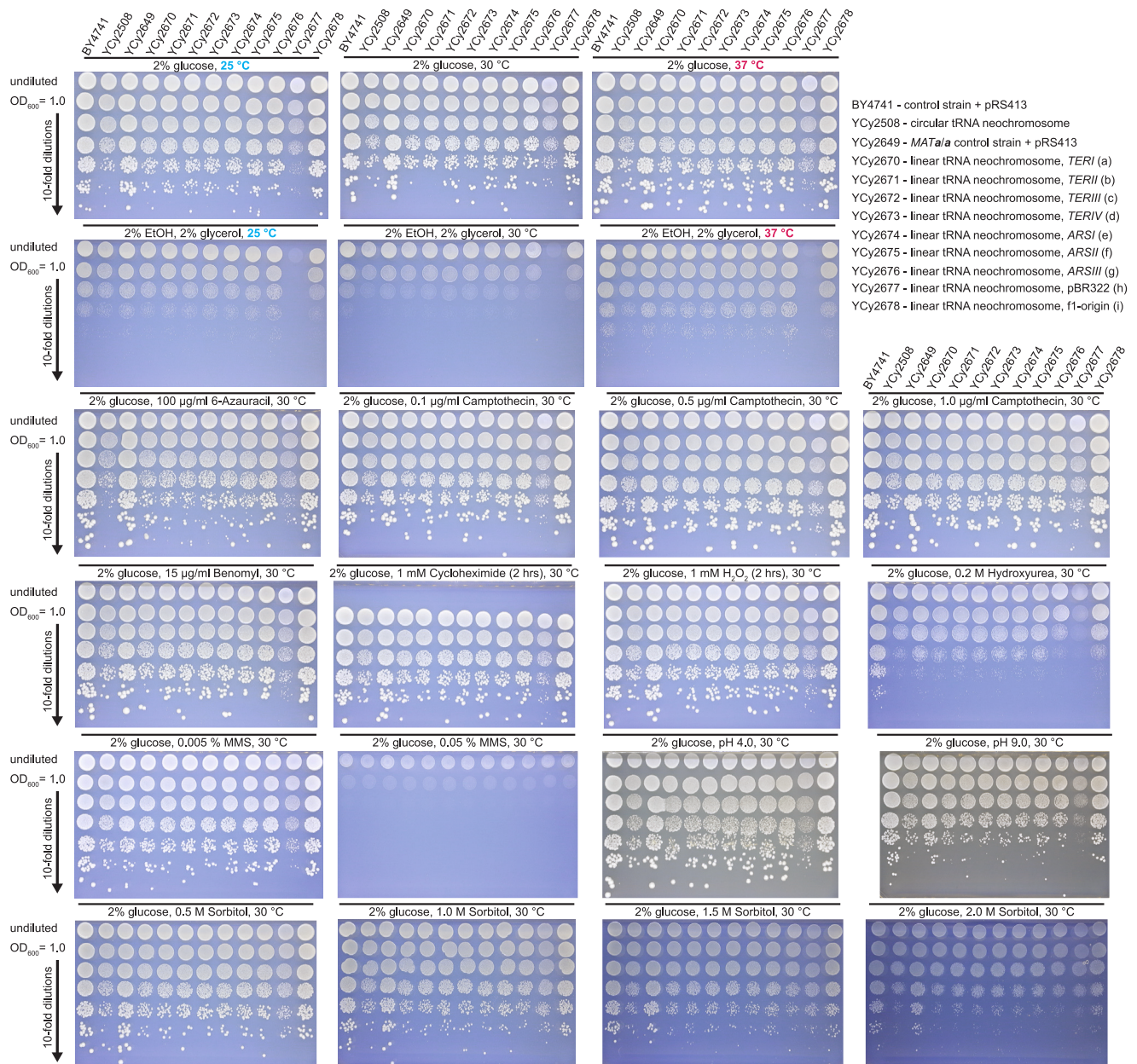


**Figure S4. Phenotyping tRNA neochromosome derivatives across a range of 22 growth conditions, related to Figure 3**

Each panel shows a single media condition with identical strain distribution of one circular and nine linear derivatives. In each panel, the top row represents the undiluted overnight culture, followed by a 10-fold serial dilution from a culture normalized to an  $OD_{600}$  of 1.0 (second row and below). Similar growth patterns can be observed throughout each assay, except for 6-azauracil and 0.2 M hydroxyurea where the growth deficiency of the tRNA neochromosome strains increases. The strain YCy2677 was later revealed to be a mitochondrially deficient  $\rho^-$  mutant (indicated by a lack of growth on non-fermentable carbon sources). All spotting assays were performed on SC-His at 30 °C for 72 h, unless specified otherwise. Carbon source and alteration are stated above each panel. See Figure 3A for visualization of linearization sites.

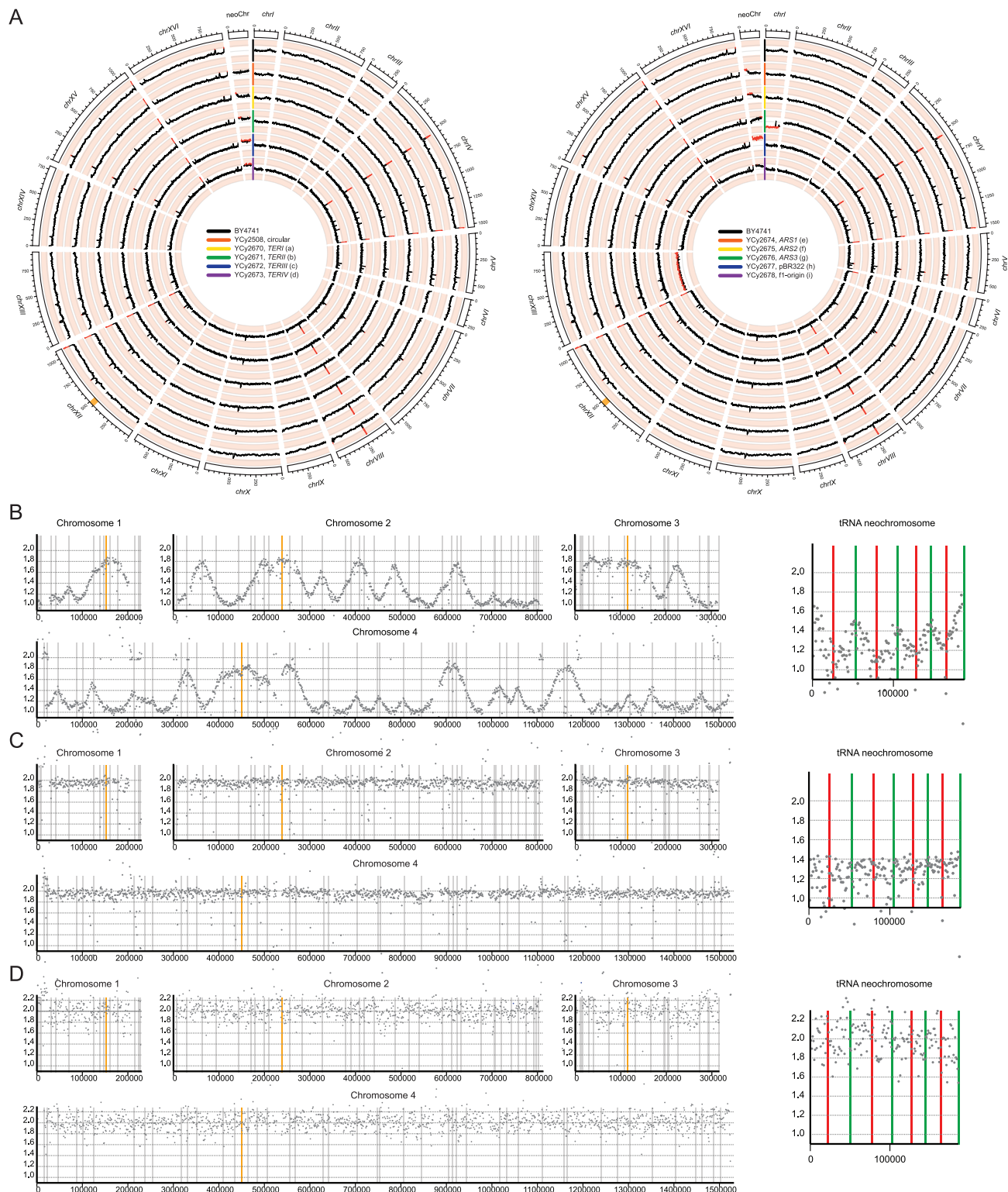


**Figure S5. Short-read tRNA neochromosome sequencing data and DNA-replication profiling of S phase and G1 phase cells in a circular tRNA neochromosome variant (YCy2508), related to Figures 3, 4, and 6**

(A) The Circos plots indicate sequence read coverage for tRNA neochromosome variants obtained from stationary phase cells in comparison to BY4741. Linearization locations are indicated in the center of each circle, with different colors denoting each strain. The sequencing coverage was normalized within each

(legend continued on next page)

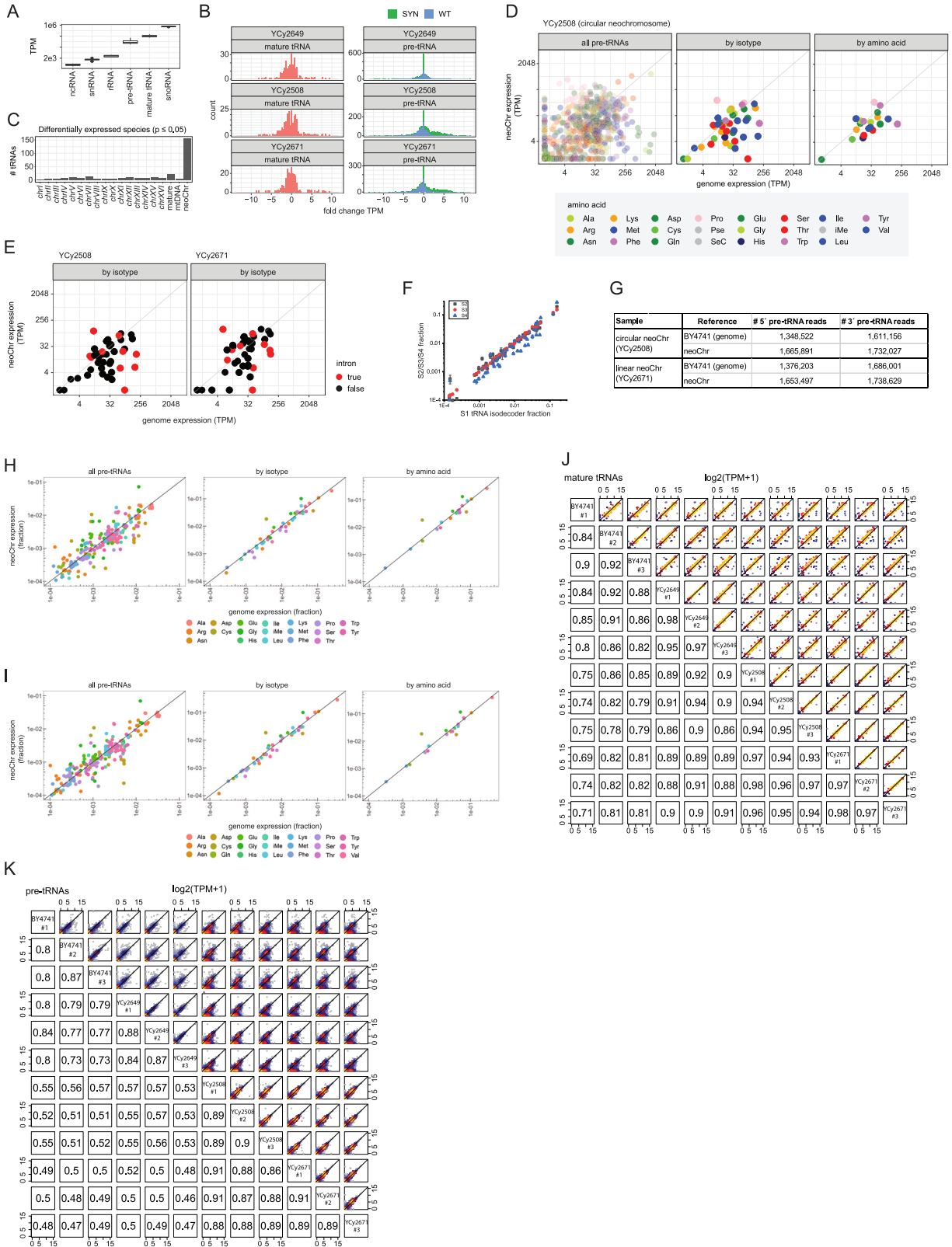
---

sample to visualize aneuploidies, corresponding to  $\geq 1.5$ - and  $< 0.5$ -fold coverage (scale from 0 to 2; indicated by red coverage lines for threshold passing). A moving window average function (5,000 bp average 500 bp steps) was applied to smoothen the curves using a custom R script. The rDNA region, indicated orange in chromosome XII, was excluded from plotting. In both plots the outermost ring is the control strain BY4741. Coverage analysis indicates a  $-1$  aneuploidy for *chrI* in YCy2676 and a  $+1$  aneuploidy for *chrXIII* in YCy2677. Notably, the strains containing the tRNA neochromosome linearized at suboptimal positions (YCy2674 to YCy2678) show alterations in tRNA neochromosome coverage; however, no size alteration was detected during size analysis (Figure 3). There are no segmental coverage alterations specific to an individual strain. Observed peaks correspond to known variations such as CUP1-1/CUP1-2 in *chrVIII*, known to have variable number of tandem repeats and can further be present as extrachromosomal circular DNA (eccDNA). Plots are generated using Circos.<sup>111</sup> Sequencing data is available at NCBI BioProject PRJNA884518.

(B) DNA-replication profiling of S phase and G1 phase cells in a circular tRNA neochromosome variant (YCy2508), (B–D) *ARS* (gray or green), *CEN* (orange), *TERI-IV* (red). Replication pattern of S phase cells. Peaks correspond to origins of replication, and pattern is indistinguishable from strains without the tRNA neochromosome.<sup>112</sup>

(C) Replication pattern of  $\alpha$  factor-arrested cells (G1). All chromosomes show a normalized read abundance of  $\sim 2$ -fold, while the tRNA neochromosome shows a lower abundance of  $\sim 1.4$ -fold.

(D) Replication pattern analysis of nocodazole-arrested cells (G2). Only data for *chrI* to *chrIV* and the tRNA neochromosome are shown.



(legend on next page)

**Figure S6. tRNA-seq and MSR-seq of circular and linear tRNA neochromosome variants, related to Figure 4**

The figure displays results for YCy2508 (circular tRNA neochromosome), YCy2649 (BY4741 + pRS413 control), and YCy2671 (linearized tRNA neochromosome). For (A)–(E), (J), and (K), results are from tRNA sequencing; for (F)–(I), results are from MSR-seq.

(A) Quantification of all sequenced small RNA species.

(B) Distribution of expression fold changes measured for mature and pre-tRNA species, originating either from the synthetic tRNA neochromosome or the native genome in a strain without the neochromosome (YCy2649) and strains with either a circular version of the neochromosome (YCy2508) or a linear version (YCy2671).

(C) Number of differentially expressed tRNA species on each chromosome ( $p \leq 0.05$ ).

(D) Pairwise pre-tRNA expression levels for all pre-tRNAs originating from the neochromosome, compared with levels measured from the native loci they were designed to replace (left). Alternatively, pre-tRNA expression levels were aggregated and averaged (median) by isotype (center) or amino acid (right). Pearson correlation coefficient ( $r$ ) reported for each association. Colors denote the amino acid with which the tRNA species is charged.

(E) As in (D), with colors corresponding to the presence or absence of introns. TPM, transcripts per million. No significant differences were observed in pre-tRNA levels between samples with and without introns for either the linear tRNA neochromosome ( $p > 0.45$ ) or the circular tRNA neochromosome ( $p > 0.98$ ), as determined by the Mann-Whitney U test.

(F) MSR-seq shows similar results for pre-tRNA abundances. Correlation of mature tRNA expression at the isoacceptor level. S1: BY4741 (YCy2409); S2: circular tRNA neochromosome (YCy2508); S3: 2n BY4741 (YCy2649); S4: linear tRNA neochromosome (YCy2671). R values of the linear fits are 0.991 (S1-S2), 0.997 (S1-S3), 0.888 (S1-S4), 0.988 (S2-S3), 0.920 (S2-S4), and 0.872 (S3-S4).

(G) Mapping statistics of reads containing tRNA precursors, either the upstream sequence (up) or downstream sequence (down) of the tRNA gene. Mean read counts from 3 biological replicates for each sample are shown.

(H) Correlation of tRNA precursors of identical tRNA sequences containing the upstream sequence from the native chromosomes (x axis) and the circular tRNA neochromosome (y axis) at the level of individual tRNA genes (left), grouped by isoacceptors (middle), and amino acids (right). For clarity, only upstream (and not downstream) mapped genes are shown. Genes are colored by amino acids. R values of linear fits are 0.889 (S2 gene), 0.967 (S2 isoacceptor), and 0.956 (S2 amino acid).

(I) Correlation of tRNA precursors of identical mature tRNA sequences containing the upstream sequence from the native chromosomes (x axis) and the linear tRNA neochromosome (y axis) at the level of individual tRNA genes (left), grouped by isoacceptors (middle), and amino acids (right). For clarity, only upstream (and not downstream) mapped genes are shown. Genes are colored by amino acids. R values of linear fits are 0.917 (S4 gene), 0.975 (S4 isoacceptor), and 0.961 (S4 amino acid).

(J) Comparative tRNA expression between sample replicates. Strain IDs are indicated in the middle of each chart. Pairwise mature tRNA expression levels across all strains and replicates.

(K) Pairwise pre-tRNA expression levels across all strain and replicates. Numeric values denote Pearson correlation coefficient ( $r$ ). TPM, transcripts per million.

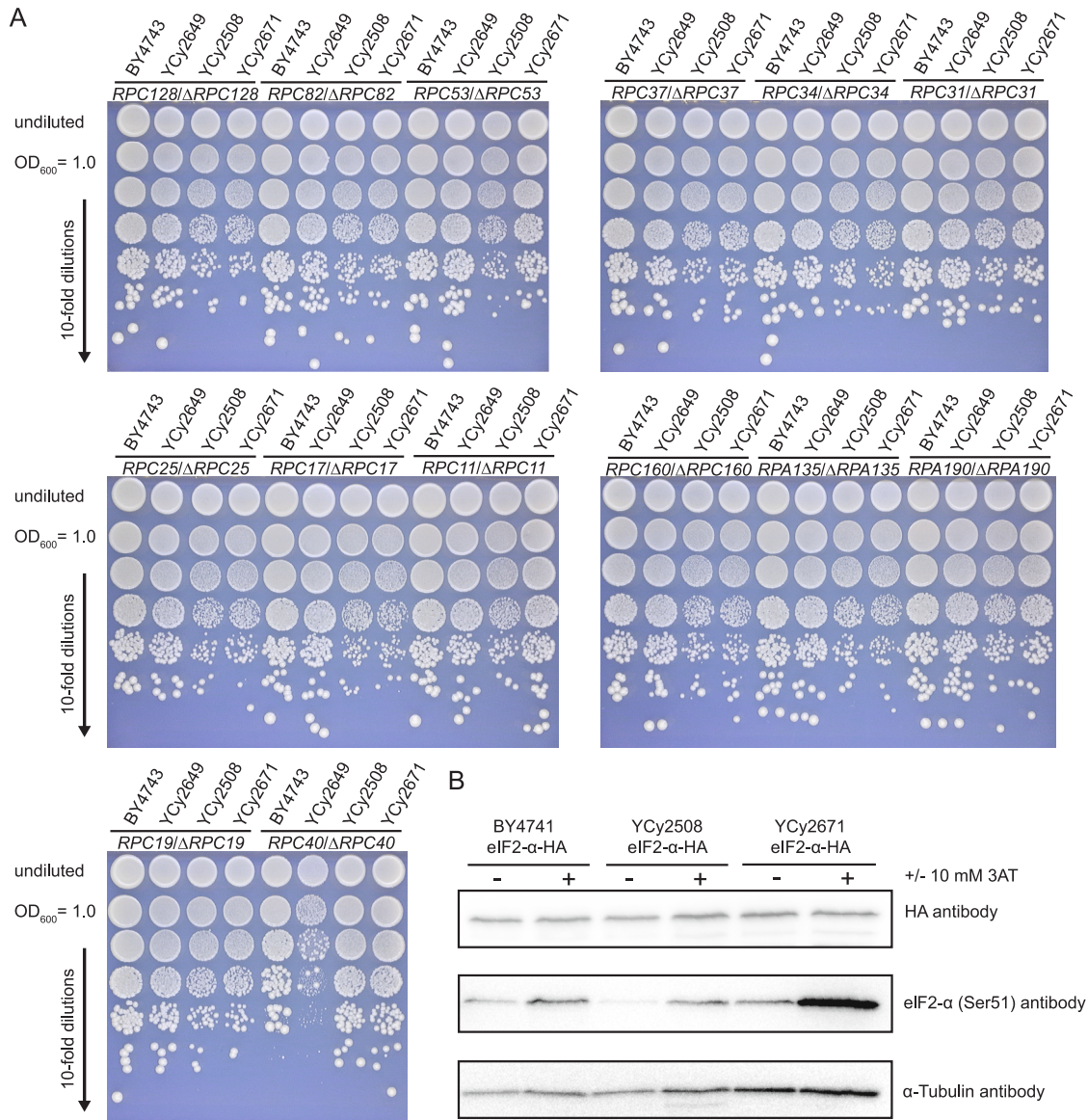


**Figure S7. RNAPIII- and RNAPI-specific and shared subunit deletion and eIF2- $\alpha$  Ser51 phosphorylation, related to Figure 4 and STAR Methods**

(A) In the above figure, heterozygous diploids were generated with single-subunit deletions of RNAPIII, RNAPI, or shared subunits. Growth media conditions are SC-His, 2% glucose at 30°C for 72 h. In each panel, the top row represents the undiluted overnight culture, followed by a 10-fold serial dilution from a culture normalized to an OD<sub>600</sub> of 1.0 (second row and below). BY4743 is the wild-type diploid control, YCy2649 is the *MATa/a* control, YCy2508 is the homozygous diploid housing a circular tRNA neochromosome, and YCy2671 is a homozygous diploid strain containing a linear variant of the tRNA neochromosome.

(B) eIF2- $\alpha$  Ser51 phosphorylation does not show increased levels in strains containing the tRNA neochromosome, related to STAR Methods. To investigate the phosphorylation levels of eIF2- $\alpha$  at position Ser51, western blot analysis was performed with phosphorylation-specific and HA epitope antibodies for the circular and a linear tRNA neochromosome strains, compared with BY4741.  $\alpha$ -tubulin was used as a loading control. 3-amino-1,2,4-triazole (3AT), a histidine analog, was used to induce amino acid starvation and served as a positive control for eIF2- $\alpha$  Ser51 phosphorylation. In all three strains, an increase of phosphorylation levels is visible after 3AT treatment. Three biological replicates of the experiment were performed, and a representative detection is shown.

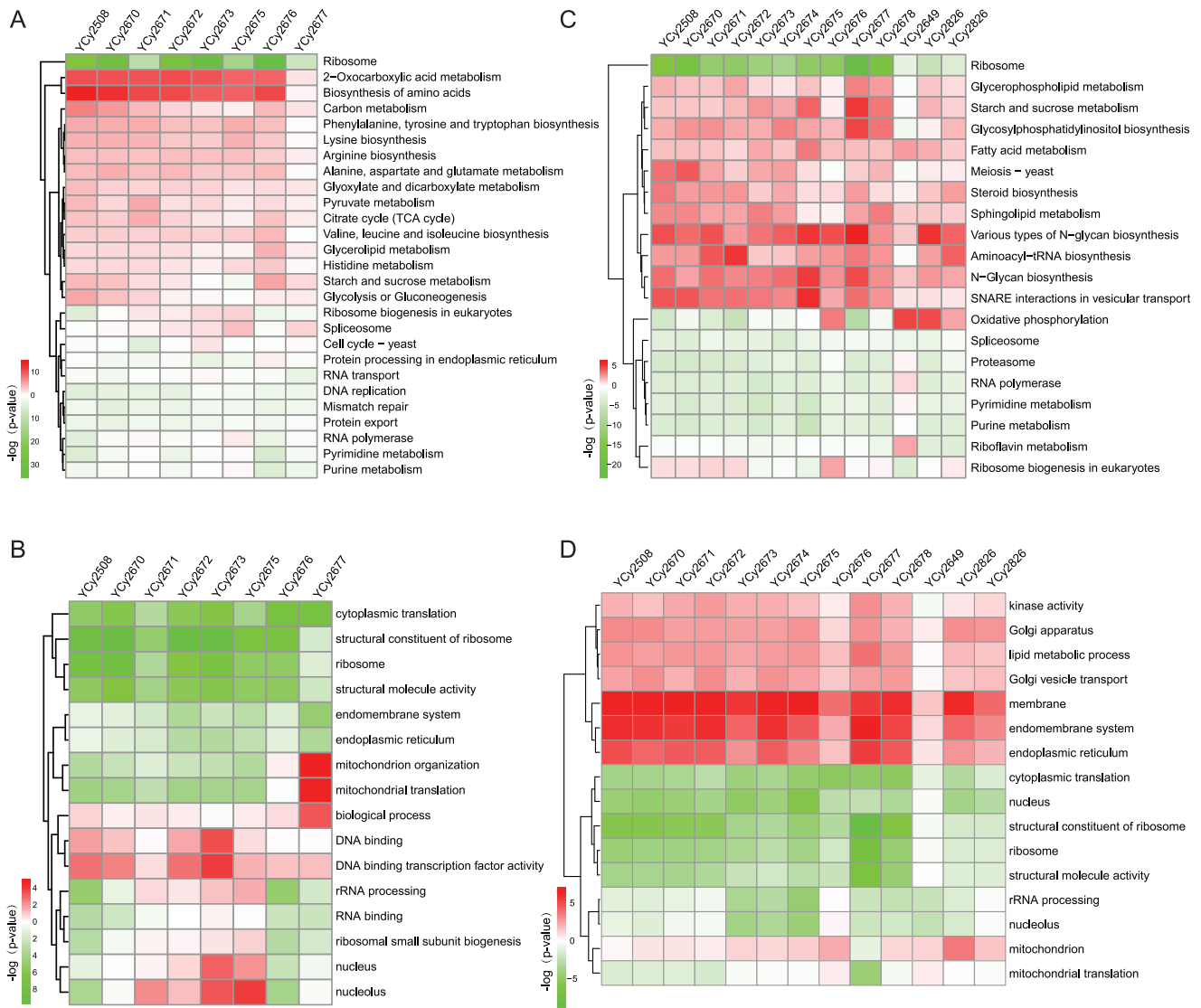


**Figure S8. RNA sequencing and proteomics profiling for all analyzed tRNA neochromosome strains, related to Figure 5**  
(A–D) (A) and (B) denote differential expression of circular tRNA neochromosome strains normalized to the homozygous diploid control strain (YCy2649), and (C) and (D) indicate proteomic analysis of the same strains. (A) KEGG and (B) GO analysis demonstrate a general upregulation of amino acid biosynthesis and a downregulation of translational processes. YCy2677 is the  $\rho^-$  strain that explains the upregulation of mitochondrial processes. Upregulated and downregulated features are labeled in red and green, respectively, with color intensity indicating significance level. (C) KEGG and (D) GO analysis following proteomics globally show a similar pattern to that of transcriptomics. However, an additional increase in membrane-associated proteins and endoplasmic reticulum can be observed. Upregulated and downregulated features are labeled in red and green, respectively, with color intensity indicating significance level.